Max-Planck-Institut für Meteorologie
Max Planck Institute for Meteorology

Long-term interactions between ice sheets and climate under anthropogenic greenhouse forcing

Simulations with two complex Earth System Models

Miren Vizcaino

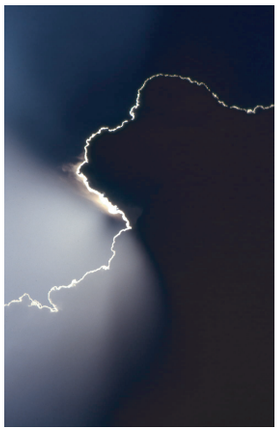

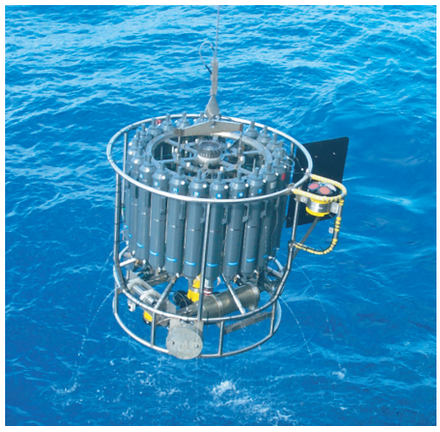

Berichte zur Erdsystemforschung 30/2006

Reports on Earth System Science

Hinweis

Die Berichte zur Erdsytemforschung werden vom Max-Planck-Institut für Meteorologie in Hamburg in unregelmäßiger Abfolge herausgegeben.

Sie enthalten wissenschaftliche und technische Beiträge, inklusive Dissertationen.

Die Beiträge geben nicht notwendigerweise die Auffassung des Instituts wieder.

Die "Berichte zur Erdsystemforschung" führen die vorherigen Reihen "Reports" und "Examensarbeiten" weiter.

Notice

The Reports on Earth System Science are published by the Max Planck Institute for Meteorology in Hamburg. They appear in irregular intervals.

They contain scientific and technical contributions, including Ph. D. theses.

The Reports do not necessarily reflect the opinion of the Institute.

The "Reports on Earth System Science" continue the former "Reports" and "Examensarbeiten" of the Max Planck Institute.

Anschrift / Address

Max-Planck-Institut für Meteorologie
Bundesstrasse 53
20146 Hamburg
Deutschland

Tel.: +49-(0)40-4 11 73-0
Fax: +49-(0)40-4 11 73-298
Web: www.mpimet.mpg.de

Layout:

Bettina Diallo, PR & Grafik

Titelfotos:
vorne:
Christian Klepp - Jochem Marotzke - Christian Klepp
hinten:
Clotilde Dubois - Christian Klepp - Katsumasa Tanaka

Berichte zur Erdsystemforschung 30 2006

Long-term interactions between ice sheets and climate under anthropogenic greenhouse forcing

Simulations with two complex Earth System Models

Dissertation zur Erlangung des Doktorgrades der Naturwissenschaften
im Departement Geowissenschaften der Universität Hamburg
vorgelegt von

Miren Vizcaino
aus Madrid, Spanien

Hamburg 2006

Reports on Earth System Science 30 2006

ISSN 1614-1199

Miren Vizcaino
Max-Planck Institut für Meteorologie
Bundesstr. 53
20146 Hamburg
Germany

Als Dissertation angenommen
vom Departement Geowissenschaften der Universität Hamburg

auf Grund der Gutachten von
Prof. Dr. Hartmut Grassl
und
Dr. Uwe Mikolajewicz
Hamburg, den 23. Oktober 2006
Professor Dr. Kay-Christian Emeis
Leiter des Departements für Geowissenschaften

ISSN 1614-1199

Long-term interactions between ice sheets and climate under anthropogenic greenhouse forcing

Simulations with two complex Earth System Models

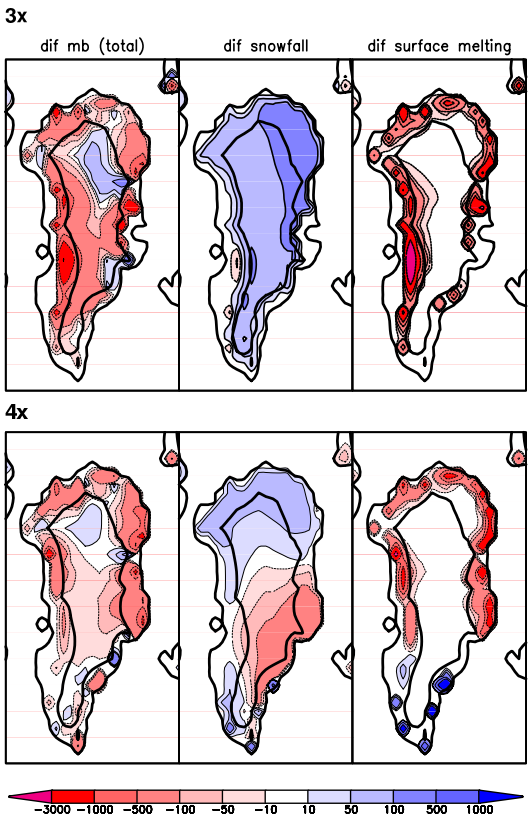

Miren Vizcaino

Hamburg 2006

"José Arcadio Buendía pagó los treinta reales y los condujo hasta el centro de la carpa, donde había un gigante de torso peludo y cabeza rapada, (...) custodiando un cofre de pirata. Al ser destapado por el gigante, el cofre dejó escapar un aliento glacial. Dentro sólo había un enorme bloque transparente, con infinitas agujas internas en las cuales se despedazaba en estrellas de colores la claridad del crepúsculo. Desconcertado, sabiendo que los niños esperaban una explicación inmediata, José Arcadio Buendía se atrevió a murmurar:
-Es el diamante más grande del mundo.
-No -corrigió el gitano-. Es hielo."

"José Arcadio Buendía paid the thirty reales and led them into the center of the tent, where there was a giant with a hairy torso and a shaved head, (...) watching over a pirate chest. When it was opened by the giant, the chest gave off a glacial exhalation. Inside there was only an enormous, transparent block with infinite internal needles in which the light of the sunset was broken up into colored stars. Disconcerted, knowing that the children were waiting for an immediate explanation, José Arcadio Buendía ventured a murmur: 'It's the largest diamond in the world'. 'No,' the gypsy countered. 'It's ice.' "

Cien años de soledad
Hundred years of solitude
Gabriel García Márquez

Contents

Abstract

The ice sheets of Greenland and Antarctica store the largest amount of continental water on Earth. Changes in their mass balance due to the climate change associated with the increasing atmospheric concentration of greenhouse gases could produce important changes in the sea level. Besides, changes in their mass balance could have an impact on ocean circulation via modified meltwater fluxes and on the atmosphere via changes in albedo and topography.

Most of the studies of the mass balance of the ice sheets focus on the evolution until the year 2100. Some of them do not include the effect of changes in the dynamics of the ice sheets on the total mass balance. In this study an ice sheet model is bi-directionally coupled to two different Earth System Models. It has been used to study the multi-century evolution of global ice sheets in scenarios of anthropogenic greenhouse forcing, the impact of their mass balance changes on the climate system, and how these changes can modify their own mass balance. The use of General Circulation Models for the ocean and atmosphere in both Earth System Models permits a proper identification of these potential ice sheet-climate feedbacks.

The Earth System Models used in this study are ECHAM3/LSG2/LPJ/-HAMOCC/SICOPOLIS (ESM1) and ECHAM5/MPI-OM/LPJ/SICOPOLIS (ESM2). Several stabilisation and IPCC SRES scenario simulations have been performed with ESM1. Changes in the North Atlantic Meridional Overturning Circulation (NAMOC) are mostly driven by increased atmospheric moisture fluxes, with a minor contribution from meltwater fluxes from the Greenland ice sheet (GrIS). The mass balance of the GrIS has been found to be very sensitive to changes in the northward heat transport due to the weakening/collapse of the NAMOC in the simulations. The mass balance of the Antarctic ice sheet is dominated by increased snowfall rates in all the simulations.

The ice sheet-atmosphere feedbacks related to albedo and atmospheric circulation were found not to be relevant for the mass balance of the Greenland ice sheet until the ice sheet decayed to 3/4 of its original area and volume. The sign

of these feedbacks was found to be positive, with a dominant role of the albedo changes.

First results of a model with bidirectional coupling of an ice sheet to an AOGCM (model ESM2) without flux corrections are presented. The results with ESM2 show stronger melting rates of the GrIS than with ESM1 and positive contribution of the Antarctic ice sheet to sea level rise in the high stabilisation scenario 4xCO_2.

Chapter 1

Introduction

The ice sheets of Greenland and Antarctica store the largest amount of continental water on Earth. If the water stored in these continental-sized ice masses would be released to the world oceans, the sea level would rise by approximately 70 m (Church *et al.*, 2001). They represent 97% of the world's glacier surface and hold 99.85% of the global glacier volume. Changes in the mass balance of these ice sheets due to climate change associated with the rising concentration of greenhouse gases could significantly affect the global sea level. Besides, the location of these ice sheets close to the sites of deep water formation could affect the strength of the meridional overturning (Stouffer *et al.*, 2006) and therefore the northward heat transport by the ocean, with potential consequences for the regional climates. Changes in the area and shape of the ice sheets can modify the surface albedo and the general circulation of the atmosphere.

1.1 Ice sheets and climate

Ice sheets can modify the climate by several processes:

1. Changes in the topography of the ice sheets can modify the *general circulation of the atmosphere*. Modelling studies, for instance, indicate that the path of the jet stream is strongly modified by topography (Manabe and Broccoli (1985), Kutzbach and Wright (1985), Cook and Held (1988)).

2. Changes in the glacier mask can modify strongly the surface *albedo*.

3. Freshwater fluxes from the ice sheets can modify the *ocean circulation* via changes in ocean water density (Stouffer *et al.*, 2006).

4. Changes in the amount of water stored by the ice sheets modify *sea level* and therefore the land-sea distribution. At the time of the Last Glacial Maximum (21-18 ky BP), for instance, the sea level was approximately 130 m lower than at

present.

The discharge of meltwater from the northern hemisphere ice sheets has been proposed as the triggering mechanism for abrupt climate change in the past at the time of the Younger Dryas (Berger and Killingley (1982), Broecker *et al.* (1988), Maier-Reimer and Mikolajewicz (1989)). The high albedo of the ice sheets has played a very important role in the glacial-interglacial transitions during the glacial cycles of the Pleistocene. Manabe and Broccoli (1985) found that the topographic and albedo effects of ice sheets alone explain much of the northern hemisphere cooling identified in paleoclimatic records of the last glacial maximum.

1.2 The mass balance of ice sheets

Ice sheets gain mass by accumulation of snow (snowfall and deposition by wind-drift). The snow is gradually transformed to ice via compaction (from the density of 100-200 kg/m^{3}of fresh snow to approximately 910 kg/m^3, which is the density of ice). Ice sheets loose mass (ablation) by melting at the surface (when surface temperatures reach the melting point) or at the base with subsequent runoff or evaporation of meltwater. Some water can refreeze within the snow, and some snow may sublimate or be blown off the surface. Ablation can also take place by discharge of ice into a floating ice shelf or a glacier tongue, from where the ice is lost by basal melting due to ocean heat supply and by calving of icebergs. Net accumulation takes place at high altitudes and net ablation at lower altitude. To compensate for net accumulation and ablation, ice flows downhill by internal deformation and by sliding and bed deformation at the base. Horizontal fluxes of ice are controlled by the gradient of topography, the ice thickness, the effective ice viscosity (which varies by several orders of magnitude with the range of temperatures in the ice column, Paterson (1994)), and the basal thermal and physical conditions (presence of meltwater and/or deformable sediment).

Ice velocities range from several meters per year at the ice divides to several hundred or thousand of meters per year at ice shelves and ice streams. Variations in ice velocities due to changes of the viscosity of the ice have time scales of several thousand years, due to the slow time-scales of heat diffusivity in the ice column. Variations associated with the presence of meltwater at the base, which produces sliding of the ice column, have shorter time-scales. They have been proposed as the mechanism behind Heinrich events (MacAyeal (1993), Payne (1995), Calov *et al.* (2002)) and behind the surging behaviour of outlet glaciers and ice streams.

Four components determine the current and future volume changes of the polar ice sheets: 1) the long-term background evolution as a result of ongoing

ice-dynamic adjustment to past environmental changes as far back as to the last glacial period, 2) the effect of current and future surface mass-balance changes, 3) the ice dynamic response to these surface mass balance changes due to changes in the velocity field associated to changes in the surface slope and ice thickness, and 4) other ice-dynamic responses related to changes in the ice-sheet base or at the grounding line (lubrication of the base by percolated meltwater, disintegration of ice shelves or glacier tongues,...).

1.3 The Greenland ice sheet (GrIS)

The Greenland ice sheet has an area of 1.71 x 10^6 km^2 and stores 2.85 x 10^6 km^3 of freshwater. This volume is equivalent to 7.2 m of sea level (Church *et al.*, 2001). The mean thickness of the ice is therefore 1.7 km. The ice sheet occupies 82% of the surface of Greenland. The maximum height of the ice sheet is at the northern dome (3247 m). The height of the southern dome is 2960 m.

The Greenland ice sheet first formed approximately 7 million years ago and was definitively established 3 million years ago (Zachos *et al.* (2001), Larsen *et al.* (1994)). During the last interglacial (127 ky BP) global sea level was approximately 5-6 m higher than at present (Stirling *et al.* (1998), Vezina *et al.* (1999)). According to the modelling studies of some authors, as Letreguilly *et al.* (1991b) and Ritz *et al.* (1997), the contribution from the Greenland ice sheet to these high sea levels was relatively modest, approximately 1-2 m of sea level equivalent (SLE), and the high sea levels were mainly due to the disintegration of the West Antarctic ice sheet (Mercer, 1978). Other authors propose a substantial contribution to the sea-level rise from the Greenland ice sheet: 4-5.5 m of SLE (Cuffey and Marshall, 2000) and 2.2-3.4 m SLE (Otto-Bliesner *et al.*, 2006).

At present the mean annual accumulation over the ice sheet is 1.4±0.1 mm/yr of SLE (Church *et al.*, 2001). Summer temperatures on the Greenland ice sheet are high enough to cause widespread melting, which accounts for half of the ice loss. The remainder is discharged as icebergs or into small ice shelves.

1.4 The Antarctic ice sheet (AIS)

The Antarctic ice sheet is the largest single mass of ice on Earth. It covers an area of 12.37 x 10^6 km^2 and contains a volume of 25.71 x 10^6 km^3 of ice. The volume is equivalent to 61.1 m of sea level (Church *et al.*, 2001). Two major sub-ice sheets can be distinguished in Antarctica, separated by the Transarctic Mountains: the

East Antarctic Ice Sheet (EAIS), and the West Antarctic Ice Sheet (WAIS). The WAIS is a marine-based ice sheet, i.e., most of its bed lies well below sea level and its edges flow into floating ice shelves. Most of the ice from WAIS is discharged into the huge ice shelves of Rönne-Filchner and Ross in the Weddell and Ross Seas, respectively. The volume of the WAIS is 6 m SLE.

The widespread glaciation of Antarctica took place at the Eocene-Oligocene boundary, about 35 million years ago (Zachos *et al.*, 2001). The associated shift of temperatures at that time represents one of the most relevant reorganisations of global climate in earth's history. At that time, the opening of the Southern Ocean gateways, the Drake Passage and the Tasman Gateway led to the formation of the Antarctic Circumpolar Current and hence to the isolation of the Antarctic continent. Declining atmospheric carbon dioxide concentration and the orbital configuration contributed to the onset of a persistent Antarctic glaciation.

The accumulation over the ice sheet is 5.1±0.2 mm/yr of SLE (Church *et al.*, 2001). Antarctic temperatures are so low that there is virtually no surface runoff (10±10 x 10^{12} kg/yr, Church *et al.* (2001)). The ablation takes place by ice discharge into floating ice shelves, which experience melting and freezing at their base and eventually break up to form icebergs (iceberg production rates are 2072±304 x 10^{12} kg/y, (Church *et al.*, 2001)).

1.5 Recent estimates of changes in the mass balance of ice sheets

The mass balance of ice sheets can be estimated by taking the difference between ice input and ice output fluxes or by monitoring changes in ice sheet elevation as a proxy for volume changes (measurements must be corrected for isostatic adjustments of bedrock elevation and for changing density of the snow and ice column). Precipitation rates can be estimated from field measurements. Output fluxes can be calculated from ice-velocity measurements using interferometric synthetic-aperture radar (InSAR).

Monitoring changing ice volume by altimetry from aircraft or satellite is increasingly important. Although some altimetry data were collected in the 1970s, comprehensive mass-balance observations did not begin until the early 1990s. Recent observations have documented changes in Greenland and Antarctica including notable increases in ice discharge, especially since the mid- to late 1990s (Rignot and Thomas (2002), Krabill *et al.* (2004)). In Antarctica, altimetry-derived estimates show thickening in EAIS but thinning along the Amundsen Coast of

WAIS (Curt *et al.* (2005), Wingham *et al.* (1998), Shepherd *et al.* (2002)).

Velicogna and Wahr (2006) used measurements from time-variable gravity to determine mass variations of the Antarctic ice sheet during 2002-2005, finding a mass decrease equivalent to 0.4± 0.2 mm of global sea level rise per year, with most of the mass loss coming from the WAIS.

Measurements of ice velocity made with satellite radar interferometric methods have recorded a doubling of the velocities of several Greenland outlet glaciers over the past five years (Rignot and Kanagaratnam (2006), Joughin *et al.* (2004)). About half of the discharge from the ice sheet is through 12 fast-flowing outlet glaciers, most of them with 10 to 20 km width at their seaward margin. The breaking up of the floating tongues or ice shelves of several of these glaciers in the past few years has been also observed (Joughin *et al.*, 2004). Increased velocities maybe linked to the loss of the mechanical buttressing effect of the ice tongues (Rignot and Kanagaratnam (2006), Joughin *et al.* (2004), Alley *et al.* (2005)). Other mechanism that has been proposed to explain these increased velocities is basal lubrication via meltwater reaching the glacier bed trough crevasses (Zwally *et al.*, 2002). In the Antarctic Peninsula, the disintegration of large ice shelves was followed by velocity increases of between two and eight times (Scambos *et al.*, 2004). Large glaciers feeding Amundsen Coast ice shelves have thinned and accelerated by up to 26% over the last three decades, with perturbations extending more than 200 km inland (Shepherd *et al.* (2002), Thomas *et al.* (2004), Joughin *et al.* (2003)). The breakup of ice shelves and ice tongues could have been triggered by increased surface meltwater production penetrating into surface crevasses and/or ocean basal melting (Shepherd *et al.* (2003), Payne *et al.* (2004)).

1.6 State of the art in modelling the future mass balance of ice sheets

1.6.1 Modelling of surface mass balance changes

For the Third Assessment Report (TAR) "Climate Change 2001" from the IPCC, the sensitivity of the ice sheets' surface mass balance to a local increase of temperatures was studied with multiple regression analyses, simple meteorological models and General Circulation Models (GCMs). In most of the studies with GCMs, a high-resolution Atmospheric General Circulation Model (AGCM) was driven by the output from a low-resolution transient AOGCM experiment for a limited duration of time (f.i. 5 years in the study from Ohmura *et al.* (1996)). The typical resolution employed was T106, since a resolution of at least 100 km is

estimated to be needed to resolve the orographic forcing of precipitation along the margins of the ice sheets. Melting rates estimated either via calculations based on the surface energy balance or via calculations based on the observed relationship between melting and the summer temperatures. For Greenland, the estimates of the TAR of the sensitivity to a 1°C local warming range between +0.1 and +0.4 mm/yr of sea level equivalent (Van de Wal and Elkholm (1996), Ohmura *et al.* (1996), Smith (1999), Janssens and Huybrechts (2000), Wild and Ohmura (2000)). For Antarctica, the estimates are close to -0.4 mm/yr of global sea level equivalent (Huybrechts and Oerlemans (1990), Giovinetto and Zwally (1995), Ohmura *et al.* (1996), Smith *et al.* (1998), Wild and Ohmura (2000)).

In more recent studies the surface mass balance has been calculated at higher resolution (tens of kilometres or less). Climate change was simulated either with high-resolution AGCMs or perturbing an observational climatology with the output of a model of lower resolution. Ablation was calculated either by methods based on temperature-index methods or by energy balance modelling. An example of such modelling approaches is the work of Wild *et al.* (2003). They used a temperature-index method at a 2 km resolution and the output from ECHAM4 at resolution T106. They found lower melting rates than found in a previous study conducted with ECHAM4 (Wild and Ohmura, 2000) where surface melting was calculated with an energy balance scheme at the resolution of the atmospheric model (T21). Wild *et al.* (2003) attributed this difference to the reduced ablation area on the higher-resolution grid.

Bugnion and Stone (2002) used a snowpack model with climate forcing from ECHAM4 and MIT 2D in order to estimate the current mass balance of the Greenland ice sheet and its changes over the 21^{st} century. Snowpack models permit the representation of the refreezing of surface meltwater within the snowpack and albedo variations due to snow aging, its conversion to ice, and presence of surface meltwater.

1.6.2 Modelling of total mass balance changes

As explained before, the total mass balance of the ice sheets does not only depend on the surface mass balance, but also on changes in the dynamics of the ice sheet. In order to include dynamical changes in the assessment of total mass balance changes, a thermomechanical ice sheet model is required. The word thermomechanical refers to the coupling of the dynamics and ice temperatures via viscosity changes, sliding, and other processes.

For the TAR, the ice sheet model of Huybrechts and de Wolde (1999) was

integrated using temperature and precipitation fields obtained by perturbing a present day climatology according to the geographically and seasonally dependent patterns predicted by the T106 ECHAM4 model (Wild and Ohmura, 2000). The time-dependent patterns were scaled with the averaged changes over the ice sheet from several AOGCMs run under the IS92a scenario. From 1990 to 2090, Greenland contributes 0.01 to 0.03 m and Antarctica -0.07 to -0.01 m to global sea level according to the results of this study.

Several modelling studies have been performed for time periods of several centuries to millennia: Van de Wal and Oerlemans (1997), Warner and Budd (1998), Huybrechts and de Wolde (1999), Greve (2000). These studies have been performed with ice sheet models passively coupled to Earth System Models of Intermediate Complexity (EMICs) or forced by simple parameterisations of changes in the temperature and snowfall forcing. More sophisticated simulations of the bi-directional interaction between climate and ice-sheets under anthropogenic climate change have been performed more recently via the coupling of the ice sheets to AOGCMs. These studies will be introduced in the next section.

1.7 Ice sheets as components of Earth System Models

For paleo-studies several Earth System Models of Intermediate Complexity have been used with a bi-directionally coupled ice sheet model, for instance, in order to investigate the role of the ice-sheet feedbacks during the last glacial inception, approximately 117 ky BP (Wang and Mysak, 2002; Kageyama *et al.*, 2004; Calov *et al.*, 2005).

Very few anthropogenic climate change modelling studies account for the modifications of climate due to changes in the mass balance of the ice sheets. Huybrechts *et al.* (2002) and Fichefet *et al.* (2003) interactively coupled a Greenland ice sheet model with an AOGCM in order to investigate the effect of varying freshwater fluxes on the oceanic circulation of the time between 1970 and 2100. The coupling was only performed between the ice sheet model and the ocean model in these studies. Changes in the geometry (shape and extent) of the Greenland ice sheet were not given to the atmospheric component in these models.

The first study with a fully bidirectional coupling of a dynamical ice sheet model to an AOGCM is that of Ridley *et al.* (2005), who used a dynamical three-dimensional ice sheet model coupled to the AOGCM HadCM3 in order to study the response and feedbacks of the GrIS to anthropogenic climate change. They

showed the almost complete disappearance of the Greenland ice sheet after 3000 years in a 4xCO_2 simulation. The North Atlantic Meridional Circulation was not significantly modified by the release of freshwater from the GrIS. Atmospheric regional changes over the ice sheet acted as a negative feedback for the disintegration of the GrIS.

1.8 Objectives and outline of this study

The objective of this study is to explore the long-term (multi-century) interactions between the ice-sheets in a climate forced with higher concentrations of greenhouse gases. The tool used for this study is a dynamical ice-sheet model bi-directionally coupled to two different complex Earth System Models. The core of both Earth System Models is a coupled Atmosphere-Ocean General Circulation Model (ECHAM3 T21/LSG and ECHAM5 T31/MPI-OM). Other relevant components of the physical and biogeochemical climate system (land vegetation, ocean biogeochemistry) are modelled within these Earth System Models. The use of a dynamical ice sheet model permits the inclusion of changes in the ice flux in calculations of the total mass balance of the ice sheets. The bi-directional coupling of the ice sheet model to the climate permits the study of the modifications of climate caused by the changes in the mass balance of the ice sheets (via albedo, topographic and freshwater discharge changes), which potentially could also be important for the evolution of the ice sheets themselves. The use of General Circulation Models in this modelling approach permits a proper investigation of these processes by which ice sheets can modify climate.

For the calculation of the mass balance two different coupling schemes have been used with the Earth System Models: in the case of the first Earth System Model, the scheme for the calculation of melting (*degree-day method*) is based on parameterisations which relate atmospheric temperatures to melting rates; while in the case of the second Earth System Model a more sophisticated scheme based on the balance of heat fluxes at the ice sheet surface (*energy balance method*) is used.

Two main type of questions will be addressed with the tool used in this study: the first group refers to the different mechanism playing a role in the evolution of future ice sheets (changes in surface melting, snowfall rates, and ice dynamics); the second, to the role played by ice sheets in future climate.

The structure of this thesis is as follows. In Chapter 2 the Earth System Model ECHAM3/LSG2/LPJ/HAMMOC3/SICOPOLIS (ESM1) will be introduced. In Chapter 3 the simulated ice sheets of the control climate will compared to ob-

servations. In Chapter 4 the multi-century evolution of global ice sheets under greenhouse stabilisation scenarios will be investigated with the ESM1. In Chapter 5 the long-term response of global ice sheets to the SRES emission scenarios B1, A1B and A2 will be investigated with the same model. The Greenland ice sheet disappears within 5000 years under the forcing from the high emission scenario A2. In Chapter 6 the process of disintegration of the Greenland ice sheet under this scenario will be shown, and its impact on the climate and on the evolution of the ice sheet itself (via positive or negative feedbacks between the ice sheet and the climate). The ESM2 ECHAM5/MPI-OM/LPJ/SICOPOLIS will be introduced in Chapter 7. The results with this model for greenhouse stabilisation scenarios 2xCO2 and 4xCO2 will be shown in Chapter 8. Chapter 9 consists of general conclusions and an outlook.

Chapter 2

Model description of ESM1

In this chapter the Earth System Model ECHAM3/LSG2/HAMOCC3/LPJ/-SICOPOLIS (also referred to as ESM1 or MPI/UW in this thesis and other publications) will be described, with special emphasis on the ice sheet component and its coupling to other components. The structure of the chapter is as follows: first the ice sheet model (ISM) will be introduced, then the rest of components of the model will be described, and then the coupling of the ice sheet model to the full Earth System Model will be explained.

2.1 The ice sheet model SICOPOLIS

SICOPOLIS (SImulation COde for POLythermal Ice Sheets), by Ralf Greve (Greve, 1995), is a three dimensional thermomechanic (i.e., it includes the dependence of the flow of ice on its temperature) ice-sheet model. It integrates the time-dependent equations governing ice-sheet extent and thickness, ice velocity, temperature, water content and age for any specific grounded ice as a response to external forcing. This is given by (i) surface temperature, (ii) surface mass balance (snowfall and surface melting), (iii) sea level, and (iv) geothermal heat flux.

The model equations are subjected to the *shallow ice approximation* (SIA); that is, they are scaled with respect to the aspect ratio ε (ratio of typical thickness to typical length),[1] and only first order terms are kept. The SIA yields hydrostatic pressure conditions and ice flow governed by the gradients of pressure and the shear stresses in horizontal planes, t_{xz}, t_{yz}. The influence of the normal-stress deviators, t^D_{xx} , t^D_{yy} , t^D_{zz} , and the shear stress in vertical planes, t_{xy},

[1] This ratio is approximately 10^{-3} in ice sheets

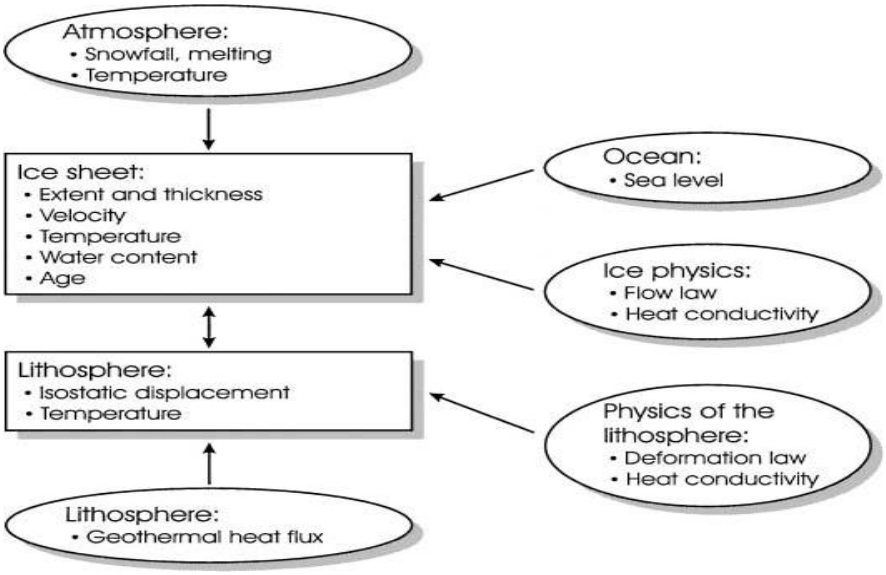

Figure 2.1: Scheme of the model SICOPOLIS.

is negligible. *Accelerations are neglected* in the momentum balance, so that the velocity field behaves quasi-stationary ("Stokes flow"). The horizontal velocity is a local function of the ice thickness, the surface slope and the temperature and water content in the ice column. It always points in the direction of the steepest surface descent.

The model does not include the special dynamics of ice shelves. The movement of ice shelves in nature is driven by the pressure gradient and by the gradients of t^D_{xx} , t^D_{yy} , t^D_{zz} and t_{xy} (precisely the stresses that are neglected in the SIA for ice sheets). The compressive stresses t_{ii} are exerted by the lateral margins that confines the ice shelves and by pinning points. The horizontal shear (t_{xz}, t_{yz}) is, on the contrary, very small.

Although not including the dynamics of ice shelves, the model allows the expansion of the ice sheet into the adjacent shallow ocean, in order to allow, for instance, the glaciation of the Hudson Bay during the last glaciation.

2.1.1 Ice-thickness equation

The basic equation of the model is the ice-thickness H equation:

$$\frac{\partial H}{\partial t} = -\frac{\partial q_x}{\partial x} - \frac{\partial q_y}{\partial y} + a_s - \frac{P_b}{\rho} \tag{2.1}$$

where a_s is the accumulation-ablation term, $\mathbf{q}$ is the vertically integrated velocity, P_b is the basal melting rate, x and y are the horizontal coordinates, and t is time.

2.1.2 Formulation of the ice flow

Ice is treated as a viscous power-law material. The strain rate components (which are also the velocity gradients) are related to the stress components through the *constitutive relation*

$$\boldsymbol{D} = EA(T')f(\sigma)\boldsymbol{T^R} \tag{2.2}$$

where $\boldsymbol{D}$ is the strain-rate tensor $[ms^{-2}]$,$\boldsymbol{T^R}$ is the deviatoric (or frictional) stress-tensor (units: N/m^2), σ is the effective shear stress, *f(σ)* is the *creep response function*, E is the enhancement factor, and *A(T')* is the rate factor. The rate factor *A(T')* is defined as function of the homologous temperature *T'* (i.e., the difference of the temperature T to the melting temperature T_m). The rate factor *A(T')* accounts for the dependence of the deformation of the ice with temperature. The enhancement factor $E \geq 1$ accounts for the increased softness of ice containing impurities (such as dust) and/or anisotropy. Glacial ice has been found to be softer than interglacial ice (Paterson, 1991).

The effective shear stress σ is defined as a function of the components of the deviatoric stress tensor : $\sigma = \sqrt{\frac{1}{2} tr(\boldsymbol{T^R})^2}$. It is an invariant, hence independent of the coordinate system.

The creep response function is defined as

$$f(\sigma) = \sigma^{n-1} \tag{2.3}$$

with n=3, (n=1 is valid for a Newtonian viscous material, for which deformation rates are linearly dependent on the stresses). The case n=3 is called *Glen's law*.

The deviatoric stress tensor $\boldsymbol{T^R}$ differs from the full stress tensor in that the hydrostatic component is subtracted: $\boldsymbol{T^R} = -p\mathbf{1} + \boldsymbol{T^R}$.

With the SIA, the stresses[2] are set to

$$\sigma_{zz} = -\rho g(h - z) \text{ normal stress} \tag{2.4}$$

$$\left.\begin{aligned} \sigma_{xz} &= -\rho g \tfrac{\partial h}{\partial x}(h - z) \\ \sigma_{yz} &= -\rho g \tfrac{\partial h}{\partial y}(h - z) \end{aligned}\right\} \text{ shear stresses} \tag{2.5}$$

[2]Stresses with equal indexes *ii* are called *normal stresses*. They represent some form of compression or extension. *Shear stresses* are denoted by indexes ij, (with $i \neq j$) and they are essentially a traction that acts to deform the ice block in the horizontal plane.

where ρ is ice density, g is the gravitational constant, h is the vertical coordinate of the ice surface, and z is the vertical coordinate at the point where the stresses are calculated.

These shear stresses are zero at the surface and have a maximum at the base. The normal stress is also zero at the surface (the atmospheric pressure is considered negligible compared to the other stresses). All the other components of the stress tensor are ignored in the SIA.

The resulting effective shear stress σ is:

$$\sigma = \rho g(h-z)\sqrt{(\frac{\partial h}{\partial x})^2 + (\frac{\partial h}{\partial y})^2} \tag{2.6}$$

Defining the surface slope α_s as

$$\alpha_s = \sqrt{(\frac{\partial s}{\partial x})^2 + (\frac{\partial s}{\partial y})^2} \tag{2.7}$$

where s is the surface plane, the horizontal velocities v_x, v_y are

$$\begin{array}{l} v_x(z) = v_{x,b} - 2(\rho g)^3 \alpha_s^2 \frac{\partial s}{\partial x} \int_{base}^{z} A(T')(s-z)^3 dz \\ v_y(z) = v_{y,b} - 2(\rho g)^3 \alpha_s^2 \frac{\partial s}{\partial y} \int_{base}^{z} A(T')(s-z)^3 dz \end{array} \tag{2.8}$$

where $v_{x,b}$, $v_{y,b}$ are the basal velocities.

Integration of the velocity equations for an hypothetical isothermal column with no sliding at the bed ($v_{x,b}$, $v_{y,b} = 0$) would give for the surface velocity $v_h(z=s)$:

$$v_h(z=s) = \frac{A(T)}{2}(\rho g \alpha)^3 H^4 \tag{2.9}$$

The vertical velocity is obtained from the *incompressibility* assumption for ice (ice is considered incompressible, like water but unlike snow):[3]

$$\frac{\partial v_x}{\partial x} + \frac{\partial v_y}{\partial y} + \frac{\partial v_z}{\partial z} = 0 \tag{2.10}$$

2.1.3 Heat transfer

The temperature equation in the ice column is given in the SIA by:

[3]This assumption does not hold in the snow and firn at the top of an ice-sheet. The approach in SICOPOLIS and many other ice sheet models is to assume that all the ice column is incompressible glacial ice.

$$\frac{\partial T}{\partial t} = -v_x \frac{\partial T}{\partial x} - v_y \frac{\partial T}{\partial y} - v_z \frac{\partial T}{\partial z} + \frac{1}{\rho c} \frac{\partial}{\partial z} \left(\kappa \frac{\partial T}{\partial z} \right) + \frac{2}{\rho c} E A(T') f(\sigma) \sigma^2 \qquad (2.11)$$

where c is specific heat of ice and κ is the conductivity of ice.

Equation 2.11 relates temperature change with advection, vertical heat conduction, and heat production generated by internal friction. The SIA eliminates lateral heat conduction.

The most relevant processes of thermal advection in ice sheets are the transport downwards of cold ice beneath ice divides and the transport of cold ice down the glacier along flowlines.

Thermal diffusion does not lead to a uniform, isothermal temperature distribution in the glacier in general, because the top and bottom surfaces are pinned to cold and warm extremes. This causes a continuous transfer of energy upwards into the ice: the geothermal heat energy penetrates slowly upwards in the ice, "resisted" by the very cold atmosphere temperatures. The thermal conductivity of ice is rather intermediate, (better insulators are air or snow; ice is similar in that sense to most geological materials), so the time scale at which changes in air temperature penetrate into the ice sheet is pretty long. For instance, some parts of the Greenland ice sheet still have temperatures matching the cold environment of the last glacial period.

The production of heat by internal friction is concentrated in the lower section of the ice sheet. This gives a *positive feedback* for the movement of ice, because warm ice deforms more than cold ice: hence, more deformation yields more heat, higher temperatures yield more deformation. In this way, steep and deep areas of the ice sheet produce a lot of deformational heat and are often at the melting point well above the glacier bed. Since the model considers sliding only in melting regions, the basal sliding also plays a very important role in this feedback mechanism. These processes are considered by some authors (MacAyeal (1993), Calov *et al.* (2002)) to be the key point, for instance, for large scale surges of the former Laurentide Ice Sheet during the last glacial.

Pressure Melting Point Depression

Ice melts at different temperatures when it is under pressure. The higher the pressure is, the lower is the melting point. All other materials behave oppositely, increasing the melting point with pressure. Because water is denser than ice, it tries to reach under high pressure the most compacted configuration. The depression of the melting point T_m with pressure is modelled as follows in SICOPOLIS:

$$T_m = T_0 - \beta^* p = T_0 - \beta \frac{p}{\rho g}, \tag{2.12}$$

where $T_o = 0°$ C, $\beta^*$is the Clausius-Clapeyron constant, and the Clausius-Clapeyron gradient $\beta = \rho g \beta^*$corresponds to the temperature gradient in temperate ice.

Basal melting rate

Whenever the base is at the melting point, basal melting rates P_b^w are calculated according to:

$$P_b^w = \frac{1}{L}\left\{\kappa \frac{\partial T}{\partial z} - \kappa_r \frac{\partial T^+}{\partial z} + ((v_{sl})_x \sigma_{xz} + (v_{sl})_x \sigma_{yz})\right\} \tag{2.13}$$

where κ is the heat conductivity of ice and v_{sl} the basal sliding velocity (difference between ice velocity and lithosphere velocity). The basal melting rate is given by the difference between the heat coming from the bedrock $\kappa_r \frac{\partial T^+}{\partial z}$ and the heat transported upwards into the ice $\kappa \frac{\partial T}{\partial z}$, plus the frictional heat produced by the basal stresses.

Boundary conditions: temperatures at the uppermost layer of the ice-sheet.

For the surface temperature T_s (temperature of the uppermost layer of the ice column) the firn temperature at 15 m depth is taken. Experimentally this 15 m-depth temperature is found to be equal to the mean annual air temperature plus a correction due to refreezing of meltwater. The seasonal temperature penetrates through diffusion only into the upper 15 m of ice. It gives an annual temperature wave in the near-surface ice (Paterson, 1994).

This temperature T_s is corrected according to the equation 2.31 described further down. Meltwater refreezing can add latent heat and give mean annual temperatures a few degrees higher than the mean annual air temperature.

2.1.4 Lithosphere

The temperature equation in the rock is

$$\rho_r c_r \frac{dT}{dt} = \kappa_r \nabla^2 T, \tag{2.14}$$

where κ_r is the conductivity of the lithosphere, ρ_r is the density, and c_r is the heat capacity. For the boundary condition at the lithosphere base, the flux of heat into the lithosphere is given by

$$\kappa_r \nabla T = Q_{geo} \tag{2.15}$$

where Q_{geo} is the geothermal heat flux.

The response of the lithosphere on the varying ice load is treated by a local-lithosphere-relaxing-asthenosphere model in which the asthenospheric time lag τ_V is the only parameter. A local force balance between buoyancy and ice load for a vertical column of transect area dA with ice thickness $H = h$ -b is considered to calculate the sinking depth $\Delta b(x, y, t)$ of the lithosphere into the asthenosphere below it:

$$\rho_a g \Delta b dA = \rho g H dA, \tag{2.16}$$

where ρ_a is the density of the asthenosphere. Equation 2.16 assumes that vertically moving lithosphere columns do not interact with each other, and have no horizontal velocity. The steady-state position of the lithosphere, b_{ss}, is given by

$$b_{ss} = b_0 - \Delta b = b_0 - \frac{\rho}{\rho_a} H \tag{2.17}$$

where $b_0(x, y, t)$ is the position of the relaxed ice-free steady-state lithosphere.

Due to the asthenosphere's viscosity, this equilibrium is not reached instantaneously, but with a certain time lag τ_V. The evolution equation for the position of the lithosphere surface $z = b(x, y, t)$ is

$$\frac{db}{dt} \equiv \frac{\partial b}{\partial t} = -\frac{1}{\tau_V} \left[b - (b_0 - \frac{\rho}{\rho_a} H) \right] \tag{2.18}$$

For a fixed thickness H this corresponds to an exponential approach of b towards the equilibrium state b_{ss}.

2.1.5 Numerics of the model

The numerical solution is based on a finite-difference integration technique, for which the σ-transformation, mapping of vertical columns onto the [0,1] interval, is carried out. The model domains of ice and lithosphere are treated separately in order to simplify the implementation of the boundary and transition conditions at the interfaces. An Arakawa-C-grid (Arakawa and Lamb, 1977) is applied in the model, where the velocity components are defined in between grid points, and

other variables (water content, temperature, positions of free surface and bedrock, ...) are defined on grid points. This grid is used in most of the current ice-sheet models based on finite differences.

For the solution of the ice thickness equation, four numerical methods can be used in SICOPOLIS. These are (i) explicit scheme, (ii) alternating-direction implicit scheme (ADI), (iii) over-implicit ADI scheme and (iv) over-implicit scheme with iterative SOR solution of the system of linear equations. For a detailed discussion of the differences on the application of this schemes, see Greve and Calov (2002).

2.1.6 Specification of physical quantities

Rate factor *A(T')*

It follows an Arrhenius type law for T' < -10° C, supplemented by four values in the regime T' < -10°C (Paterson, 1994):

$$\begin{aligned} A(T' = 0°\mathrm{C}) &= 3.2 \cdot 10^{-24}\mathrm{s}^{-1}\mathrm{Pa}^{-3} \\ A(T' = -2°\mathrm{C}) &= 2.4 \cdot 10^{-24}\mathrm{s}^{-1}\mathrm{Pa}^{-3} \\ A(T' = -5°\mathrm{C}) &= 1.6 \cdot 10^{-24}\mathrm{s}^{-1}\mathrm{Pa}^{-3} \\ A(T' = -10°\mathrm{C}) &= 0.49 \cdot 10^{-24}\mathrm{s}^{-1}\mathrm{Pa}^{-3} \\ A(T' < -10°\mathrm{C}) &= A_0 e^{-\frac{Q}{R(T_0+T')}} \end{aligned} \tag{2.19}$$

with $T_0 = 273.15$ K , the activation energy $Q = 60$ kJ mol^{-1} , the universal gas constant R and the coefficient $A_0 = 3.985{\cdot}10^{-13}$s^{-1} Pa^{-3}. All other values in the interval 0 < T' < -10° C are obtained by linear interpolation.

Sliding law

For the calculation of the basal velocity $\boldsymbol{v}_\mathrm{b}$, no-slip is prescribed (adhesion condition) if the basal ice is at $T < T_m$. If basal ice is at melt temperature T_m, a Weertman-type sliding law is used:

$$\begin{aligned} \boldsymbol{v_b} &= \boldsymbol{0} && \text{if } T < T_m \\ \boldsymbol{v_b} &= -\tfrac{C_{sl}}{\rho g}\tfrac{||\boldsymbol{t}||^p}{(\rho g h)^q}\tfrac{\boldsymbol{t}_{||}}{||\boldsymbol{t}||}, \quad \text{with } p = 3\ ,\ q = 2 && \text{if } T = T_m \end{aligned} \tag{2.20}$$

where C_{sl}= 10^5 yr^{-1} (Greve, 1997) is the sliding coefficient; $t_{||}$ is the basal shear traction in the bed plane, and $\rho g H$ is the overburden pressure. Following Calov (1994) and Calov and Hutter (1996), this sliding-law is applied as

$$\boldsymbol{v_b} = -C_{sl} H ||\mathrm{grad}\ h||^2 \mathrm{grad}\ h \tag{2.21}$$

Enhancement factor E

The enhancement factor E is used to take into account that glacial ice is less viscous than interglacial ice, probably due to differences in dust content and/or induced anisotropies (Fisher (1987), Paterson (1991), Paterson (1994), Svendsen and Hutter (1996)). The values used for the set-up of the simulations performed with ESM1 and ESM2 are $E = 3$ for the Northern Hemisphere and $E = 5$ for the Southern Hemisphere Greve (1997).

Relaxed bedrock b_0

The relaxed bedrock is calculated from equation 2.17,

$$b_0 = b_{ss} + \Delta b = b_{ss} + \frac{\rho}{\rho_a} H \tag{2.22}$$

The present bedrock is assumed to be in equilibrium for this calculation. That is, for the steady-state position of the bedrock the present values of the bedrock are used:

$$b_{ss} \cong b_{Present} \tag{2.23}$$

This assumption is not true, since the bedrock is still in a process of uplift since the onset of the deglaciation. Some other areas are suffering the inverse process. Since no accurate measurements on global coverage of the uplift rates are available, this error cannot be easily reduced. Some studies of the present day imbalance of ice thickness and bed elevation have been conducted with the ice sheet model of Huybrechts for Antarctica (Huybrechts, 1992) and with a coupled ice-sheet/bedrock model for Greenland (Le Meur and Huybrechts, 1998).

Geothermal heat flux

For the northern hemisphere the global mean value Q_{geo}^{mean}= 55 mW/m^2 (Sclatter *et al.*, 1980) is used. For the southern hemisphere, a two-dimensional map $Q_{geo}(x,y)$ is applied in order to account for the unequal distribution of the geothermal heat flux in the Antarctic continent due to different age of the bedrock on the East and West sections (Sclatter *et al.*, 1980). Two different values Q_{geo}^{E} and Q_{geo}^{W} are used in the West and East area, with a transition area of 1000 km. Outside of Antarctica, the value of the geothermal heat flux is fixed to the global mean value Q_{geo}^{mean}= 55 mW/m^2:

$$Q_{geo} = \begin{cases} Q_{geo}^{mean} & \text{if lat} > -60^\circ \\ \frac{1}{2}(Q_{geo}^{E} + Q_{geo}^{W}) + \frac{1}{2}(Q_{geo}^{E} - Q_{geo}^{W}) \cdot \left(-\tanh\left(2 \cdot \frac{\alpha}{\alpha_w}\right)\right) & \text{if lat} \leq -60^\circ \end{cases} \tag{2.24}$$

where α is the distance to the meridian 30° W. This meridian was chosen because it is parallel to the Transarctic Mountains, which are approximately the dividing line for the old East Antarctic bedrock and the newer West Antarctic bedrock. α_w is the half-width of the transition area.

The values used for Q_{geo}^{E} and Q_{geo}^{W} are:

$$Q_{geo}^{E} = 45 \text{ mW/m}^2$$
$$Q_{geo}^{W} = 70 \text{ mW/m}^2$$

following Sclatter *et al.* (1980). In this study the values given for the geothermal heat fluxes in Antarctica are speculative, since no good measurements are available. Antarctica is divided into four areas according to the age of the bedrock: (i) 0-250 Ma (Mesozoic and Cenozoic) , (ii) 250-800 Ma, (iii) 1700 Ma, and (iv) > 1700 Ma and for every area the mean heat flux from bedrock of similar age from the other continents on Earth is used.

About other physical quantities

The geothermal heat flux is imposed at a distance H_r under the base of the ice in order to account for the thermal inertia effects of the lithosphere. Other physical quantities are specified in the table 2.1.

2.1.7 Set-up of the model

Grid

The Northern and Southern Hemispheres are projected separately to a polar stereographic map with standard parallels at 71°N and 71°S. The reference longitude is 44°W for the first case (in order to place Greenland centred in the map) and 0° in the second case. A horizontal resolution of 80 km is used, which corresponds to 157 x 157 points in each grid. Each grid domain covers an area of 12480 x 12480 km^2. The vertical resolution is 21 grid points in the ice region and 11 grid points in the lithosphere.

Table 2.1: Standard values of physical quantities used for the simulations in this study. References: ρ, β: Calov (1994); τ_v, ρ_a: Abe-Ouchi (1993); κ, c, $\rho_r c_r$, and κ_r : Ritz (1987); L: Blatter (1991).

Symbol	Quantity	Value
ρ	Density of ice	910 kg/m^3
κ	Heat conductivity of ice	$9.828\mathrm{e}^{-0.0057T[K]}$ Wm^{-1} K^{-1}
c	Specific heat of ice	(146.3+7.253T[K]) Jkg
L	Latent heat of ice	335 kJ kg^{-1}
β	Clausius-Clapeyron gradient	8.7$\cdot$ 10^{-4} Km^{-1}
υ	Water diffusivity	0
$\rho_r c_r$	Densitiy x specific heat of the lithosphere	2000 kJ m
κ_r	Heat conductivity of the litosphere	3 W m^{-1} K^{-1}
τ_V	Time lag for the bed adjustment	3000 a
ρ_a	Density of the asthenosphere	3300 kg m^{-3}
H_r	Thickness of the lithosphere	5 km

Numerics

The numerical procedure used in the solution of the ice-thickness equation is the implicit method (see 2.1.5).

Topography

The present topography of the bedrock is constructed based on ETOPO5 (ETOPO5, 1988) land and sea-floor elevations, which are gridded with a resolution of 5' in latitude and longitude. For the area of the present Greenland ice sheet this data set provides the ice surface instead of the bedrock. There the bedrock data of Letreguilly *et al.* (1991a) with 20 km resolution are applied. For Antarctica, the ice-thickness and bedrock data set of BEDMAP (Lythe *et al.*, 2001) is used. The total volume of grounded ice from the digital map is 25.68 x 10^6 km^3 for Antarctica (for comparison, the figure from Church *et al.* (2001) is 25.71 x 10^6 km^3).

2.1.8 Parameterisation of ice shelves.

Since ice shelves are not specifically modelled, several parameterisations have been included in order to keep the Antarctic grounding line at its current position. Otherwise the ice sheet would extend until the limit of the continental shelf. These parameterisations consist of a modification of the dynamics of marginal ice, and the introduction of calving and ocean melting rates for marginal ice. Besides, a sub-grid calculation of the position of the grounding line according to the flotation criterion is performed.

Changes in the dynamics

In order to increase the velocities in the floating ice domain, the sliding coefficient for equation 2.20 is set at $C_{sl} = 10^7$ yr^{-1}, which is 100 times the value for temperate grounded ice.

Ocean melting

An ocean heat flux is applied to the floating ice. Two different processes are considered:

1. Frontal melting Q^{oc}_{fm}: applied to the surface of the walls of the floating ice in contact with the water. A value of 62 W/m^2 is used.

2. Bottom melting heat flux Q_{bm}^{oc}: applied over the bottom surface of the floating ice. A parameterisation according to the depth of the water column is implemented : the heat flux is proportional to the depth of the water column under the ice h_w until a maximum value Q_{bm}^{c}, which is reached for a water column h_w^*.

$$Q_{bm}^{oc} = Q_{bm,max}^{oc} \cdot \left[1 - \max\left(h_w^* - \frac{h_w}{h_w^*}\right)\right] \tag{2.25}$$

The values used are : $Q_{bm,max}^{oc} = 5$ Wm^{-2}, h_w^*= 100 m.

For the values of Q_{fm}^{oc} and Q_{bm}^{oc} measurements in the present Antarctic ice shelves have been used as reference (Jacobs *et al.*, 1992). This study shows that the highest melt rates occur near ice fronts and deep within sub-ice cavities.

Calving

Calving is a process which involves fracture generation and propagation processes and is known to be dependent on ice thickness and temperature, water depth, tidal forcing, coastal/embayment geometry, the flux of ice across the grounding line, and presence of water-filled crevasses weakening overall ice shelf competence by forcing of vertical crack propagation. The governing physics for calving and ice shelf breakup are still not fully understood and may not be deterministic. It is known that the calving increases with higher temperatures in the ice.

Here a very simple parameterisation for the calving is introduced. Wherever the floating ice reaches a thickness h_{cl}^* below 200 m, it is calved. With an exception: in order to allow the movement of the grounding line, this parameterisation is not applied near the grounding line (the points of floating ice in contact with grounded ice are not allowed to be calved).

2.2 The Earth System Model ECHAM3/-LSG2/HAMOCC3/LPJ/SICOPOLIS

The Earth System Model ECHAM3/LSG2/HAMOCC3/LPJ/SICOPOLIS (also referred to as ESM1 in this thesis and as MPI/UW in publications with the results of this model) has as core a coupled atmosphere-ocean General Circulation Model (AOGCM). It includes the main physical and biogeochemical components of the Earth System via fully-coupled models of the ocean biogeochemistry (modelled with HAMOCC, Maier-Reimer (1993)), land vegetation (modelled with LPJ, Sitch

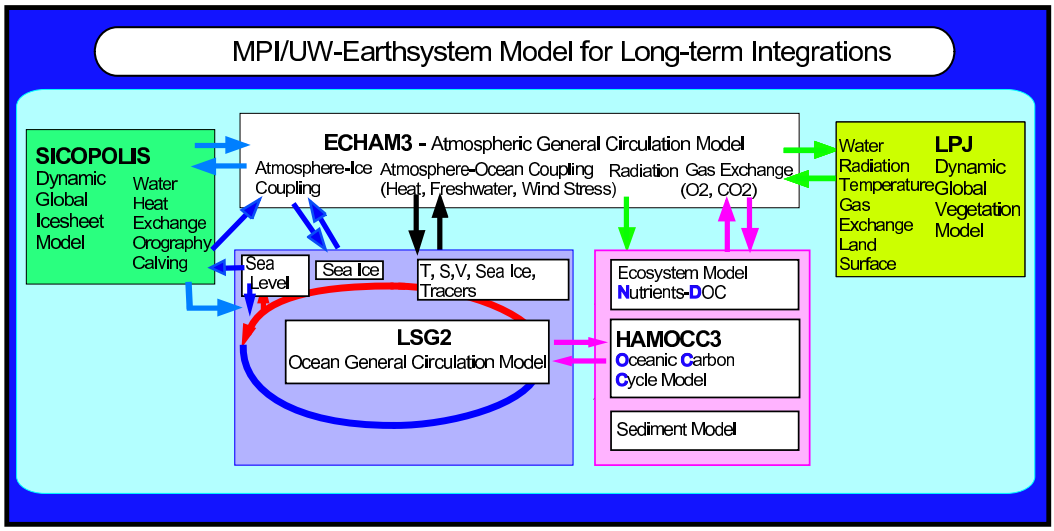

Figure 2.2: The Earth System Model ECHAM3/LSG2/HAMOCC3/LPJ/-SICOPOLIS

et al. (2003)), and ice sheets (modelled with a three dimensional model SICOPOLIS). The ocean biogeochemistry and land vegetation models allow for the modelling of the carbon cycle. The model allows multi-century and multi-millennia experiments due to its coarse resolution (T21 for the atmosphere model) and to the use of a periodically synchronous technique.

In the following each model component of the Earth System Model will be described, as well as the exchange fields at the interface with other model components. A scheme of the coupled model is shown in fig. 2.2. In 2.2.2 the periodically synchronous coupling technique will be explained.

2.2.1 Description of components

The atmospheric GCM ECHAM3 (Roeckner *et al.*, 1992) has a resolution of T21 (approximately 5.6°) in the horizontal and a vertical resolution of 19 vertical layers. The prognostic variables are vorticity, divergence, temperature, humidity, surface pressure and cloud water. The time step is 40 minutes.

The ocean model LSG2 is an improved version of the model LSG by Maier-Reimer (1993). It is used with a horizontal resolution of 5.6° in two overlapping grids (64 x 64 points on an Arakawa E grid). The vertical resolution is 22 vertical layers, with thickness varying with depth from 50 m in the uppermost layer to almost 800 m at 5600 m depth. The thickness of the bottom cell is variable, allowing a smooth representation of the topography. The time step of the model is 5 days, but a time-step of 1 day is used for the thermodynamics of the surface

layer. Several sub-grid-scale parameterisations have been included in the version 2 of LSG. A simple dynamic sea ice model is included in LSG2. The advection velocity is the sum of the velocity of the uppermost ocean layer and a wind-derived component (2% of the wind velocity with geostrophic rotation of 19°). A simple water conserving runoff model is also included in the ocean model. A constant bucket depth of 50 cm is used everywhere. The time dependent transport direction is determined using the direction of the strongest topography gradient. The topography can be changed via changes in the ice sheet thickness and isostatic rebound of the lithosphere in response to former ice loads. Since the land-sea mask of the Earth System Model is derived from the ECHAM3 mask, some ocean points on the Arakawa E grid do not have a neighboring "wet" velocity point. These grid points are treated as isolated lakes with a constant depth of 50 m.

The coupling time-step between atmosphere and ocean is one day. The ocean supplies distributions of sea surface temperatures and sea ice to the atmosphere, whereas the atmosphere supplies fluxes of heat, momentum and mass.

The coupled Atmosphere Ocean General Circulation Model runs with two flux corrections: an artificial freshwater export from the North Atlantic/Arctic to the North Pacific of 0.14 Sv and an additional easterly wind stress in the tropical oceans. The additional freshwater export improves substantially the representation of the Atlantic overturning circulation and oceanic heat transport. This correction is needed because, due to its course resolution and the only partially resolved synoptic variability, the atmospheric model produces a too strong convergence of atmospheric moisture transports within the Arctic and the adjacent land areas. The wind-stress correction is designed to improve the representation of the climate in the tropics, especially the position of the intertropical convergence zone.

The dynamic global vegetation model LPJ (Sitch *et al.*, 2003) simulates the spatial distribution of ten plant functional types (PFTs) over the earth, and within each PFT four living biomass and three litter carbon pools are defined. A grid cell can contain more than one PFT, and has two common soil carbon pools. For each PFT, photosynthesis and autotrophic and heterotrophic respiration are the main processes determining the carbon fluxes. Besides that, establishment and mortality are modelled explicitly, as well as the phenology changes over the year. LPJ supplies surface properties to the atmosphere model: background albedo (the albedo of the snow-free surface), vegetation cover and roughness length. The horizontal resolution and the grid of LPJ are the same as for the atmosphere model. The calculated fluxes of carbon in LPJ are used for the calculation of the atmospheric CO_2 concentration. The time step of the coupling of the terrestrial

vegetation model with the other components is 1 year.

The marine carbon cycle is represented with the model HAMOCC3 (Maier-Reimer (1993);Winguth *et al.* (1994)). The trace substance fields are advected within the LSG2 model using the identical advection scheme as for temperature and salinity. Temperature, salinity and sea ice fields for the calculation of the biogeochemistry are taken from the ocean model, incoming shortwave radiation and wind speed from the atmosphere model. The atmospheric CO_2 partial pressure and vertical gradients of carbon are linked with three pumping mechanisms (Volk and Hoffert, 1985): 1) the solubility pump with high solubility at low temperatures, and two biological pumps, which are 2) the dominating "soft tissue pump" caused by the formation of organic material and depletion of nutrients and carbon in the surface water and 3) the counteracting $CaCO_3$ pump. Phosphate (PO_4) is treated as the only nutrient-limiting tracer for photosynthesis in order to avoid the complication arising from denitrification and nitrogen fixation. Export production (EP), the amount of primary production transported from the euphotic zone into deeper layers is parameterised by the availability of light, temperature T (in °C), nutrients (PO_4), and vertical mixing ν:

$$EP = \frac{\frac{r(T,L)\cdot 50\,\mathrm{m}}{\nu}}{\frac{PO_4^2}{PO_4+P_0}} \tag{2.26}$$

with a growth rate *r(T,L)* following a formula of Smith (1936). The temperature dependence follows Eppley (1972). The light function $g(L)$=$0.005 L_{sw}$ takes the shortwave radiation L_{sw} from ECHAM3. P_0 =0.02 mmol $m^{-3}$is the nutrient half saturation constant. Production of opal forming species is simulated as function of EP and silica variability. $CaCO_3$ production is controlled by export production, the competing opal production, and by a temperature dependent formulation $\frac{a}{1+a}$ with

$$a = \exp\left(0.1°\mathrm{C}^{-1} \cdot (T - 10°\mathrm{C})\right) \tag{2.27}$$

Remineralisation of particulate organic carbon (POC) is modelled according to a temperature and oxygen dependent formulation. At the sea floor, the carbon and silica budget is closed with a single layer sediment module for opal, $CaCO_3$ and POC. The time step of the ocean biogeochemistry is 1 month.

2.2.2 The Periodically Synchronous Coupling Technique

Long term integrations with this Earth System Model, despite its course resolution, are still computationally very expensive. More than 90% of the computer

time is consumed by the atmosphere model. On time scales longer than decades, the memory of the physical system resides in the slower components (ocean, ice sheets), whereas the long-term memory of the atmosphere is rather small. Voss and Sausen (1996) made use of this and introduced the periodically-synchronous coupling technique for atmosphere-ocean GCMs. The technique is based on alternating periods of fully synchronous integrations and periods where the ocean is driven in stand-alone mode by fluxes from previous synchronous integration periods. In order to increase as much as possible the length of the ocean-only periods, a two-dimensional energy balance model was introduced to solve problems at the ice-edge with the build-up of unrealistically thick sea ice (Mikolajewicz *et al.*, accepted).

During the ocean-only periods an archive of several different years of atmospheric data is used. A proper length of this archive is needed in order to represent the mean climatological forcing and its variability as well. A too-long archive has the disadvantage of introducing an artificial delay in case of changing climate. An archive length of 8 years was found to be the minimum length in order to obtain an acceptable approximation of the mean climate and variability (Mikolajewicz *et al.*, accepted). Two different approaches are followed for the length of the only-ocean periods: a) a simple one, where periods of 2 synchronous years alternate with periods of 8 ocean-only years, and b) a more interactive one, yielding a higher reduction in computer time, where the length is calculated from the actual state of the ocean. In the second case, the model is switched into the fully synchronous mode only when sea surface temperatures and sea ice properties are very different than the ones used for calculation of the atmospheric forcing. The maximum permitted length of the ocean-only periods in the mode b) is 48 years.

For the land vegetation and ice sheet models a similar approach is adopted, but the decision for a potential end of the simulation period without atmospheric GCM is made in the ocean model.

2.3 Coupling of the ice sheet model

2.3.1 Forcing fields and calculation of the surface mass balance: the degree-day scheme.

The atmospheric forcing of the ISM consists of seasonal 2-m atmospheric temperatures and precipitation rates. A flux correction has been applied for both the 2-m temperatures and precipitation rates: instead of using directly the atmospheric fields, anomalies from the AGCM are used superimposed on the present

climatology from ERA40 (Uppala *et al.*, 2005). Precipitation anomalies have been preferred to ratio anomalies (an option preferred in some other studies) for mass conservation purposes.

In order to account for the differences in the reference topography of the fields from the ERA40 climatology and the atmospheric data from the AGCM two corrections have been applied for the near-surface temperature and precipitation fields. For the near-surface temperatures a linear height correction with lapse rate -6.5° C/km (environmental lapse rate) has been applied. For precipitation rates P, an exponential height-desertification correction has been applied. Precipitation rates are reduced by 50% per km above the height $h_0 = 2$ km (Budd and Smith, 1979):

$$P = P(h_{ref}) = \begin{cases} \exp\left(\gamma_p \left[\max(h, h_o) - h_0\right]\right), & h_{ref} \leq h_0 \\ \exp\left(\gamma_p \left[\max(h, h_o) - h_{ref}\right]\right) & h_{ref} \geq h_0 \end{cases} \tag{2.28}$$

where h_{ref} is the height at which precipitation rates are calculated and $\gamma_p = -0.6931$ km^{-1} is the coefficient from the exponential law.

Precipitation rates P are converted into accumulation rates S by an empirical formulation (Marsiat, 1994), which relates them to the seasonal near-surface temperatures T:

$$S_{mam} = P_{mam}\mathrm{x} \begin{cases} 0, & T_{mam} \geq 7°\mathrm{C} \\ (7°\mathrm{C} - T_{mam})/17°\mathrm{C}, & -10°\mathrm{C} \leq T_{mam} \leq 7°\mathrm{C} \\ 1, & T_{mam} \leq -10°\mathrm{C} \end{cases} \tag{2.29}$$

for the season March-April-May (sub-index mam) and similarly for other seasons.

The surface melting is parameterised according to Calov (1994) following the degree-day model by Braithwaite and Olensen (1989). This method couples the melting rate m linearly to the air-temperature excess above 0° C:

$$m = \begin{cases} \beta T_c & T_c > 0 \\ 0 & \text{otherwise} \end{cases} \tag{2.30}$$

where T_c is the near-surface temperature and β is the so-called degree-day factor. A different factor β is employed for the melting of snow, β_{snow} =3 mm water equivalent (WE) day^{-1} °C^{-1}, and for the melting of ice: β_{ice}=12 mm WE day^{-1} °C^{-1} for the northern hemisphere and β_{ice}=8 mm WE day^{-1} °C^{-1} for the southern hemisphere (Reeh (1991), Greve *et al.* (1999), Calov *et al.* (1998)).

Air temperatures are assumed to follow a sinusoidal annual cycle with amplitude the difference between the summer and annual temperatures T_{summer}-T_{ma},

and additional variations due to the diurnal cycle and changing weather conditions are treated as normally-distributed statistical variations with standard deviation σ_{stat}= 5°C (Greve *et al.*, 1999).

There is a simple parameterisation accounting for refreezing.

The ice-surface temperature T_s is assumed to be equal to the mean annual air temperature T_{ma} unless the formation rate of superimposed ice, M^*, exceeds the ice-melting rate, M. In this case, an empirical firn-warming correction due to the latent-heat release of the remaining superimposed ice is applied (Reeh, 1991):

$$T_s = T_{ma} + \max\{\mu_{fwc}(M^* - M);\ 0\} \tag{2.31}$$

with the firn-warming correction coefficient $\mu_{fwc} = 24.206°$ C m^{-1} a.

Due to the differences in the size of the atmospheric grid (T21) and the ice sheet grid (80 km), a downscaling technique is needed. First the atmospheric data is bi-linearly interpolated onto the ice sheet model grid, and then the same algorithm as for the flux corrections is used in order to account for height differences. The time step for the ISM is 1 year.

2.3.2 Fields passed from the ice sheet model to the atmosphere and ocean components

The ice sheet model provides the following fields to other components of the Earth System Model: topography and albedo changes (via changes in the glacier mask) to the atmosphere and freshwater fluxes to the ocean. An atmospheric model grid point (resolution T21) is defined as glacier if at least 50% of its area is glaciated according to the interpolated ice-covered area from the SICOPOLIS grid. Freshwater fluxes are treated differently in the case of being supplied to the ocean as ice and in the case of being supplied as liquid water. The first case corresponds to calving and basal melting due to ocean heat supply, the second case to surface melting and basal melting due to geothermal heat fluxes. The distinction is made in order to account for the heat exchange between the cryosphere and the ocean.

The albedo feedback.

Changes in the topography and glacier mask passed from the ice sheet model to the atmospheric model can modify the albedo via two processes:

1) The albedo of glaciated surfaces differs from the albedo of non-glaciated surfaces.

2) The albedo of glaciated surfaces depends on the temperature of the grid point, in order to account for sub-scale areas inside the atmospheric grid point at melt temperature (the presence of meltwater reduces strongly the albedo). Changes in the topography of the glaciated areas can produce changes in the surface temperature via the height-effect (decrease of temperatures with increasing height). These temperature changes can modify the albedo of land ice if they are within a certain range close to the melt temperature (T_m= 273.15 K).

The parameterisation of the albedo of snow-covered areas in the atmospheric model ECHAM3 (DKRZ, 1994) will be described in the following.

In the atmospheric model ECHAM3, in the snow-covered areas the surface albedo changes from its background value α_{Sb} through the snow depth Sn value and the albedo of snow/ice surface α_S as follows:

$$\alpha_{Surf} = \alpha_{Sb} + (\alpha_S - \alpha_{Sb}) \cdot \frac{Sn}{Sn + Sn^*} \tag{2.32}$$

where S_n^*=0.01 m a critical snow depth. For $Sn >> Sn^*$ the surface albedo approaches the albedo of snow.

The albedo of snow and ice on land surfaces, α_S, depends on the surface type (t_S), the surface temperature (T_S), and the fractional forest area (a_f) over land. For $T_S \geq T_m = 273.15\,K$ (i.e., for melting of snow or ice), α_s is fixed at a relatively small value, $\alpha_S = \alpha_{Smin}(t_S, af)$. α_S is larger, $\alpha_S = \alpha_{Smax}(t_S, a_f)$, for cold surfaces ($T_S \leq T_0 = 263.15\,K$), according to Robock (1980). Over land, the respective snow albedos are assumed to depend on the fractional forest area ($0 \leq a_f \leq 1$) according to:

$$\begin{aligned} \alpha_{S_{min}}(a_f) &= a_f \cdot \alpha_{Smin}(a_f = 1) + (1 - a_f) \cdot \alpha_{Smin}(a_f = 0) \\ \alpha_{S_{max}}(a_f) &= a_f \cdot \alpha_{Smax}(a_f = 1) + (1 - a_f) \cdot \alpha_{Smax}(a_f = 0) \end{aligned} \tag{2.33}$$

In the temperature range $T_0 < T_S < T_m$, $\alpha_S = \alpha_S(T_S, t_S, a_f)$ is obtained by linear interpolation

$$\alpha_S = \alpha_{Smax} - (\alpha_{Smax} - \alpha_{Smin}) \cdot \frac{T_S - T_0}{T_{melt} - T_0} \tag{2.34}$$

with the minimum and maximum surface albedos α_{Smin} and α_{Smax} (Robock (1980) for snow albedos; Kukla and Robinson (1980) for the parameterisation of the albedo of land ice) as shown here in this table:

		α_{Smin}	α_{Smax}
land ice (ice sheets)		0.6	0.8
snow on land	for a_f=0	0.4	0.8
	for a_f=1	0.3	0.4

Chapter 3

Initialisation of the model and control ice sheets

In this chapter the initialisation of the ice sheet model and the Earth System model will be described. The ice sheet model has to be initialised with a long spin-up in order to account for the memory of the temperatures of the ice column to past climates. The topography, total volume and area, and velocities of the ice sheets of the control simulation, with pre-industrial CO_2 concentration, will be compared to available measurements.

3.1 Initialisation of the model

For the initialisation of the Earth System model, a spin-up simulation over 10,000 years has been performed. This simulation started from a previous model state. During this spin-up simulation the flux corrections for the ice sheet model were calculated.

For the initialisation of the ice sheet model two glacial cycles have been simulated with a simple climatic forcing. A time-dependent temperature anomaly from ice cores (from the central Greenland GRIP (Dansgaard *et al.*, 1993) for the northern hemisphere and from the VOSTOK ice core ((Jouzel *et al.*, 1993) and (Jouzel *et al.*, 1996)) for the southern hemisphere) has been superimposed to the present climatology from ERA40 (Uppala *et al.*, 2005) for the near-surface temperature forcing.

A linear relationship between temperature and precipitation changes has been used for the precipitation forcing. For sea level forcing the SPECMAP δ^{18}O record (Imbrie *et al.*, 1984) is used via the conversion (Greve *et al.*, 1999)

$$z_{sl}[m] = -34.83\,\mathrm{m} \cdot \left(\delta^{18}O[\%] + 1.93\right) \tag{3.1}$$

where z_{sl} is the sea level expressed in meters.

3.2 The reference ice sheets and comparison with measurements

A control simulation (CTRL) over 2250 years with the coupled Earth System Model is described in detail in Mikolajewicz *et al.* (accepted). The mean atmospheric concentration of CO_2 is 279.5 ppmv. This control simulation will be used as reference simulation for the anthropogenic climate change experiments. In the following, the simulated ice sheets of CTRL will be analysed and compared with available measurements.

3.2.1 Area and topography of the reference ice sheets

The reference northern hemisphere ice sheets from the control simulation have an area of 2.15±0.02 x 10^6m^2. These ice sheets are located mainly on Greenland. Other glaciated areas are simulated in Svalvard, Iceland, Baffin Island, Ellesmere Island and the Rocky Mountains (fig. 3.1). These glaciated areas are placed at locations which correspond to actual glaciers and ice caps (see fig. 3.2).

According to (Church *et al.*, 2001), the area of the Greenland ice sheet is 1.71 x 10^6km^2, and its volume leads to 7.2 m SLE. The simulated northern hemisphere ice sheets have a volume of 8.6 m SLE. Main differences of the control Greenland ice sheet with the topography from ETOPO5 (ETOPO5, 1988) are found in northeast Greenland, where thickness anomalies are as large as 500-800 m (fig. 3.3). These differences in northeast Greenland explain most of the difference of volume between the simulated and measured ice sheet. The middle part of the ice sheet is 100-200 m lower than the measured one.

In the southern hemisphere, all simulated glaciated points are placed on Antarctica. The simulated area of the Antarctic ice sheet (12.70±0.02 x 10^6km^2) exceeds by 3% the measured area (Church *et al.*, 2001). Its volume (66.94±0.19 m SLE) is 9% bigger. All numbers given here correspond only to grounded ice, that is, the area and volume of the ice shelves have not been counted. The ice excess is placed in West Antarctica and the area of the Amery Ice Shelf (fig. 3.3). The grounding line is placed in the right position almost everywhere,

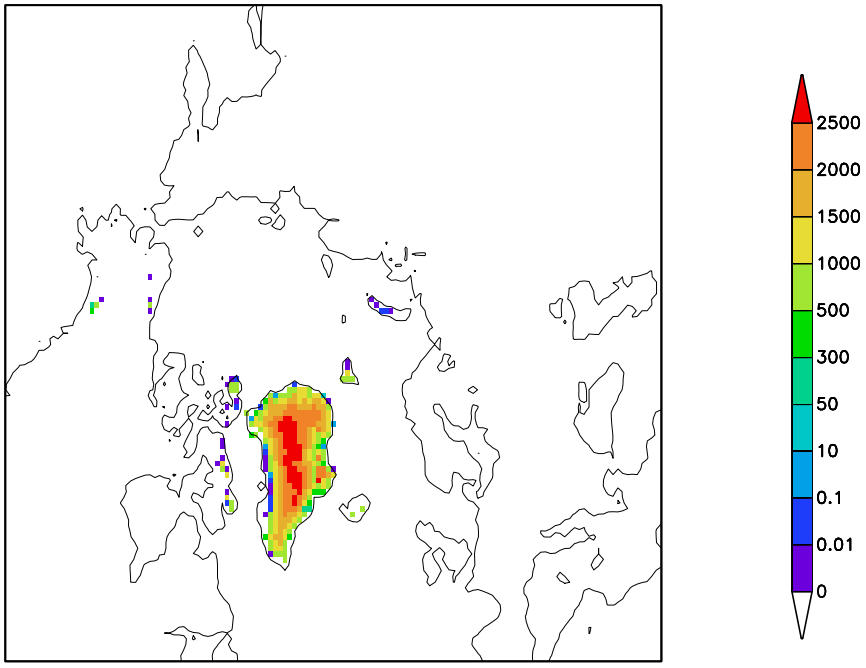

Figure 3.1: Mean thickness [m] of the northern hemisphere ice sheets from the control simulation in the ice-sheet model grid. The black contour line corresponds to the model isoline for the topographic height=0 m.

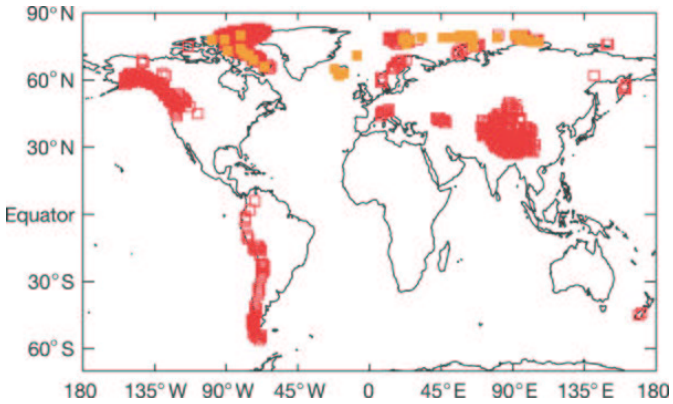

Figure 3.2: Worldwide location of grid cells containing glaciers(red) and individual icecaps (yellow). From Raper and Braithwaite (2006).

except for the Ronne Ice Shelf, where it is placed a bit further inside, and for the Antarctic Peninsula, more extended than the real one.

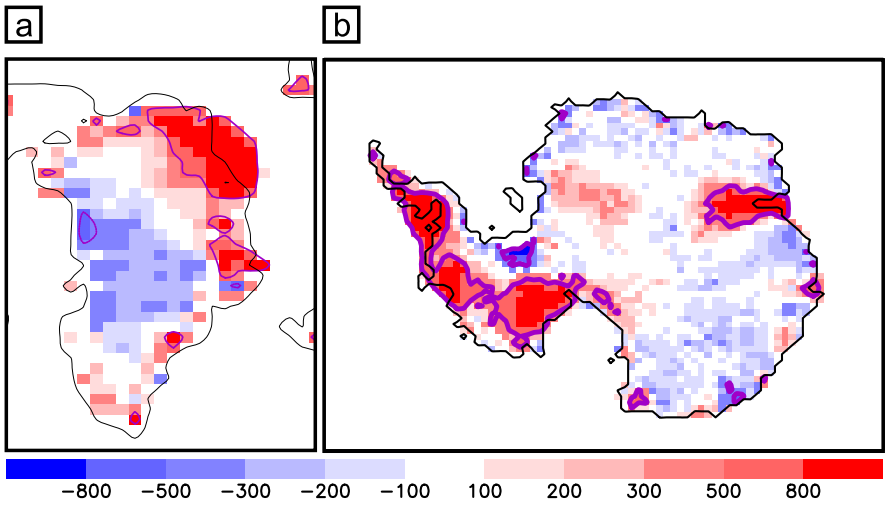

Figure 3.3: Comparison of the topography [m] of the simulated CTRL ice sheets with measurements from ETOPO5 (ETOPO5, 1988):(a) Greenland ice sheet and (b) Antarctic ice sheet. The purple line delimits the area with changes exceeding 500 m. The black line of a) corresponds to the ETOPO5 isoline for 0 m height, while the black line of b) corresponds to the grounding line of the measured ice sheet.

3.2.2 Dynamics of the control ice sheets.

The vertically integrated mean velocities of the Greenland ice sheet from CTRL and shown together with the measurements from Joughin *et al.* (2004) in fig. 3.4. The general pattern agrees well with observations: lower velocities (several m/yr) in the interior and higher velocities at the margins (several hundreds of m/yr). The areas with velocities between 25 and 100 m/yr are in general properly modelled. Due to the resolution of the model, the exact location of the fast outlet glaciers and ice streams can not be resolved. For instance, the fine structure of the ice stream in the northeast is not modelled.

The pattern of mean balance velocities of the grounded ice of the Antarctic ice sheet from CTRL agrees reasonably well with measurements (fig. 3.5). Low velocities are simulated in the highest areas of the interior of the East and West Antarctic ice sheets. Velocities increase towards the margins.

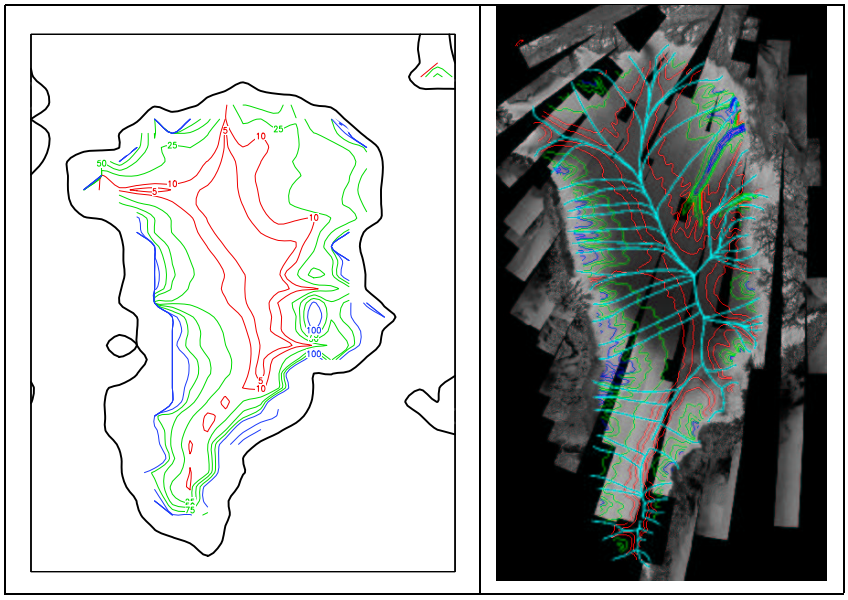

Figure 3.4: Vertically integrated mean velocities (red, green, and blue) and drainage divides (cyan) over the Greenland ice sheet: left panel) from the control simulation; right panel) measurements from Joughin *et al.* (2004). The 5 and 10 m/yr contours are shown in red, the 25, 50, and 75 m/yr contours in green. Velocities of 100 m/yr and larger are shown at 100 m/yr intervals (blue).

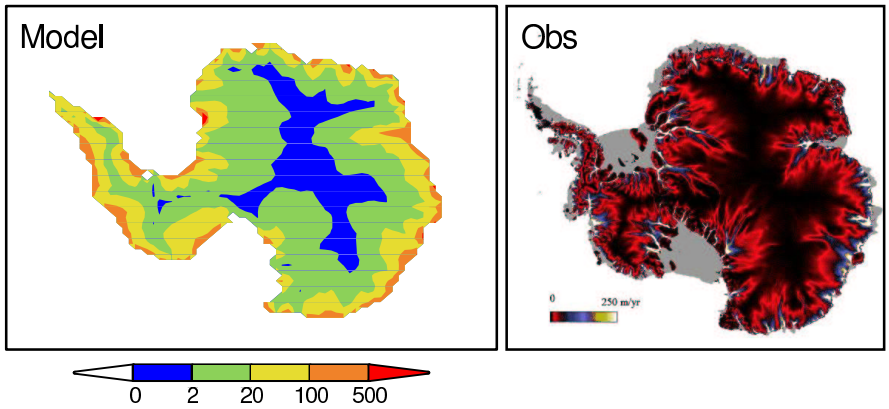

Figure 3.5: Vertically integrated mean velocities over the Antarctic ice sheet from the control simulation and from measurements from Bamber *et al.* (2000).

3.3 Summary and conclusions

The modelled reference ice sheets are in general in agreement with observations. Most of the glaciated areas simulated in the northern hemisphere correspond to the Greenland ice sheet. Some other glaciated areas are modelled on the current locations of glaciers and ice caps. Main differences in the topography of the modelled Greenland ice sheet with measurements exist in the northeast, where the ice sheet extends into the shelf area. The grounding line position of the simulated Antarctic ice sheet is in general at the right location. The volume of the Antarctic ice sheet is overestimated by 9%. The dynamics of the ice sheets are in general well modelled, except for the small scale (tens of km) features (outlet glaciers, ice-streams).

Chapter 4

Multi-century evolution of global ice-sheets under greenhouse stabilisation scenarios modelled with ESM1

4.1 Introduction

The increasing concentration of greenhouse gases in the atmosphere is expected to cause rising global mean temperatures (Houghton *et al.*, 2001). The warming is expected to be stronger at higher latitudes, due to the positive feedbacks of reduced snow-cover and sea-ice. Simple model simulations (Gregory *et al.*, 2004) have shown that, for an uniform regional warming of more than 3 K, the mass balance of the Greenland ice sheet will become negative and the ice sheet will begin to decay. Due to its location close to the areas of deep water formation, meltwater fluxes from Greenland could potentially cause a reduction of the strength of the ocean meridional overturning circulation.

Beside the potential from the ice sheets to modify the ocean circulation, another major climatic impact is of interest regarding the evolution of ice sheets: its contribution to sea level changes.

4.2 Simulations set-up

In order to explore the long-term evolution of global ice sheets under anthropogenic climate change and their feedbacks onto the climate, two different sets

of experiments have been performed with the Earth System Model ECHAM3/-LSG2/HAMOCC/LPJ/SICOPOLIS: 1) stabilisation scenario runs, where the atmospheric concentration of CO_2 is increased from pre-industrial level by 1% per year until reaching 2x, 3x and 4x the pre-industrial level and then the concentration is kept constant; and 2) IPCC scenario runs A1B, A2 and B1, where emissions of carbon instead of CO_2 concentrations have been prescribed. The stabilisation scenario runs will be analysed here, the SRES scenario simulations will be analysed in the next chapter.

Three main experiments will be analysed in this chapter. Atmospheric concentration of CO_2 is prescribed in these as follows: increase from pre-industrial concentration of 280 ppmv with 1% per year, until stabilisation at 2 times, 3 times and 4 times pre-industrial concentration. The experiments will be referred to as 2x, 3x and 4x. In 2x, the stabilisation level is reached in year 70; in 3x, in year 105; in 4x, in year 140. The simulations have a length of 1000 years.

For some of the scenarios some additional runs have been performed where the feedbacks between the ice sheets and the climate are ignored. The comparison of these simulations with the fully coupled ones is meant to facilitate the identification of the feedbacks between the ice sheets and the other components of the climate system. The simulations where the feedbacks of ice sheets are not taken into account will be named as *_1w (1w meaning one-way coupling).

A control simulation (CTRL) has been performed with a length of 2250 years and a prognostic pre-industrial concentration of CO_2.

An asynchronous coupling technique (Voss and Sausen (1996), Voss *et al.* (1998)) is applied with a fixed ratio of 2 years of fully-synchronous simulation of all components of the Earth System Model, followed by a period of 8 years of only-"slow" components (all but the atmosphere: ocean, ice sheets, vegetation).

All simulations are listed in table 4.1.

4.3 Global changes in the atmosphere and ocean

The mean global temperature increases in all the simulations. The increase in the mean global near-surface temperature is 2.1 K (2x), 3.2 K (3x) and 4.2 K (4x) at the end of the simulations (fig. 4.1). These increases indicate a relatively low climate sensitivity of this Earth System Model compared to other modelling results. Near-equilibrium runs from the latest IPCC report (Houghton *et al.*, 2001) have a mean sensitivity of 3.5 K for doubling of CO_2 .

The global temperature increase rate is strongest when the atmospheric CO_2 concentration is still rising. After stabilisation, global temperatures continue

Name	Length	Description
CTRL	0-2250	pre-industrial concentration of CO_2
2x	0-1000	1 % increase of CO_2 until stabilisation at 2xCO_2
3x	0-1000	1 % increase of CO_2 until stabilisation at 3xCO_2
4x	0-1000	1 % increase of CO_2 until stabilisation at 4xCO_2
*_1w	0-1000	One-way coupling: the feedbacks from ice sheets are ignored
*_CTPP	0-1000	Precipitation rates prescribed (mean rates from CTRL)
3x_FIXTOP	0-1000	As 3x, with fixed topography: the simulation neither allow for the height albedo feedback nor for changes in the ice flux.
3x_FIXADV	0-1000	As 3x, with fixed advection: integrated vertical velocities are prescribed.

Table 4.1: List of experiments.

rising due to the delay associated with the storage of heat by the ocean (Voss and Mikolajewicz, 2001). In the 4x simulation a period of slight decrease of the global mean temperature can be traced between years 200 and 400. This is, as it will be shown in the next paragraph, related to significant changes in the global ocean circulation.

Reduced formation of North Atlantic Deep Water (NADW) and a decline in the strength of the meridional overturning circulation (MOC) take place in all the simulations. In 2x and 3x this reduction in the strength of the MOC is modest and it reaches values only slightly lower than those of the control simulation after a century from the time of maximum reduction. In 4x, on the contrary, the strength of the MOC is steadily decreasing with time, until reaching minimal values. It does not recover by the end of the simulation. The causes for this reduction in the strength of the MOC and the role played in it by the ice sheets will be analysed in 4.4.

The two-dimensional pattern of temperature change shows stronger warming over the continents than over the oceans for all the simulations. Arid regions show a stronger warming. Northern high latitudes experience also a stronger warming than other regions, due to the positive snow and sea ice albedo feedback. Over the North Atlantic a regional weak warming or even net cooling takes place. This local minimum of temperature change is connected to the changes in the strength of the MOC.

The hydrological cycle is enhanced in all greenhouse simulations. Locally in the North Atlantic weaker anomalies/reduction of precipitation are seen associated with the low warming signal/net cooling in this region. For anthropogenic climate change simulations, the model shows a mean increase of the global mean precipitation of 5.1% for a CO_2 doubling, compared to the reference average 6.6% from the IPCC 2001 report (Houghton *et al.*, 2001).

4.4 Freshwater fluxes from Greenland and ocean circulation

The reduction in the North Atlantic Meridional Overturning Circulation in all the stabilisation simulations is related to increased stratification, caused by positive freshwater flux anomalies and surface warming. These positive freshwater flux anomalies reach values as high as 0.2 Sv in the 4x simulation (fig. 4.1). The comparison of net freshwater fluxes into the Arctic and North Atlantic basins between the simulations 2x, 3x and 4x and the corresponding simulations for which

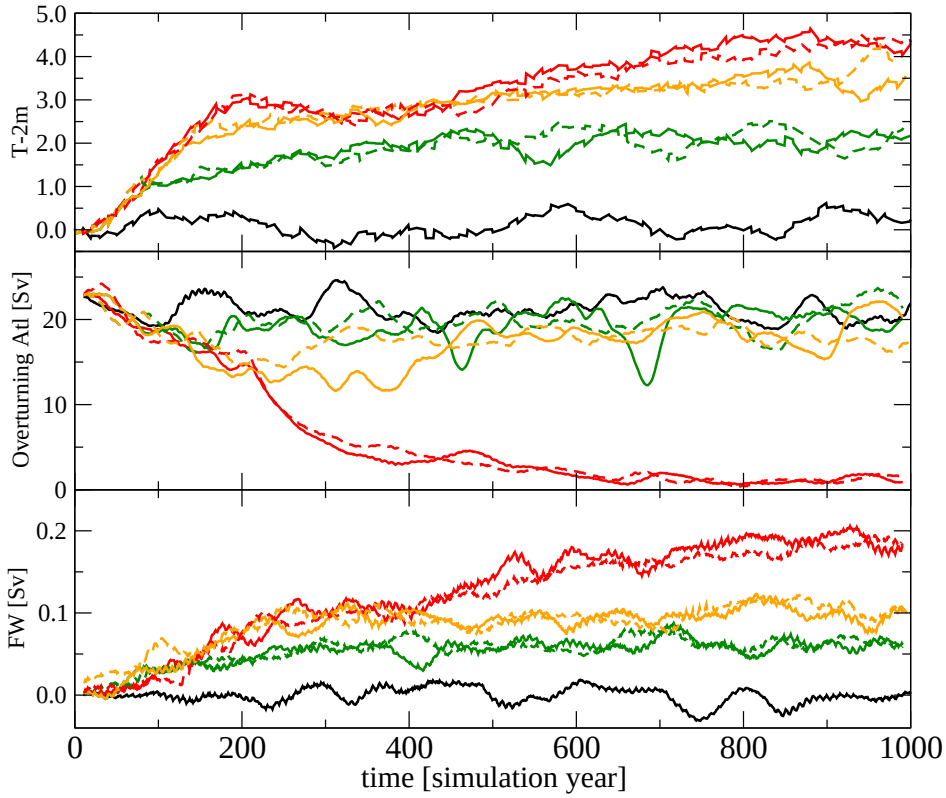

Figure 4.1: (a) Changes in the near surface (2-m height) temperature [K} for the 2x (green lines), 3x (yellow) and 4x (red) stabilisation scenarios relative to CTRL (black). Dashed lines represent the simulations where the feedback of the ice sheets is not included. (b) Strength of the north Atlantic meridional overturning at 30°N and at 1500 m depth [Sv]. (c) Anomalies to CTRL of net freshwater fluxes into the North Atlantic [Sv]. All time-series are 20-year running means.

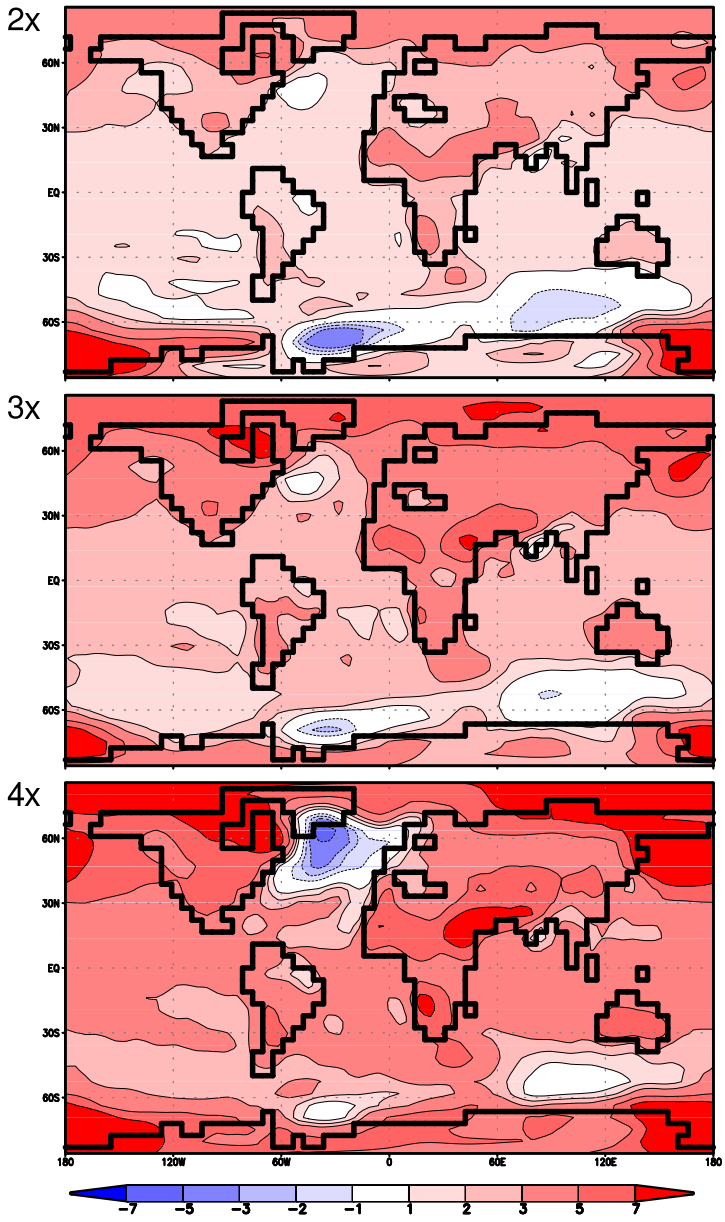

Figure 4.2: Global distribution of changes in the annual near-surface air temperature [K] for the simulations 2x, 3x and 4x compared to CTRL. Years 900-1000.

the feedbacks from the ice sheets (including freshwater fluxes) are not included is shown in fig. 4.1. Except for the simulation 4x, the total net freshwater fluxes in the simulations including the extra meltwater from the ice sheets are not significantly higher than the total net freshwater fluxes in the simulations *_1w for which the extra-input from the ice sheets is not included. At the time of the collapse of the MOC in the simulation 4x, the total freshwater input into the North Atlantic basin is approximately 0.1 Sv. The contribution from the northern hemisphere ice sheets to this is less than 0.005 Sv. From year 400, the freshwater fluxes from the northern hemisphere ice sheets do not exceed 0.02 Sv in the simulation 4x. The relative contribution of the ice sheets to net freshwater flux is less than 10% of the total in the simulation 4x.

There are no substantial differences in the strength of the NAMOC between the simulations including the extra meltwater from the ice sheets and the simulations with meltwater fluxes as in CTRL. Thus the Greenland ice sheet does not play a major role in the changes in stratification in the North Atlantic in these simulations. Instead, increased atmospheric moisture transport into the North Atlantic drainage basin is the cause of the weakening of the MOC.

4.5 Evolution of the Greenland ice sheet

4.5.1 Regional climate change in Greenland and surroundings.

The regional climate changes in and close to Greenland in these simulations are the result of the combination of two effects: 1) a global signal associated with high global concentration of greenhouse gases, and 2) a local regional signal associated with the changes in the strength of the NAMOC and its associated meridional heat transport. The first signal is warm and wet; the second one either reduces the magnitude or reverts the sign, depending on the scenario, of the temperature and precipitation changes caused by the high concentration of greenhouse gases. The combination of the signals 1) and 2) produces a meridional gradient of temperatures over Greenland, with the higher positive anomalies in the north and weaker/negative ones in the south (fig. 4.4). In the simulation 4x, where the MOC collapses completely, this gradient is strongest: lower temperatures than in CTRL occur in the southern part of Greenland and higher temperatures occur in the northern half.

The meridional gradient of temperature anomalies over the ice sheet is stronger in winter than in summer (not shown). In the simulations 2x and 3x, summer

positive anomalies of temperatures are lower than the annual mean anomalies (fig. 4.3). In 4x, where the climate of Greenland is highly influenced by a cold anomaly in the North Atlantic, summer temperature anomalies are not as cold as the annual ones. Summer is the season of main interest for the mass balance of the Greenland ice sheet, since surface melting takes place during this season.

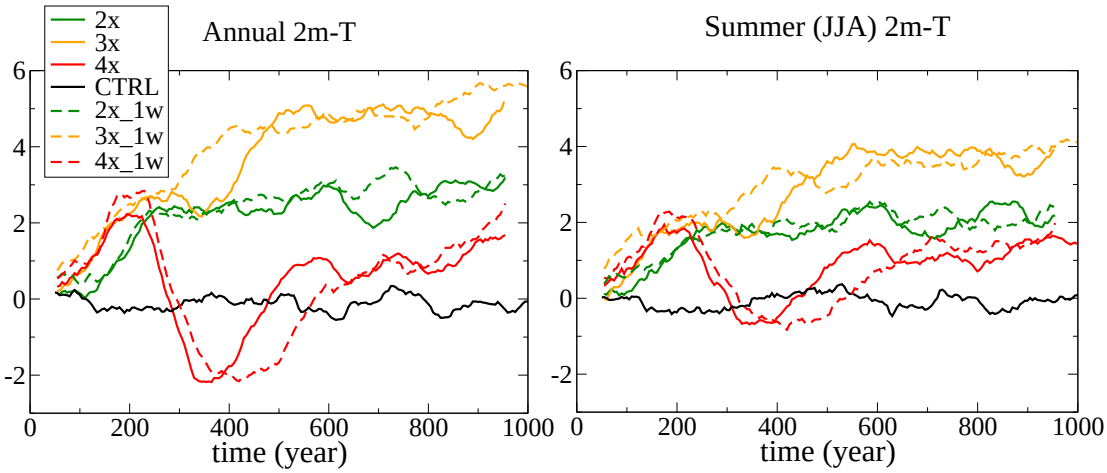

Figure 4.3: Time series of near-surface annual and summer temperature changes [K] averaged over the reference area of the reference Greenland ice sheet (from CTRL). The temperatures have been all referred to the reference height of the Greenland in CTRL via a correction with a lapse rate of -6.5°C/km. 20-year running means are displayed.

In the simulations 2x and 3x the mean summer temperature over the Greenland ice sheet area increases by 2 K and 4 K by the end of the simulations (fig. 4.3, right). In 3x a rapid increase of summer temperatures until year 200 is followed by a period with only minor changes in the mean summer temperature, which lasts until year 400. During this period the MOC has weakened significantly and then has initiated a recovery until reaching a state not far from the reference one of the control simulation. From year 400, temperatures increase over the Greenland ice sheet, and from year 600 onwards they do not show major changes.

The evolution of the temperature change over Greenland is significantly different in the simulation 4x when compared to 2x and 3x. After an initial increase of temperatures until year 200, a strong decrease follows. The mean summer temperature is lower than in the control run for a century, and afterwards (from year 400) begins to increase. Between years 600 to 1000 the mean temperature anomaly is approximately 1.3 K.

Precipitation changes behave similarly to temperature changes. While the

Greenland ice sheet receives more precipitation than in control everywhere in the simulations 2x and 3x, in the simulation 4x the pattern of precipitation changes presents a strong gradient over the ice sheet. Less precipitation falls in the south-east of the Greenland ice sheet, while the other parts of Greenland receive more than in the control run. This different pattern of precipitation changes in 4x with respect to 2x and 3x is responsible for a different role of accumulation changes in the total mass balance of the ice sheet in the simulations 2x and 3x, when compared to 4x. This will be shown in the next section.

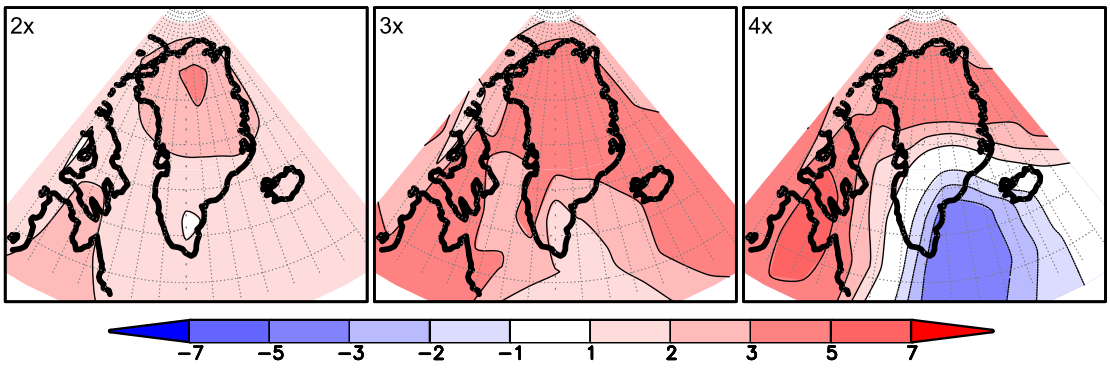

Figure 4.4: Changes in the summer (JJA) temperature [K] over Greenland by the end of the simulations (mean over the period 900-1000).

4.5.2 Changes in the mass balance of the Greenland ice sheet

The integral volume of the Greenland ice sheet decays in all the stabilisation scenario simulations 2x, 3x and 4x (fig. 4.15a). By the end of the simulations, the loss of volume is equivalent to a sea level rise of 25 cm in 2x, 1 m in 3x and 40 cm in 4x. The loss of mass is significantly higher in the simulation 3x than in 4x, although the signal of global warming is stronger in 4x, as shown before. The reasons for the lower loss of total mass in 4x are to be found in the regional climate change over Greenland. As previously shown, in the simulation 4x, the location of the centre of the negative temperature signal associated with the collapse of the MOC is located not far from the southeast coast of Greenland. The climate of the Greenland ice sheet in 4x is colder than in CTRL in the the southern third of Greenland, and colder than in 3x for the rest. Consequently, melting rates are much higher in 3x than in 4x and a stronger decay of the Greenland ice sheet occurs in 3x.

The area of the Greenland ice sheet does not change very much (fig. 4.5). By the end of the 2x simulation, only some isolated grid points in the ice sheet model (the size of each grid point is approximately 80 km x 80 km) have become ice-free. In 3x, the strongest changes occur at the east margin in the middle part of the island. In 4x, while some isolated points become ice-free at the north of the ice sheet (those points being common with points becoming ice-free in the simulation 3x), some other experience the opposite transition in the south, due to the reduced melting rates there.

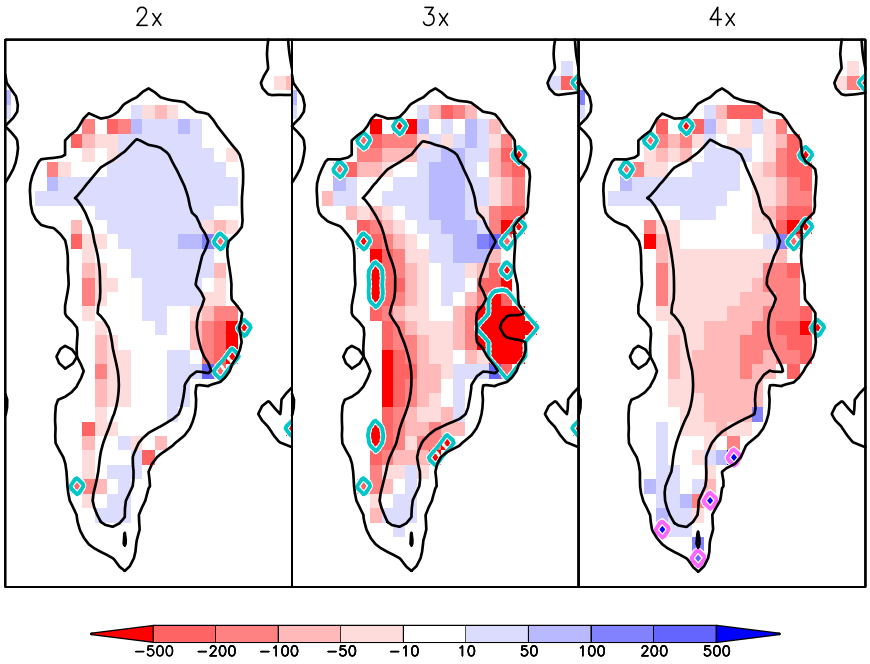

Figure 4.5: Changes in ice thickness [m] and grounding line position (blue line: area becoming ice free; pink line: area becoming iced) in the Greenland ice sheet for the period 900-1000 for the simulations 2x, 3x and 4x minus CTRL. In black: contour lines for heights z=0 m and z=2000 m.

Changes in the mass balance in 2x and 3x

By the end of the simulations, 2x and 3x show a similar pattern of two-dimensional distribution of thickness changes (fig. 4.5), with reduced thickness in the margins of the ice-sheet in the ablation area (where ablation exceeds accumulation) due to increased melting rates, and increased thickness in part of the accumulation area (where accumulation exceeds ablation) due to enhanced snowfall. In 3x, most of the of the area of the ice sheet higher than 2000 m (the Greenland Plateau), the

change in the surface mass balance (increase in snowfall- increase in surface melting) is positive (fig. 4.6). Nevertheless, an area of reduced thickness can be seen in the central part in the Plateau by the end of the simulation. The comparison of the surface mass balance of the last 100 years of the simulation shows more clearly this mismatch between the surface mass balance and the changes in the mass balance of the column of ice. While snowfall rates increase substantially almost everywhere over the ice sheet and surface melting rates increase almost only at heights lower than 2000 m, the changes in the vertically integrated mass balance of most of the Greenland Plateau are negative. These differences in the surface mass balance and the vertically integrated mass balance are explained by changes in the horizontal transport of ice. The transport of grounded ice (that is, the ice placed on land, as opposite to floating ice in ice shelves and glacier tongues) is mostly driven by gravity forces and follows the direction of the gradients of topography. The changes in the surface mass balance (increased melting dominating the surface mass balance at the margins and increased snowfall dominating the surface mass balance in the interior) cause increased gradients of topography. These increased gradients cause increased transport of ice from the interior to the margins. In some cases, this increased transport becomes the dominant term of the mass balance, and regions of positive surface mass balance experience a vertically integrated loss of mass. This is what explains the mismatch between the surface mass balance and the total mass balance in the simulations shown here. A more detailed analysis of the role of the dynamics in the mass balance budget of the Greenland ice sheet will be shown later in this chapter.

Changes in the mass balance in 4x

By the end of the simulations, 4x shows a different pattern of two-dimensional distribution of thickness changes than the simulations 2x and 3x (fig. 4.5). The middle part of Greenland shows thickness lower than in the control simulation. The total mass balance is negative in this area (fig. 4.6). This is mainly due to reduced accumulation rates. The precipitation anomaly associated with the cold anomaly in the North Atlantic leads to snowfall rates lower than in CTRL in the middle part of the island. The maximum reduction of snowfall takes place at the east coast.

By the end of the simulation and consistently with the temperature forcing described before, the southern part of Greenland has melting rates lower than in CTRL. In the rest of low elevation areas of Greenland, melting rates are lower than those of 3x (see fig. 4.12).

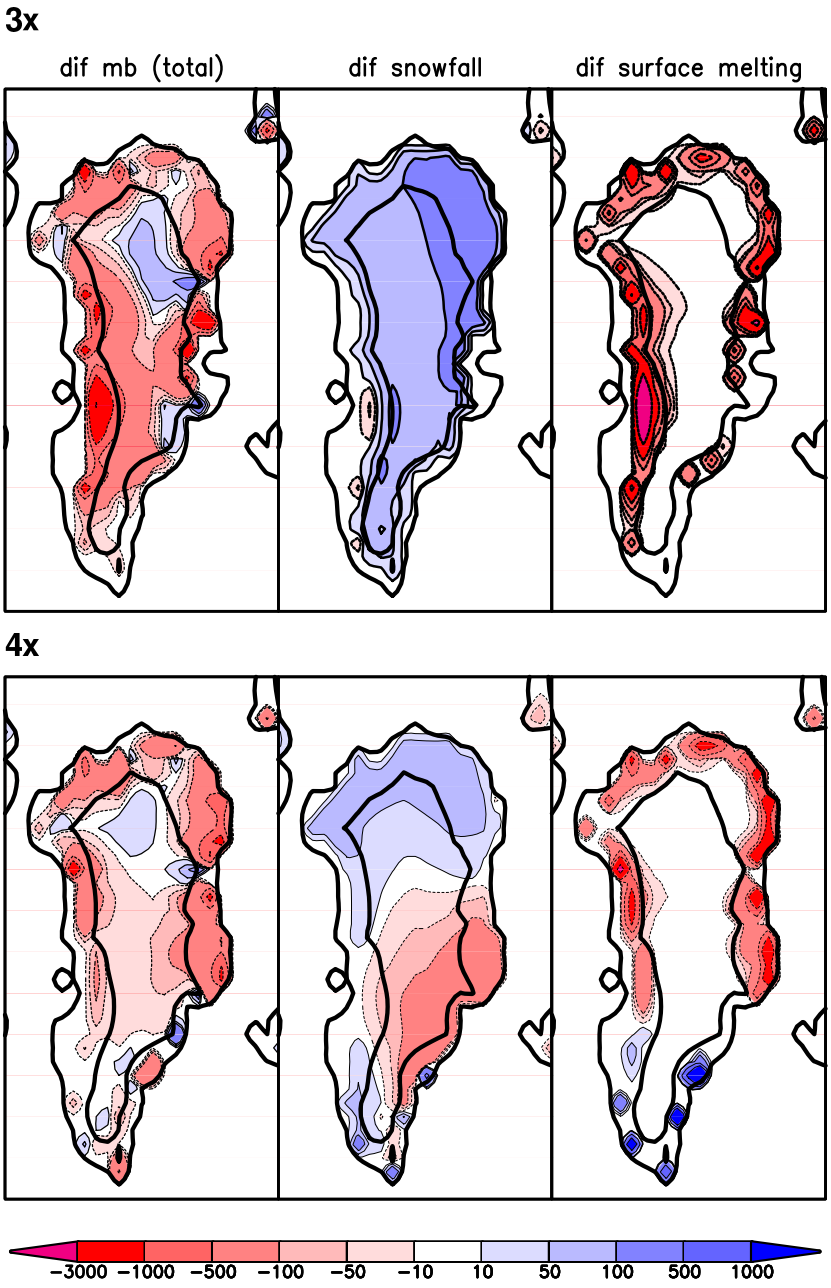

Figure 4.6: Comparison of changes in the mass balance [mm WE/yr] of Greenland for simulations 3x (upper panel) and 4x (lower panel) averaged over the period 900-1000 years: first column) Total mass balance change in the column of ice (net sum of all positive and negative terms including advection); second column) surface accumulation (snowfall); third column) surface melting. In black: contour lines for heights z=0 m and z=2000 m.

4.5.3 Feedbacks between the Greenland ice sheet and the climate system

It will be distinguished here between feedbacks between the ice sheets and the ocean (via increased freshwater fluxes from the decaying ice sheet) and feedbacks between the ice sheets and the atmosphere.

Feedbacks between the GrIS and the ocean

The freshwater fluxes from the ice sheets in these stabilisation simulations are relatively low (see fig 4.7). This is due to the combination of two factors: 1) the relatively low climate sensitivity of this Earth System Model causes a relatively modest warming of the Greenland area and 2) the location of Greenland in the area affected by the negative temperature anomaly associated with the weakening/collapse of the Meridional Overturning Circulation (MOC). Due to their small magnitude, the freshwater fluxes from Greenland do not play a major role in the changes of ocean circulation in these stabilisation scenario simulations.

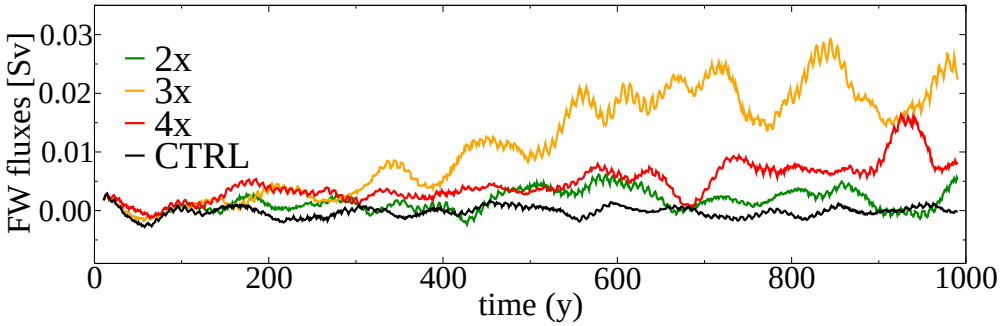

Figure 4.7: Net freshwater fluxes [Sv] from the northern hemisphere ice sheets for the experiments 2x (green), 3x (yellow), 4x (red) and CTRL (black). The time series are 20-year running means.

The mass balance of the Greenland ice sheet in these anthropogenic climate change scenarios has been shown to be highly influenced by the climatic effects of a change of the MOC, the main effect being a significant reduction of melting rates when significant weakening of the MOC occurs. This effect was shown to be particularly strong in the case of a complete collapse of the Atlantic overturning: the contribution to sea level changes from the GrIS in the simulation with $4xCO_2$ forcing, where the overturning collapses, is much lower than the contribution from a simulation with a $3xCO_2$ forcing, where the overturning weakens but recovers afterwards. Thus, in the simulation 4x, the regional climate signal associated

with a collapse of the MOC is dominant over the stronger global warming signal associated with a stronger higher CO_2 forcing.

The mechanism described before by which a weakening MOC produces such a climate effect on the Greenland ice sheet that melting rates of the ice sheet are reduced significantly can be identified as a ***potential stabilising feedback for the MOC***. The feedback loop would function as follows: higher temperatures over the Greenland ice sheet associated with higher concentrations of greenhouse gases produce an increase in melting rates. The increased freshwater fluxes from the ice sheet produce increased stratification in the areas in the North Atlantic where deep water formation occurs. This weakens the MOC. The regional climate change consequence of the weakening of the MOC reduces the warming over the Greenland ice sheet, reducing the melting rates. Lower freshwater fluxes from the ice sheet allow for a recovering of the strength of the overturning.

Feedbacks between the GrIS and the atmosphere

Changes in the area and volume of the Greenland ice sheet can have an effect on the atmosphere by two main mechanisms:

1) Changes in the topography can modify the general circulation of the atmosphere.

2) Changes in the area of the ice sheet and/or in the properties of the surface modify the albedo of the Greenland area.

The comparison of the global climates of the simulations 2x, 3x and 4x with the respective simulations where the feedbacks from the ice sheets were suppressed (2x_1w, 3x_1w and 4x_1w) shows no differences in the global climate (see fig. 4.1a). Thus the feedbacks to the atmosphere, if any, should have only a regional impact. In the following, the climate over the Greenland ice sheet in the simulations without feedbacks and the simulations with them will be compared in order to identify possible feedbacks.

The albedo of the ice sheet is approximately the same in the simulations with and without the ice sheets (fig. 4.8), except for minor changes in the simulations 2x and 3x due to changes in the glacier mask. One atmospheric grid point (in the resolution T21) becomes ice free in 2x from year 800. The same transition occurs in 3x somewhat earlier, approximately at year 600. These changes in only one of the atmospheric grid points do not produce a signal in the integrated temperature over the ice sheet (fig. 4.3).

The evolution of the integral volume of the Greenland ice sheet in the simulations where the feedbacks are suppressed show no significant differences with the simulations where the feedbacks are included (fig. 4.15a). The comparison of the

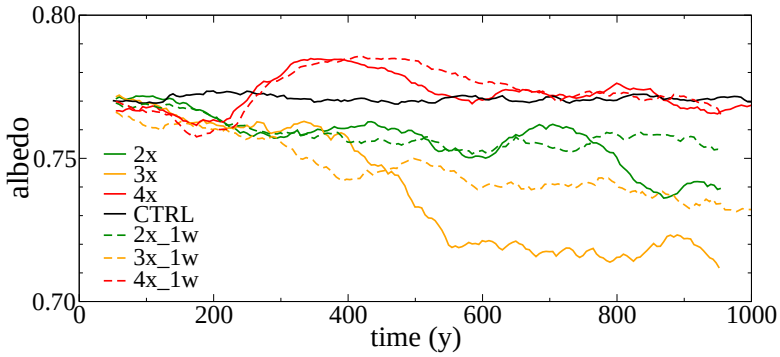

Figure 4.8: The albedo of the reference area of the Greenland ice sheet in the atmospheric model. Simulations 2x (green), 3x (yellow) and 4x (red). Dashed lines correspond to the simulations without the feedback of the ice sheets (2x_1w, 3x_1w, 4x_1w).

two-dimensional distribution of volume changes over the ice sheet by the end of the simulation shows no significant differences either. Thus the feedbacks between the GrIS and the regional climate of Greenland are not playing a major role in the evolution of the Greenland ice sheet itself in these simulations.

4.6 Evolution of the Antarctic ice sheet

4.6.1 Regional climate change in Antarctica

The temperatures over Antarctica increase in all the perturbed climates of 2x, 3x and 4x. By the end of the simulations, the mean regional near-surface temperature increase by 2 K in the case of 2x, 4 K in the case of 3x, and 5.8 K in the case of 4x, for the last 200 years (fig. 4.9). The mean temperature increase over the ice sheet is not very different between the three simulations until year 200, where the mean increase of temperatures is 2 K. While temperatures stay at this level in 2x, they experience a significant increase in 3x and 4x until the end of the simulations. This increase in temperature is stronger than the increase of the global mean temperature. This stronger increase of the temperatures long time after greenhouse gases have stabilised is related to the longer time-scales of climate change in the areas close to deep water formation sites (Voss and Mikolajewicz, 2001).

The control simulation exhibits a strong variability in the climate over the ice sheet (see the curve of near-surface temperature averaged over the ice sheet in fig. 4.9, with a standard deviation of 0.49 K). This variability has a time scale

of 400 years, and it is strongly related to the variability of the Antarctic Bottom Water formation (AABW) in the Weddell and Ross Seas in the simulations with this Earth System Model.

Precipitation rates over the Antarctic ice sheet increase in all greenhouse simulations. This increase will play an important role in the mass balance of the ice sheet, as it will be shown in the following.

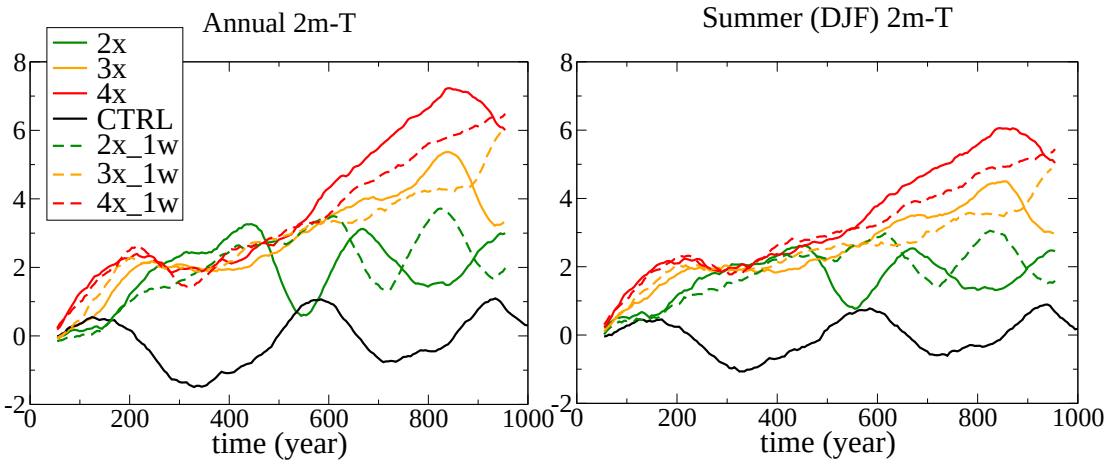

Figure 4.9: Time series of near-surface annual and summer temperature changes averaged over the reference area of the reference AIS (from CTRL). The temperatures have been all referred to the reference height of the AIS in CTRL via a correction with a lapse rate of -6.5°C/km. 20-year running means are displayed.

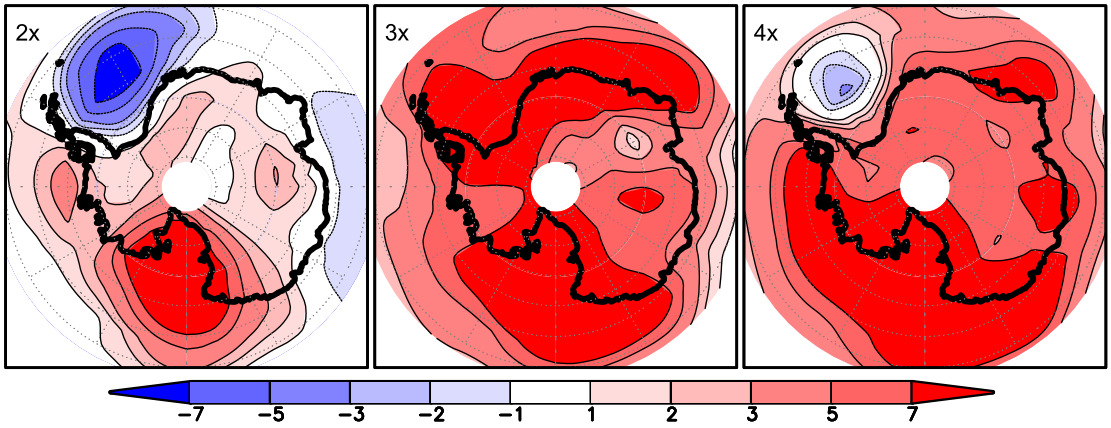

Figure 4.10: Changes in the summer (DJF) temperature [K] over Antarctica by the end of the simulations (mean over the period 900-1000).

4.6.2 Changes in the mass balance of the Antarctic ice sheet

The total volume of the Antarctic ice sheet increases in all the greenhouse simulations. The increase is approximately linear with time. By the end of the simulations, the additional volume of water stored in the ice sheet is equivalent to a sea level drop of 50 cm in 2x, 1 m in 3x, and 1.2 m in 4x (fig. 4.15b). This shows a higher storage of water in the simulations with higher increase in the concentration of greenhouse gases. The model does not simulate any abrupt change in the evolution of the Antarctic ice sheet in any of the simulations.

The changes in the mass balance are dominated by changes in accumulation. A relatively modest increase of melting rates occurs in some of the low elevated marginal areas of the ice sheet.

The two dimensional pattern of changes in ice thickness by the end of the simulations (see fig. 4.11) shows increased thickness all over the Antarctic ice sheet in all the greenhouse simulations, except for some small areas at the margin of the ice sheets, at topographic heights lower than 2000 m. The higher the prescribed atmospheric carbon dioxide concentration, the higher is the increase in thickness: for the simulation 4x the increase is maximal.

The pattern of net mass balance changes confronted to the changes in surface melting and snowfall (fig. 4.12) shows a clear dominance of the snowfall changes in the net mass balance in all the simulations. The surface melting increases only in the Antarctic Peninsula and low elevation areas (at the coast). Changes in the horizontal transport of ice are responsible for minor differences between local surface mass balance and total (vertically integrated) mass balance. No significant changes in the horizontal transport occur for the high elevation areas of the East Antarctic Plateau.

4.7 On the role of surface melting, accumulation and dynamical changes in the mass balance budget of global ice sheets

The results of these simulations of anthropogenic climate change show significant changes in the terms of the surface mass balance (surface melting and accumulation), and in the ice dynamics as well. The integral mass balance has been shown to be negative for the Greenland ice sheet, and positive in the case of the Antarctic ice sheet.

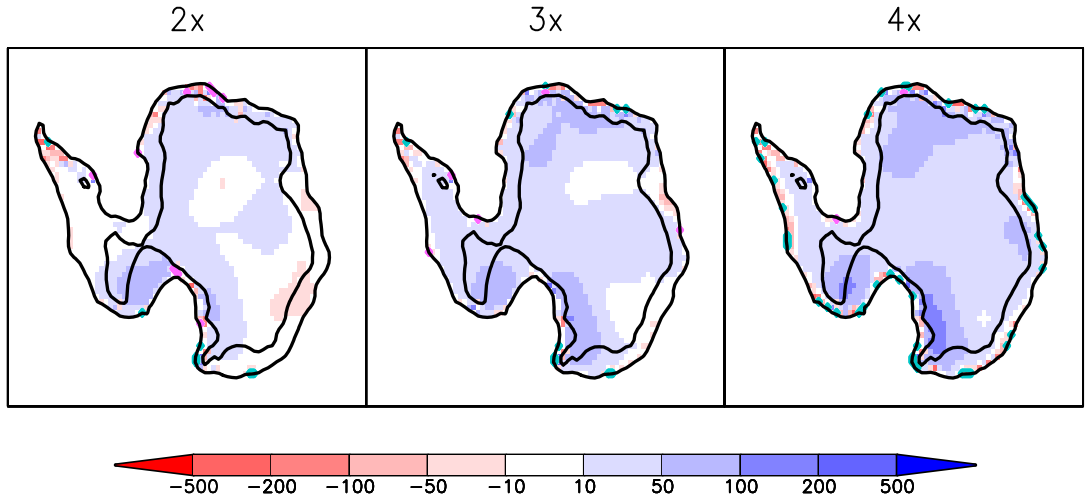

Figure 4.11: Changes in ice thickness [m] and grounding line position (blue line: area becoming ice free; pink line: area becoming iced) in the AIS for the period 900-1000 for the simulations 2x, 3x and 4x minus CTRL. In black: contour lines for heights z=0 m and z=2000 m.

This difference in the sign of the total mass balance is related to the current climate over those two ice sheets. In Greenland near-surface temperatures in summer exceed the melting point at the low elevation areas of the ice sheet, and surface melting represents approximately one half of the total mass loss. In Antarctica, on the contrary, due to the very low temperatures, surface melting on the grounded ice is insignificant and represents a very small fraction of the surface mass balance. In a perturbed climate with high concentration of greenhouse gases, a local warming over Greenland causes increased melting rates in the ice sheet, but over Antarctica the warming could not exceed the threshold to be surpassed to bring the surface of the marginal areas of the ice sheet to the melting point.

4.7.1 The case of Greenland

The term of mass balance which determines the negative sign of the integrated net mass balance of the Greenland ice sheet is the surface melting, which increases significantly due to the warmer climate over the ice sheet. What are the roles played by accumulation and dynamical changes in the total mass balance of the GrIS? Did they contribute positively or negatively to the decay of the ice sheet? Is their contribution to the total mass balance important in absolute terms or can they be ignored? What is the error associated with calculations of the mass balance of ice sheets which do not include the contribution of changes in the

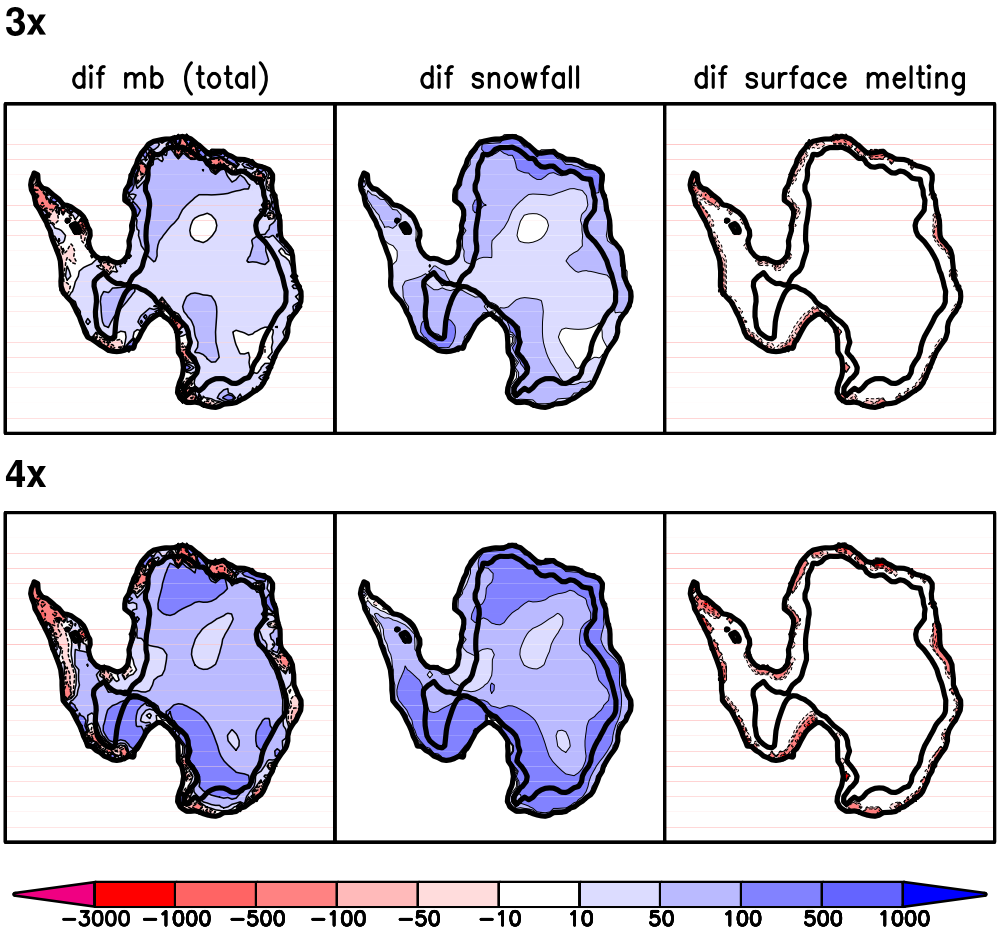

Figure 4.12: Comparison of changes in the mass balance [mm WE/ yr] of the AIS for simulations 3x and 4x averaged over the period 900-1000: first column) total change of mass in the ice column; second column) accumulation (snowfall); third column) surface Melting. In black: contour lines for heights z=0 m and z=2000 m.

dynamics? What is the relative importance of changes in accumulation versus changes in surface melting in the results presented so far in this study? Are there fundamental differences in the answer to these questions depending on the greenhouse forcing of the scenario, and on the occurrence/non-occurrence of the collapse of the MOC with its consequences for the regional climate of Greenland? These questions will be addressed in the following.

The role played by accumulation changes

Accumulation changes are positive almost everywhere over the GrIS in 2x and 3x, while this is not the case in the simulation 4x, where some areas experience lower snowfall than in the control simulation. Thus the changes in accumulation do not play the same role in the decay of the ice sheet in one case than in the other. In order to evaluate the role of accumulation changes in the total mass budget of the Greenland ice sheet, two off-line simulations have been run with the same temperature forcing from the simulations 3x and 4x, but with the precipitation rates from the control simulation. The name of these simulations is 3x_CTPP and 4x_CTPP. The purpose of running such sensitivity experiments instead of simply examining the terms of the mass balance in the simulations 3x and 4x is to account for non-linear effects. For instance, changes in the surface mass balance trigger changes in the dynamics via changes in the topographic gradients, for long-time scales as those examined here in this study.

a) In 2x and 3x

In the simulations 2x and 3x, where the signal of global warming dominates over the regional signal associated with a weakening of the MOC, snowfall rates are higher than in CTRL almost everywhere over the ice sheet (for 3x, see fig. 4.6). Thus the changes in accumulation cause a reduction of the decay rate of the Greenland ice sheet.

The volume of the GrIS in the simulation 3x_CTPP, with precipitation rates from the control simulation, is reduced by an extra 100% compared to 3x (fig. 4.13) by the end of the simulation. This indicates that, in 3x, accumulation changes reduce very significantly the rate at which the Greenland ice sheet decays, by approximately halving the decay rate.

b) In 4x

In the simulation 4x, where the climatic regional signal associated with the collapse of the deep water formation in the North Atlantic has a strong influence on the climate of the GrIS, accumulation rates are lower than those of CTRL over a large area of the ice sheet. The changes in accumulation contribute with a positive sign to the changes in the local surface mass balance in some areas and

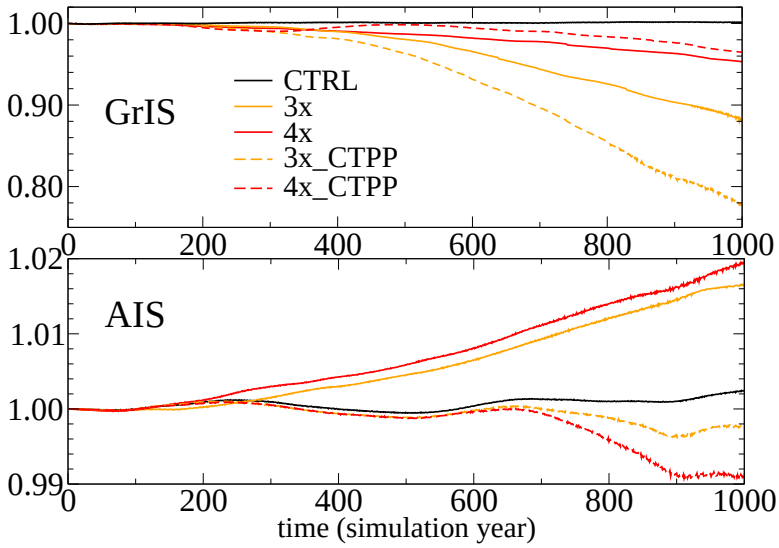

Figure 4.13: Comparison of the GrIS (a) and AIS (b) relative volume changes for the simulations 3x (yellow) and 4x (red) with others where accumulation changes where ignored, 3x_CTPP (yellow dashed) and 4x_CTPP (red dashed).

with a negative sign in others (see fig. 4.6).

In the simulation 4x_CTPP, the ice sheet model is forced with the temperature forcing from the simulation 4x but precipitation rates are kept unchanged with respect to CTRL. The Greenland ice sheet decays approximately 30% less than in the simulation 4x (fig. 4.13). Thus, *in 4x, reduced accumulation rates contribute to the decay of the ice sheet*, although the term dominating the changes in the mass balance is the surface melting.

The role played by dynamical changes

Dynamical changes can play an important role in the mass balance of ice sheets in different time-scales. At the time scales which are subject of this study two processes can potentially contribute significantly to the total mass budget: 1) the height-feedback and 2) changes in the horizontal transport of ice. The height feedback is a positive feedback for surface melting: since the height of an area of an ice-sheet is lowered due to surface melting, the ice-surface temperatures increase due to the reduced height. The increase in temperatures lead to the strengthening of melting rates. The changes in the horizontal transport of ice are caused by a) changes in the topographic gradients, those triggered by changes in the surface mass balance and b) changes in the thickness of the column of ice.

Modelling studies of changes in the mass balance of ice sheets not including

a dynamic ice sheet (snowpack models and calculations of mass balance directly from the output of GCMs) do not include any of the two processes described before. In order to evaluate if these processes are important in the total mass budget and, in case they are, at which time-scales, two off-line simulations have been performed. In the first one, the topography of the ice sheet is kept unchanged, as it occurs in the modelling approaches not including a dynamic ice-sheet. Both effects of the height-feedback and changes in horizontal transport are neglected. In the second one, the topography of the ice sheet is allowed to change, but the vertically-integrated transport at each grid point is kept constant along the simulation. In this case only the height-feedback is included and is isolated from the effect of changes in the ice flux. The simulation 3x will be used as reference simulation, since it is the stabilisation scenario simulation where strongest changes occur to the Greenland ice sheet. The simulation with fixed topography will be referred to as 3x_FIX. The simulation with fixed horizontal fluxes will be called 3x_FIXADV (FIXADV stands for fixed advection).

By the end of the simulation with fixed topography 3x_FIX, the Greenland ice sheet has decayed 60% less than in the reference simulation 3x (fig. 4.14). This indicates that the combined effect of the height feedback and the horizontal changes in the transport acts as a strong ***positive*** feedback for the decay of the ice-sheet.

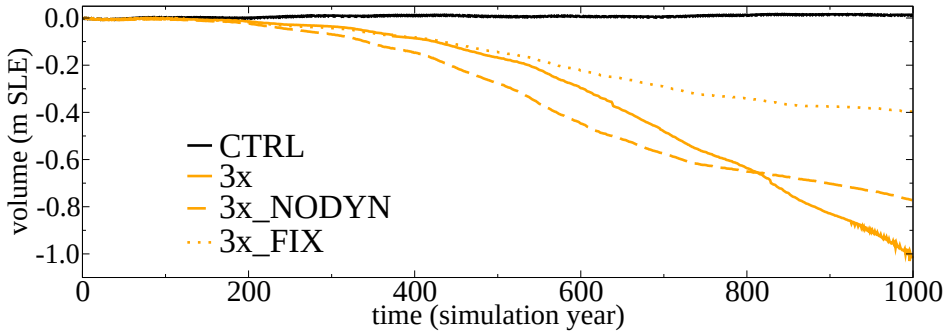

Figure 4.14: Comparison of the GrIS volume decay for the simulation 3x (solid), 3x_FIX (dotted) and 3x_NODYN (dashed).

The feedback associated with changes in the horizontal transport ***changes its sign*** along the process of decay of the ice sheet. The decay of the ice sheet is slower in the simulation with fixed fluxes 3x_FIXADV than in 3x until the ice sheet decays by approximately 8% of the original value. The initial lowering of the topography at the low marginal areas of the ice sheet in 3x triggers an increase of the horizontal flux of ice due to increased topographic gradients. This increase

flux brings extra ice to the low elevation areas, rising their topographic height. This, via the height-feedback, lowers the melting rates at the margins and acts as a ***negative*** feedback for the decay of the Greenland ice sheet. The high elevated areas originally at the accumulation area, have been lowered by this process of increased horizontal ice flux towards the margins of the ice sheet. The lowering of their topography was not sufficient, though, to bring a significant fraction of this areas to the ablation area (where ablation rates exceed accumulation rates). Later in the process of decay of the ice sheet, the reduction of height of these areas is sufficient to cause some summer melting on part of them. This additional surface melting from areas which initially did not experience any summer melting causes an increase in the total surface melting over the ice sheet. This changes the sign of the feedback caused by changes in the horizontal transport of ice, becoming a ***positive*** feedback for the decay of the ice sheet. By the end of the simulation, dynamical changes increase the mass loss of the GrIS by approximately 20%.

4.7.2 The case of Antarctica

In all the stabilisation-scenario simulations shown here, the net mass balance of the Antarctic ice sheet is positive. This is due to the low increase of surface melting rates compared with the increase in snowfall over the ice sheet. Thus, very differently to the case of Greenland, the dominant term in the surface mass balance is the accumulation. But, how much would the Antarctic ice sheet decay in this modelling approach if only the changes in surface melting would be accounted?

The role played by surface melting changes

As it was done for the study of the mass balance of the Greenland ice sheet, the output of two off-line simulations 3x_CTPP and 4x_CTPP will be compared to the evolution of the Antarctic ice sheet in 3x and 4x, respectively. These two simulations *CTPP are forced with the same temperature forcing as the simulations 3x and 4x, but the precipitation forcing is kept as in the control simulation.

The volume of the Antarctic ice sheet of the simulation 3x_CTPP evolves very similarly to the ice sheet from CTRL until year 600 (fig. 4.13). From that year, increased melting rates begin to cause a slight decrease of the volume of the ice sheet. By the end of the simulation, the Antarctic ice sheet has lost less than 0.5% of its original volume. In 3x the increase of volume by the end of the simulation is 1.5% of the original volume. Thus, surface melting changes are not important for the mass balance of the ice sheet in simulation 3x until year 600. By the end of

the simulation they reduce the effect of the dominating increase of precipitation by approximately 25%.

Similar conclusions can be drawn from the comparison of the simulations 4x_CTPP and 4x. Surface melting changes are not important until year 600. This is related to the increase in the regional warming over Antarctica that takes place there well after the greenhouse gases concentration have stabilised (see section about regional change over Antarctica). Until year 500, the average increase of temperatures does not exceed 2°C in any of the simulations. An additional warming of 2°C takes place afterwards in 3x. The increase is 4°C in the simulation 4x. A threshold for significant increase of surface melting in some low elevation areas is then surpassed. The decay of the ice sheet in 4x_CTPP is significantly higher (more than double) than in the case of 3x_CTPP. The gain of mass of the ice sheet in the simulation 4x is approximately 1.8% of the initial mass. Thus the loss of mass due to increase surface melting in 4x reduces the storage of water by approximately 40%. The figure is 25% in the case of the simulation 3x. This is consistent with the fact that accumulation rates approximately increase linearly with temperatures, but melting rates increase with a stronger pace (IPCC, 2001).

As conclusions, the results shown here suggest that:

1) The relative contribution of changes in surface melting to the total budget of the Antarctic ice sheet increases significantly with the local warming associated with the greenhouse scenario.

2) Due to the low summer temperatures of the Antarctic ice sheet, the perturbed regional climate over the ice sheet first produces a change in snowfall without any apparent change in surface melting. The warming must reach a certain threshold for the inception of summer melting. Once this threshold is reached, the relative weight of the surface melting in the surface mass balance increases significantly with increased warming.

4.8 Sea level changes

The storage of water in the AIS either compensates or exceeds the contribution to sea level rise from GrIS. By year 1000, the contribution from the ice sheets to sea level changes is close to zero in the simulation 3x, while it is a net lowering of the sea level in 2x and 4x (fig. 4.15a,b). The contribution to sea level by year 1000 from the thermal expansion of the ocean (fig. 4.15c) is 0.6 m (2x), 1.25 m (3x) and 1.5 m (4x). Maximum rate of thermal expansion occurs by year 300 in the case of 4x, being lower afterwards. The expansion has not reached an equilibrium by the end of the simulations. The net sea level rise (fig 4.15d) is maximal (+1.1m) at

year 1000 in 3x, while it reaches its maximum by the middle of the simulation in 4x (+0.9 m). This is due to the approximately linear increase of AIS volume with time (while the thermal expansion term follows an e-folding type curve), and to the small contribution of GrIS to sea level rise in comparison with 3x.

By the end of the simulations, the net sea level rise is strongest for 3x (+1.1 m) compared to 4x (+60 cm) and 2x (+20 cm). The two-dimensional pattern of sea level changes averaged for the period 900-1000 (fig. 4.16) shows the lowest sea level rise (or a lowering of the sea level for 2x) around Antarctica, due to the poleward shift of the locations of convection. Maximum sea level rise occurs in the North Atlantic and in the Arctic in 4x, due to the collapse of the deep water formation and the stable stratification. The highest sea level rise is simulated (+1.5 m) in the area of the Labrador Sea. Low sea level rise (only some tens of cm) comparable to that around Antarctica occur in the northwest Pacific, caused by the convection down to 2000 m (see Mikolajewicz *et al.* (accepted) for details about ocean circulation changes in this zone for the case of collapse of the deep convection in the North Atlantic for several simulations forced with SRES scenario emissions). The patterns of sea level changes are similar for 2x and 3x, since the ocean circulation is similar in both simulations.

It must be noted that the calculations shown here do not include the effect of redistributions of sea level due to the changes in the gravitational attraction exerted by ice masses on the ocean waters. Water piles up in the near field of an ice mass as a consequence of gravitational attraction; if the ice sheets melt (grow) the ocean will relax (will be attracted towards the ice mass) and the water will try to flow from the near field of the ice sheet to the the far field (from the far field of the ice sheet to the near field) (Mitrovica *et al.*, 2001).

4.9 Summary and discussion

The results from these stabilisation scenario simulations show a relatively small loss of mass from the Greenland ice sheet due to the relatively low climate sensitivity of this ESM and to the regional effects over the Greenland ice sheet of the weakening/collapse of the NAMOC. The relatively small meltwater fluxes from the Greenland ice sheet have been found not to play a major role in the strength of the NAMOC in the results with this ESM.

Ridley *et al.* (2005) performed a 4xCO_2 simulation with an ice sheet model bi-directionally coupled to the HadCM3 and obtained the almost complete elimination of the Greenland ice sheet within 3000 years. After the first 1000 years, the ice sheet decays to 40% of the initial volume. Their simulated global increase of

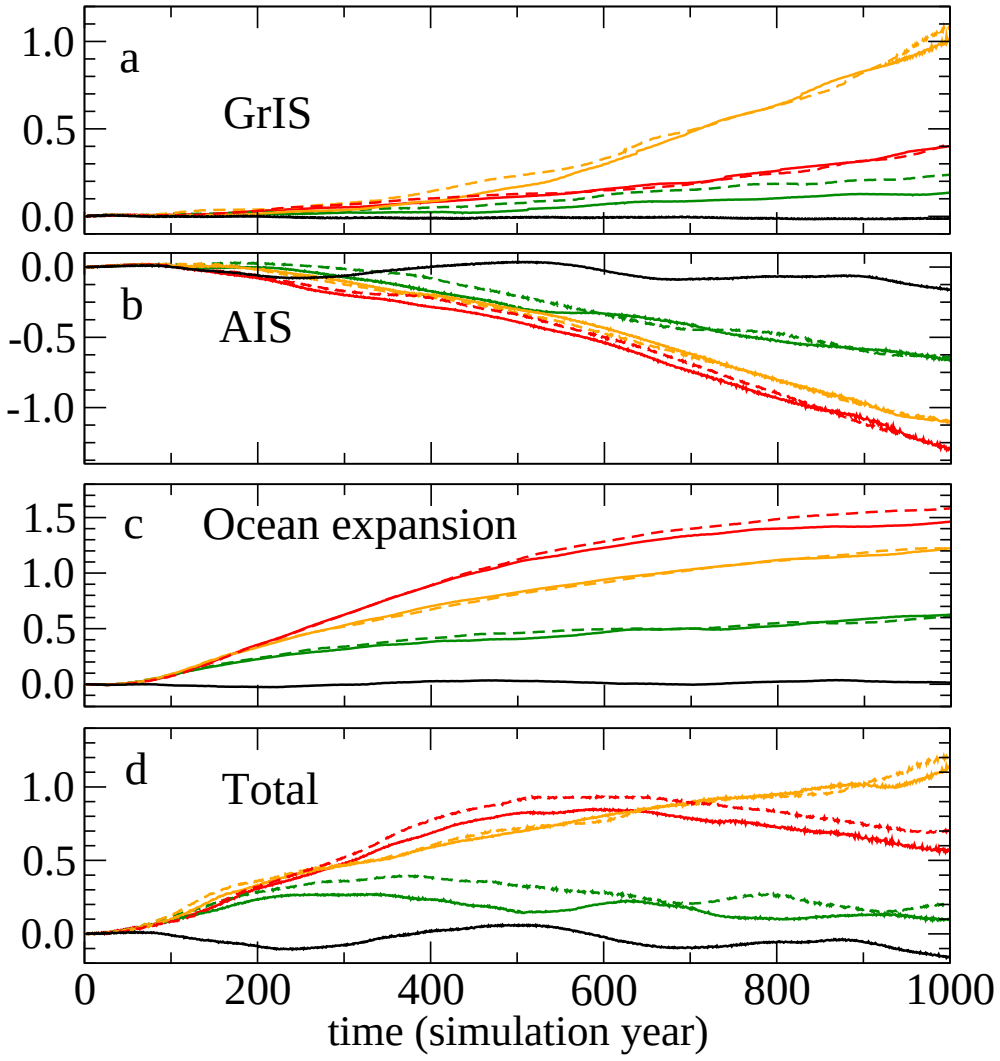

Figure 4.15: Time series of sea level changes [m] in the stabilisation simulations 2x (green lines), 3x (yellow lines) and 4x (red lines):(a) contribution from the Greenland ice sheet, (b) contribution from the Antarctic Ice Sheets, (c) contribution due to ocean expansion, (d) net sea level changes. Dashed lines represent the simulations *_1w where the feedback of the ice sheets is not included.

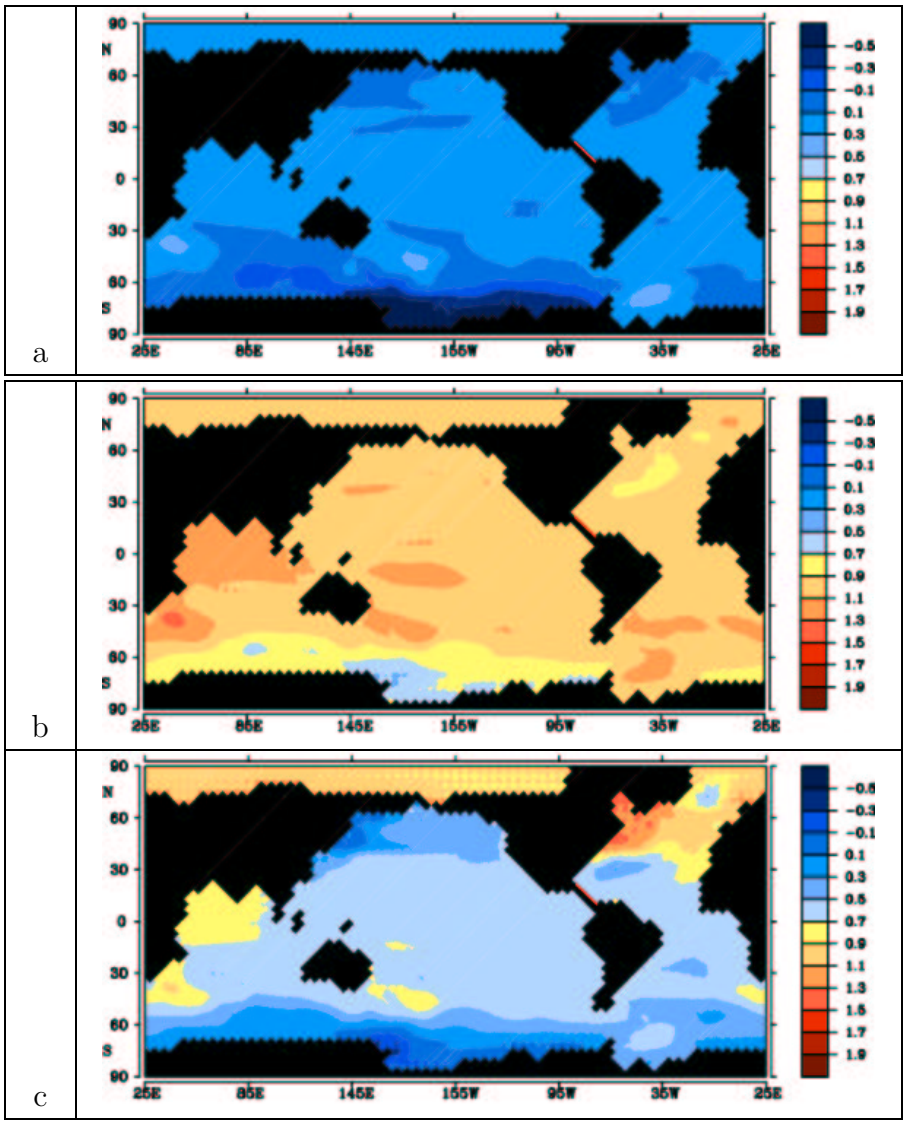

Figure 4.16: 2-dimensional pattern of changes of sea level [m] due to ocean expansion and changes in the volume of ice sheets for the simulations (a) 2x, (b) 3x, and (c) 4x.

temperatures associated with the high concentration of CO_2 is 7 K, and the local increase over Greenland is 9 K (without considering the signals due to changes in albedo and topography). These numbers are approximately 4.5 and 1.5-2 K in the results shown in this chapter.

Alley *et al.* (2005) obtained sea level rises of 1, 2, and 3 meters after 1000 year simulations with the ice sheet model from Huybrechts and de Wolde (1999) forced with the uniform increase in mean annual temperature obtained from an average of seven IPCC models used for scenarios where the CO_2 stabilised at 550, 750 and 1000 ppmv, respectively.

Huybrechts *et al.* (2002) coupled a 3-dimensional ice-sheet model of the Greenland ice sheet to the AOGCM LMD5.3- CLIO at a course resolution. The changes in the geometry of the Greenland ice sheet were not passed, however, to the atmospheric component. They applied the SRES B2 scenario to this model and found a contribution of Greenland of 4 cm to sea-level rise by 2100. About 0.03 Sv of additional freshwater fluxes enters the North Atlantic. They did not find significant changes in the patterns of climate change over the North Atlantic region compared with a climate-change run without Greenland freshwater feedback. Very differently, Fichefet *et al.* (2003) report a strong influence of the Greenland ice sheet meltwater discharge on the NAMOC until the year 2100, although the simulated freshwater fluxes (0.015 Sv) are comparable with those from the results shown here in this study. However, their control simulation showed a considerable drift towards a weaker NAMOC. Therefore the results could be affected by the model drift or their model could be close to a bifurcation point of the NAMOC, at which even very small perturbations could have a strong effect.

Regarding the Antarctic ice sheet, the results obtained with ESM1 show a net gain of mass of the ice sheet for all the stabilisation scenarios. Church *et al.* (2001) predict up to the year 2100 a continuous growth of the Antarctic ice sheet, which compensates enhanced melting rates from Greenland. Simulations with the three-dimensional ice sheet model of Huybrechts and de Wolde (1999) passively coupled to a two-dimensional climate model show a moderate and constant lowering of sea level, reaching 30 cm and 50 cm by the (calendar) year 3000 for doubling and quadrupling of CO_2 simulations, respectively. For the $8xCO_2$ scenario, the contribution of the Antarctic ice sheet to sea level rise is positive, due to increased surface melting in the margins and increased basal melting in the ice shelves caused by warmer ocean temperatures. Ice shelves are not properly modelled in the ice sheet model used in the study shown here in this thesis. Therefore a potential retreat of the grounding line in the West Antarctic ice sheet caused by the thinning of ice shelves due to enhanced ocean heat fluxes cannot be simulated. Warner and

Budd (1998) and Huybrechts and de Wolde (1999) showed that grounding line retreat along the ice shelves could happen for basal melting rates > 5-10 m yr^{-1}, demising the West Antarctic Ice Shelves after a few centuries.

4.10 Conclusions

The main conclusions that can be drawn from this study are summarised in the following:

- The contribution of the Greenland ice sheet to ocean circulation changes has been shown to be very small in this modelling study. Fresh water fluxes from the Greenland ice sheet have been found to be relatively small due to the low climate sensitivity of the Earth System Model and to the regional changes associated with the weakening/collapse of the MOC.

- In this modelling approach, the changes in the mass balance of the Greenland ice sheet have been shown to be highly influenced by the regional climate change associated with the weakening of the MOC. A substantial reduction of melting rates accompanies the collapse of the North Atlantic MOC in a simulation where the greenhouse concentrations have been set to four times pre-industrial concentrations. The contribution of the Greenland ice sheet to sea level changes is much lower than the contribution of the ice-sheet in a simulation with 3x pre-industrial levels.

-The reduction of melting rates over the Greenland ice sheet as a consequence of the regional climate changes caused by a weakening of the MOC are identified as a potential stabilising mechanism for the strength of the overturning.

-The local warming over the Antarctic ice sheet simulated for this stabilisation scenarios is not sufficient to cause surface melting to overcome the increase in snowfall over the ice sheet. Precipitation changes dominate the mass balance of the ice sheet.

-Similarly as shown by Huybrechts and de Wolde (1999) and Huybrechts *et al.* (2002), dynamical changes are found to act as a mechanism accelerating the decay of the Greenland ice sheet. Changes in the horizontal transport caused by changes in the topography, however, act to reduce the integrated surface melting in the first stages of decay of the ice sheet, until the increased transport lowers a sufficient area in the interior of the ice-sheet to a height with warmer surface temperatures permitting summer surface melting.

-The feedbacks from the ice sheets onto the atmosphere are quite small in these simulations and consequently the mass balance of the ice sheets is not significantly affected by the inclusion of these feedbacks. This does not discard the possibility

that, in case that the changes in the ice sheets due to anthropogenic climate change are stronger than those shown here, these feedbacks will need to be accounted for in order to model properly the mass balance of the ice sheet (Ridley *et al.*, 2005).

Chapter 5

Long-term response of global ice sheets to SRES emission scenarios B1, A1B and A2.

5.1 Introduction

Since the Earth System Model ESM1 includes a closed carbon cycle, carbon emissions instead of carbon dioxide concentrations can be prescribed. Several SRES scenarios were used for these carbon emissions forcing. These scenarios were designed to be used for climate projections until the year 2100. In this study, carbon emissions after 2100 are prescribed to decrease exponentially with a time constant of 150 years. Thus the purpose of the study shown in this chapter is to investigate the long-term response of the ice sheets to the anthropogenic forcing scenarios defined for IPCC.

5.2 Set-up

Several ensemble simulations have been performed for the SRES scenarios B1, A1B and A2: two realisations for the scenarios A2 and B1 and five for the scenario A1B. The simulations begin with the year 1750. For the calendar years 1750-2000 historical emissions have been used (Marland *et al.* (2005) and Houghton and Hackler (2002)), followed by several SRES emission scenarios for the period 2000-2100 (Nakićenović *et al.* (2001)). After that, an exponential decay with a time constant of 150 years was prescribed. All simulations were run until year 3000. Some of them were prolonged until the year 4000 (one for each scenario,

except for A1B, for which two simulations were continued). The simulation A2 was continued until year 9000. An additional simulation A2_1w, where the feedbacks from the ice sheets were not included, was performed for the forcing corresponding to the scenario A2. The idea is to identify the feedbacks from the ice sheets to the climate by comparing these two simulations A2 and A2_1w. This chapter will focus on the time frame between years 1750 and 4000, and the simulations A2 and A2_1w behind after 4000 will be subject of the next chapter.

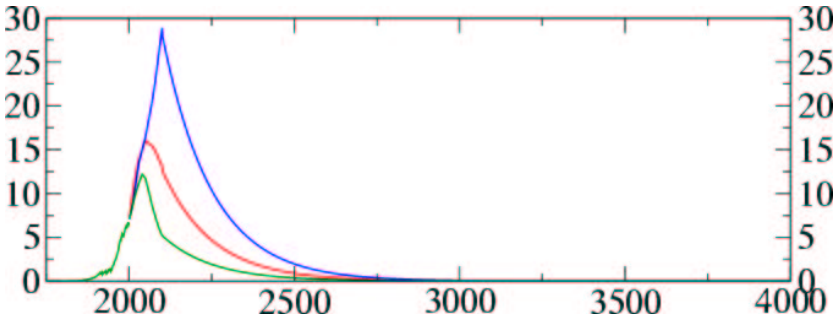

Figure 5.1: Prescribed carbon emissions [Pg C/yr] for the scenarios B1 (green), A1B (red) and A2 (blue). X-axis: time [yr].

The carbon emissions (fig. 5.1) in the high emission scenario A2 peak at 29.1 Pg C yr^{-1}in the year 2100, in the intermediate scenario A1B the peak takes place at 16.4 Pg C yr^{-1}in year 2050 and then gradually decays to 13.5 Pg C yr^{-1}in 2100. The low emission scenario B1 has its maximum of carbon emissions in 2040, with 11.7 Pg C yr^{-1}, and then the emissions decay to 4.2 Pg C yr^{-1}in 2100. Up to year 3000 the scenarios result in total emissions of 1969 (B1), 3812 (A1B) and 6568 Pg C (A2). The historical emissions up to year 2000 correspond to a total value of 439 Pg C, of which 156 Pg C are due to land use changes.

A control simulation of length 2250 years with pre-industrial concentration of carbon dioxide has been run as reference. An overview of all experiments is given in table 5.1.

A periodically synchronous coupling derived from the technique developed by Sausen and Voss (1996) has been applied (Mikolajewicz *et al.*, accepted). Until the year 3000, a ratio of 2 fully synchronous years followed by periods of 8 years of only-"slow" components (all but the atmosphere) has been used. From year 3000, the length of the periods without the atmosphere is interactively calculated, with a maximum length of 48 years.

Several simplifications were taken for these simulations: the land surface model does not include land use changes (those are represented in the emissions, but not in the distribution of vegetation from the model), anthropogenic nitrogen sources

Name	Length	Description	Size ensemble
CTRL	From 0 to 2250 (model years)	Coupled control simulation with prognostic pre-industrial CO_2 concentration	1 member
B1	From 1750 to 3000 (4000)	Emissions according to "optimistic" SRES scenario B1 2001-2100, exponential decay after year 2100	3 members
A1B	From 1750 to 3000 (4000)	Emissions according to "realistic" SRES scenario A1B 2001-2100, exponential decay after year 2100	5 members
A2	From 1750 to 3000 (4000, 9000)	Emissions according to "pesimistic" SRES scenario A2 2001-2100, exponential decay after year 2100	3 members
A2_1w	From 1750 to 7000	As A2, but prescribed ice sheets (no changes in meltwater, glacier mask or topography)	1 member

Table 5.1: Overview of the IPCC SRES scenario experiments discussed in this chapter.

were neglected, and sulphate emissions as well. Changes in dust are not modelled either.

5.3 Climate change: atmosphere, ocean, carbon cycle.

In 2100, the modelled CO_2 concentrations are 506 ppmv (B1), 656 ppmv (A1B) and 778 ppmv (A2) (see fig 5.2b). The peak concentrations are reached in 2500 for A2 (1680 ppmv), in 2330 for A1B (855 ppmv), and in 2200 for B1 (520 ppmv).

Averaged over the period 2801-3000, the simulated mean near-surface air temperature increases by 4.9 K (A2), 3.0 K (A1B) and 1.3 K (B1). Between the years 3000 and 4000 the global mean temperatures are almost constant, with a slight negative trend. This weak temperature change is due to the effects of the long-term response of surface air temperature to the early CO_2 increase and the slightly dominating response to the decaying atmospheric CO_2 concentrations caused by oceanic uptake of carbon.

The evolution of the North Atlantic Meridional Overturning Circulation (MOC) is very sensitive to the choice of the scenario. In the low emission scenario B1, the North Atlantic MOC does not experience major changes, with a maximum reduction of 2 to 3 Sv. In the high emission scenario A2, the North Atlantic MOC is reduced to 18-20 Sv by year 2100 (the long-term mean of the control simulation is 22 Sv). Less than two centuries later, in the year 2250, the deep water formation in the North Atlantic collapses completely and does not recover afterwards. The simulations forced with the intermediate scenario A1B behave similarly to A2 until year 2100. From then, however, there is a quite large scattering in the evolution of the different ensemble members. In two of the five ensemble members the North Atlantic MOC collapses between the years 2150 and 2250. In another simulation, this takes place between the years 2600 to 2750. In the remaining two ensemble members, the MOC experiences a moderate reduction but recovers afterwards. This wide range of ocean circulation changes indicates that the model is *close to a bifurcation point under the forcing corresponding to the SRES scenario A1B*. The threshold for the North Atlantic MOC is close to 10 Sv.

By year 3000, the B1 simulations show a warming of approximately 1 K over the oceans, and 1-2 K over land (fig. 5.3). The desert areas of North Africa and southwest Asia and the high northern latitudes show a warming between 2 and 3 K. In the northwest Pacific and close to the deep water formation sites of

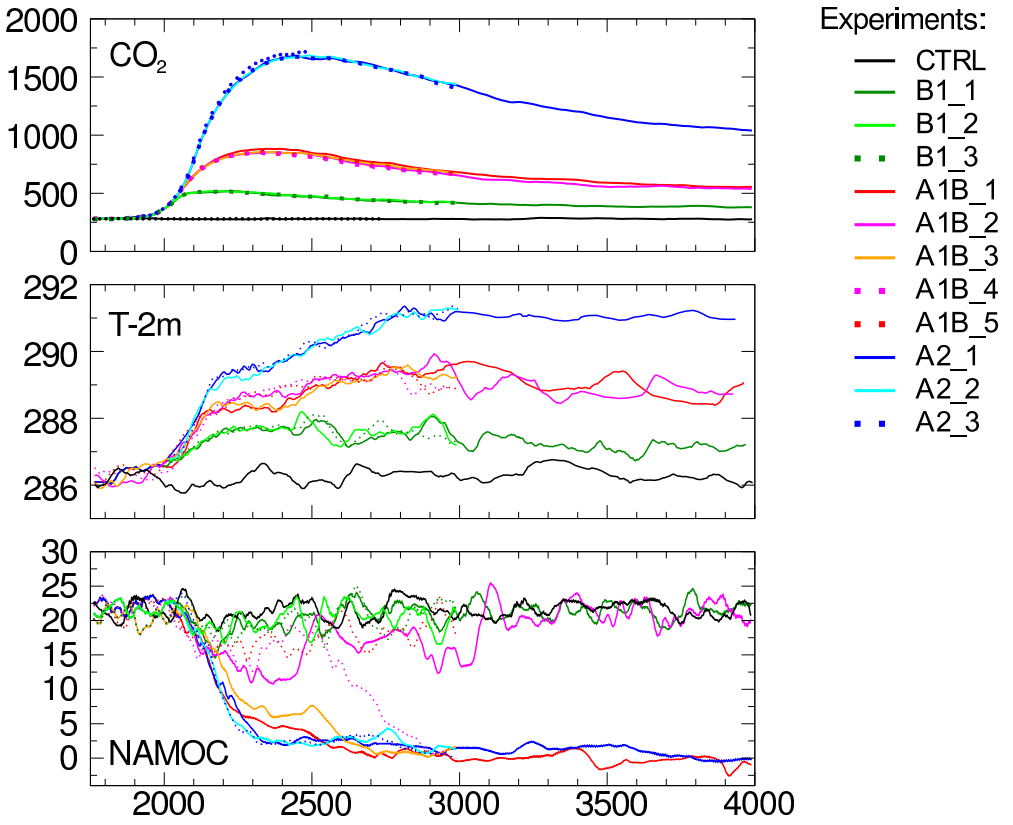

Figure 5.2: Time series of: (a) changes in the atmospheric CO_2 concentration [ppmv], (b) changes in the global mean near-surface (2-m height) temperature [K] for relative to CTRL (black), and (c) strength of the north Atlantic meridional overturning at 30°N and at 1500 m depth [Sv]. All time series are 20-year running mean values.

the Southern Ocean, reduced sea ice coverage produces a strong warming. Off southeast Greenland, a slight warming is simulated due to reduced deep ocean convection.

The spatial pattern of near-surface temperatures in the A1B simulations with a non-collapsed North Atlantic Deep Water (NADW) cell (from now on referred to as *A1B-on*, "on" referring to the active cell) is similar to the pattern of the B1 experiments, although showing stronger amplitudes, with a warming over land between 3 and 4 K. The northern latitudes show in many places a warming of more than 5 K. Over the ocean, maximum warming occurs in the Ross and Weddell Seas and in the northwest Pacific.

In the A1B simulations with a fast collapsed NADW cell (from now on referred to as *A1B-off*) a strong cooling southeast of Greenland is simulated. Strong warming occurs in the northwest Pacific and in the Ross Sea (>12 K), due to enhanced convection.

In the A2 simulations the surface warming pattern is very similar to the A1B-off. The Arctic warms by 8-9 K. A warming of more than 11 K occurs in Somalia, northeast Canada, the northwest Pacific, and the Ross Sea. A cooling of 5 K is simulated at the southeast coast of Greenland.

In all greenhouse simulations the hydrological cycle is stronger than in CTRL. Over the years 2801 to 3000, the global mean of precipitation increases by 3% (B1), 7% (A1B) and 12% (A2). The rate of precipitation changes to the temperature changes increases with increasing warming: it is 2.0%/K in B1 and 2.4%/K in A2. These values are relatively high when compared with other models.

5.4 Evolution of the Greenland Ice Sheet (GrIS)

5.4.1 Regional climate change in Greenland

As in the stabilisation scenario simulations, the climate change over the Greenland ice sheet is the result of the combination of global warming due to the high concentration of greenhouse gases and the regional signal associated with changes in the strength of the MOC. The warming signal is enhanced in the northern high latitudes via the snow and ice albedo feedbacks. The regional cold signal associated with the changes in the MOC has its centre of action southeast of Greenland. These two strong signals produce a strong gradient of temperature anomalies over the ice sheet, with high warm anomalies in the north, and modest positive/cold anomalies in the south.

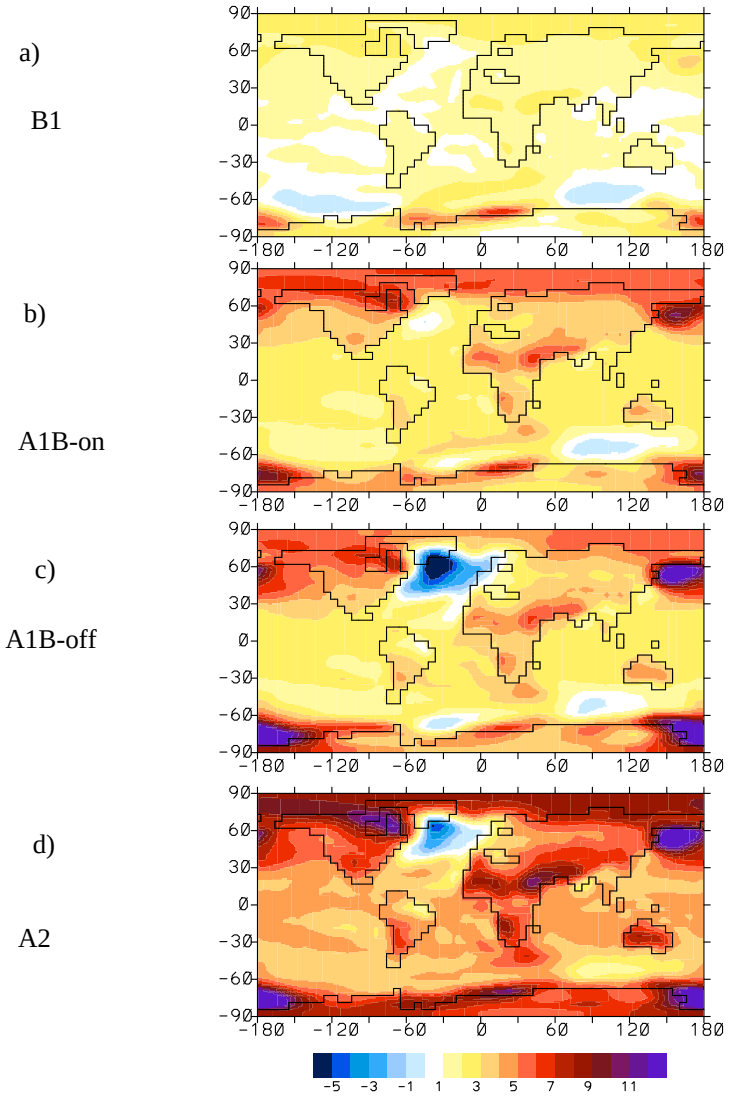

Figure 5.3: Global distribution of changes in the annual mean near-surface temperature [K] for the simulations compared to CTRL. Years 2801 to 3000.

Temporal evolution of the mean summer temperature integrated over the area of the reference GrIS

In the following, the temporal evolution of the mean temperatures integrated over the area of the control GrIS will be analysed, with focus on the summer anomalies. The magnitude of summer anomalies in the perturbed climates of the SRES scenario simulations is, in general, weaker than the magnitude of winter anomalies. This applies both for positive and negative anomalies (fig. 5.4).

In the simulations for the scenario B1, the ice sheet warms gradually until year 2500, when the summer mean temperature anomaly over the ice sheet is close to 2 K. Between years 3000 and 4000, the anomaly follows a slightly negative trend, and it is approximately 1.5 K averaged over the period 3800-4000.

The climate change over the Greenland ice sheet is extremely different among different simulations for the same scenario A1B. These huge differences in atmospheric conditions are directly related to the occurrence/non-occurrence of the collapse of the MOC.

The climate over Greenland in the simulations A1B-on and A1B-off is similar until year 2100-2200. From then, the summer temperature anomalies from the two simulations A1B-off drop abruptly. The summer mean temperature anomaly over the ice sheet becomes negative. A minimum value of -1.2 K is reached in the year 2300-2400. Then the temperatures begin to increase again, until stabilising at approximately a mean value of 0 K. From year 3000, the negative anomalies grow, stronger from year 3400 onwards. In 4000, the mean temperature anomaly over the ice sheet is close to -2 K.

Very differently, during the two simulations A1B-on the summer temperature anomaly averaged over the ice sheet is always positive. A decrease of temperatures is simulated between 2200 and 2400 only in A1B_2, while temperatures increase in A1B_1. This differences are due to a stronger weakening of the NAMOC in the simulation A1B_2. After 2400, temperatures increase also in A1B_2. By year 2600, the mean summer temperature anomaly over the ice sheet is close to 4 K. The average warming over the ice sheet is stronger between 2600-2900 than the average warming in the simulation with the SRES scenario A2. From year 2900 onwards, summer temperatures over Greenland in A1B-on begin to decrease. During the years 3200-4000, the mean summer temperature anomaly as compared to CTRL is quite stable, approximately 3 K. In the simulation A1B_4, with a "late" collapse of the NAMOC, temperatures increase until year 2500, and then decrease as consequence of the regional cooling associated with the strong weakening of the NAMOC (fig. 5.2).

The summer temperatures in the simulation A2 are similar to those from the

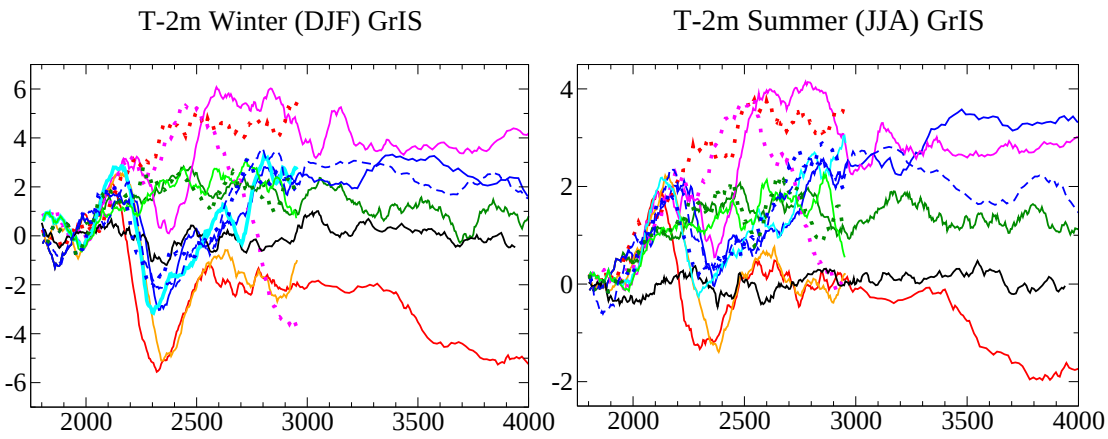

Figure 5.4: (a) Time series (20-years running mean) of near-surface winter and summer temperature changes averaged over the area of the GrIS in the reference simulation CTRL. The temperature change has been reduced to the standard topography of CTRL by applying a height correction with a lapse rate of -6.5°C/km. Colours as in fig. 5.2.

simulation A1B-on until approximately the year 2100. This similarity is due to similar global warming signal and similar strength of the North Atlantic MOC (fig 5.2). After 2100, the MOC weakens by some Sverdrups in the simulations A1B-on, but it continues losing strength in A2. The summer temperatures decrease in the simulations A2. From year 2400 an increase of temperatures takes place in A2. This increase is due to the still strong global rise of temperatures. From years 3200 to 3500, the mean summer temperature experiences an increase of more than 1 K. This increase is not related to any change either in the global mean temperature (which is very stable from years 3000 to 4000) or in the strength of the MOC (the MOC does not recover its strength by year 4000 in the simulations A2). This increase is not present either in the simulation A2_1w, where the feedbacks from the ice-sheet to the climate are not included. Hence this increase of temperatures could be related to the modifications of the climate by the ice sheet. This will be discussed afterwards when analysing the feedbacks between the Greenland ice sheet and the climate in these simulations. From year 3500 until year 4000, the mean summer temperature integrated over the Greenland ice sheet does not vary much, the mean value of the anomaly compared to CTRL being approximately 3.5 K.

The two-dimensional pattern of regional climate change over the GrIS

It has been shown that a collapse of the North Atlantic MOC has a strong impact on the regional climate over the Greenland ice sheet. For the same carbon emissions forcing in scenario A1B, the temporal evolution of the mean temperature over the Greenland ice sheet is very different in the case of a reduction of the strength of the NAMOC than in the case of collapse. In the following, the two-dimensional pattern of climate change over the ice sheet in the simulation with active MOC (A1B-on) and in the simulation with collapsed MOC (A1B-off) will be compared. The two-dimensional pattern of warming from simulation A2 will be also analysed in order to weight the contribution to the climate over Greenland of a strong greenhouse forcing and the event of the collapse of the NAMOC. The analysis will focus on two atmospheric fields: summer temperature anomalies and annual precipitation changes (fig. 5.5). The focus on summer temperature anomalies is justified by the fact that summer is the season of highest interest for the mass balance, since surface melting takes place during this season.

Differences for the A1B scenario in the cases of active/collapsed NADW cell

The pattern of changes in the near-surface temperatures in A1B-on and A1B-off averaged over the period 2800-3000 shows a strong gradient over Greenland, with maximum in the north-west direction. In A1B-on, the temperature anomalies are positive everywhere over Greenland, ranging from a minimal warming of +1 K in the southeast to a maximal warming of 5 K in the north. Temperature anomalies exceed 4 K in most of the northern half of the island.

In A1B-off, the southern half of the island experiences a cooling. Negative anomalies are minimal in the southeast (-4 K). The warming exceeds +2 K only over a small area in the northwest.

In A1B-on, the changes in annual precipitation are positive everywhere over the ice-sheet, exceeding 100 mm/yr over most of the island. Precipitation rates are lower than in control over a small area at the southeast of Greenland, over the ocean. In A1B-off, precipitation changes have a similar pattern than summer temperature changes, with a strong northwest-southeast gradient of anomalies. Half of the island receives less precipitation than in control, with the strongest reduction in the southeast. Maximal positive anomalies occur in the northwest.

To summarise these results, the main effect of the collapse of the NAMOC in the perturbed climate corresponding to the greenhouse forcing of A1B is a strong gradient of temperature and precipitation anomalies over Greenland, with negative anomalies dominating half of the area of Greenland, the maximum of the cooling occurring at the southeast coast.

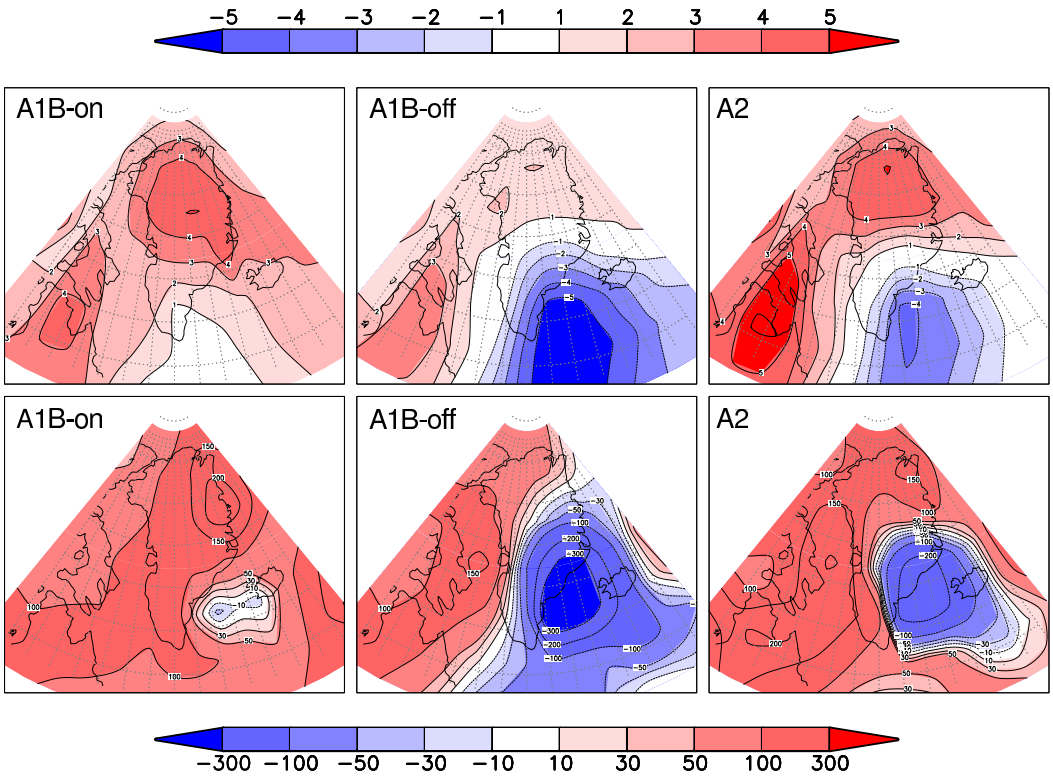

Figure 5.5: Near-surface temperature [K] anomalies in summer (JJA) (top) and annual precipitation [mm/yr] anomalies (bottom) for the longer (performed until year 4000) simulations A1B-on, A1B-off and A2 averaged over the period 2800-3000.

Competition of global warming and regional cooling in scenario A2

The NAMOC collapses in all simulations forced with the scenario A2. On the other hand, the very high carbon emissions prescribed for this scenario produce a strong global warming signal, particularly strong in most of the northern high latitudes. What is the result of the sum of these two climate change signals, the regional cold signal associated with the collapse of the MOC and the global warm signal associated with high concentration of greenhouse gases?

By the year 3000, the global mean temperature has ceased to increase in the simulations A2 and several centuries have passed since the transition in the North Atlantic from an active MOC to a collapsed MOC. At this time, only one sixth of the island approximately has temperatures lower than in control. These negative anomalies occur in the south-east. They are much smaller than the anomalies seen in the simulation A1B-off at this time, since the strong global warming signal of this simulation A2 compensates for part of the regional cooling associated with the collapse of the NAMOC. Temperature anomalies range from -3 K in the southeast to +5 K in the north of the island. The comparison with the pattern from A1B-on shows a weaker warming in the central portion of the ice sheet, but stronger warming in the north. Which of these patterns is more effective for the increase of integrated melting rates over the ice sheet? Does the global warming signal associated with the high emission scenario A2 play a more decisive role in the mass balance of the Greenland ice sheet than the collapse of the NAMOC? These questions will be addressed in the following section.

5.4.2 Changes in the mass balance of the Greenland Ice Sheet

The analysis of the changes in the mass balance of the GrIS has been split into two parts: the first describes the changes until year 3000, the second the changes occurring between years 3000 and 4000.

Until year 3000

The Greenland ice sheet looses mass in all the SRES scenario simulations (fig. 5.6). Until year 2200 the loss of mass is equivalent to less than 5 cm of sea level equivalent (SLE) in all the scenarios. By year 3000 the ice sheet has experienced a very small reduction in the case of the simulations corresponding to the scenario B1 (less than 12 cm SLE in any of the ensemble members). The strongest decay corresponds to the simulations A1B with active NAMOC, with a loss of almost 1 m SLE. Very differently, the loss of mass in the two simulations with scenario A1B

where the NAMOC has collapsed between years 2150 and 2250 is much smaller: approximately one fifth (20 cm SLE). In the simulation where the transition to a non-active NAMOC takes place between the years 2600 to 2750, the reduction of volume by year 3000 is 60 cm SLE. In the simulations from the scenario A2 a similar reduction of volume (approximately 60 cm) is reached in 3000. Thus the scenario with higher carbon emissions (A2) does not produce the maximal reduction in the Greenland ice-sheet volume, due to the regional effects of the collapse of the NAMOC.

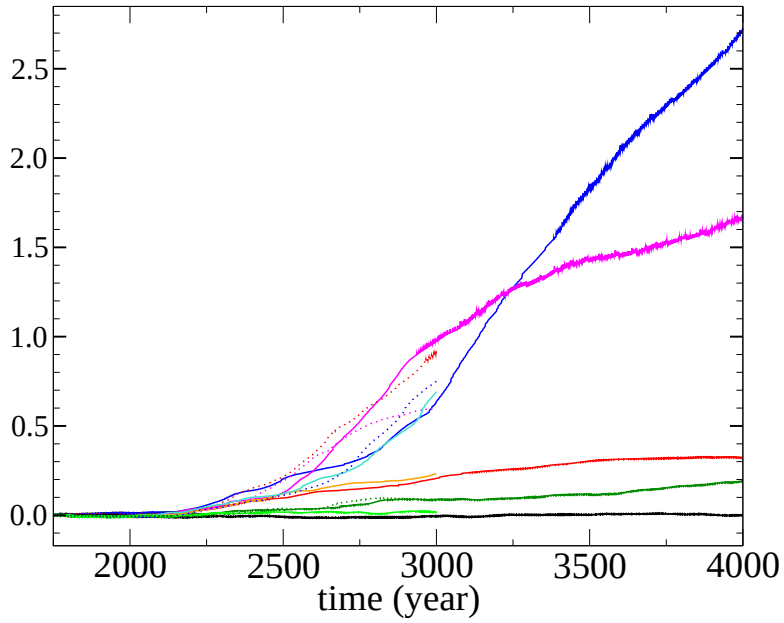

Figure 5.6: Time series of the changes in the volume of the GrIS (units: contribution to sea level rise, in m; negative values indicate sea level drop). Colours as in fig. 5.2.

In the following the two-dimensional pattern of changes of ice-thickness (fig. 5.7) will be analysed for each scenario, as well as the changes in the terms of the mass balance (fig. 5.8). Special emphasis will be given to the differences in the scenarios A1B, where the results of one simulation with active NAMOC (A1B-on) will be compared to one simulation with collapsed NAMOC (A1B-off), in order to explore the impact of the collapse of the NAMOC on the decay of the Greenland ice sheet.

Only one simulation from each scenario was continued until year 4000, except for A1B, for which two simulations were continued. These four simulations will be analysed here.

B1

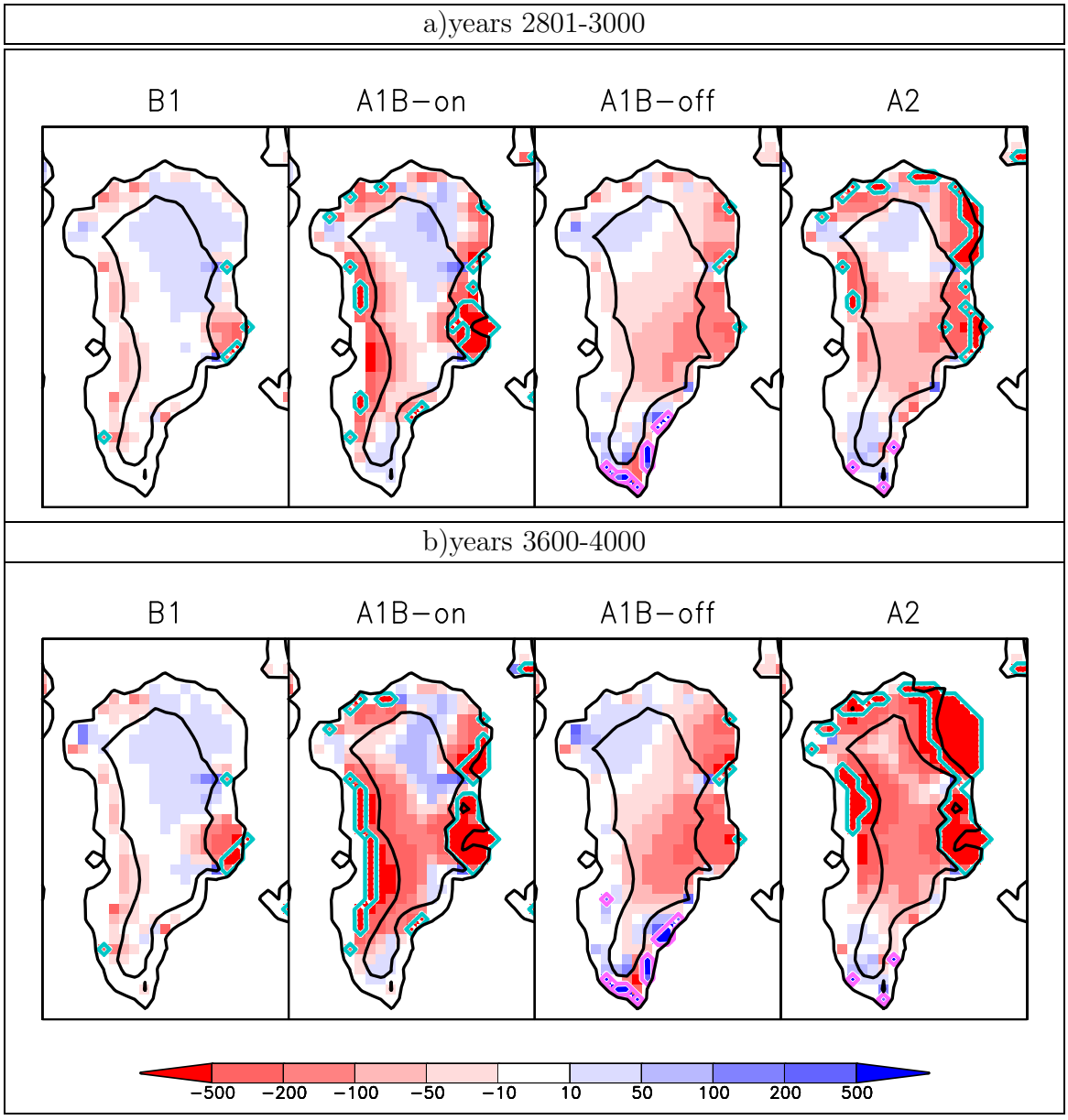

Figure 5.7: Changes in ice thickness [m] and grounding line position (blue line: area becoming ice free; pink line: area becoming iced) in the Greenland ice sheet for the period (a) 2801-3000 and (b) 3600-4000 for the simulations B1, A1B-on, A1B-off and A2 minus CTRL. In black: contour lines for heights z=0 m and z=2000 m.

By the year 3000, very small changes in the topography of the Greenland ice sheet have taken place. A modest reduction of thickness at the margins occurs, with maximal reduction in the east, where some points become ice-free. In the northern half of the ice-sheet, only a slight increase of thickness occurs over most of the high areas as a consequence of enhanced snowfall.

A1B

The pattern of changes in the ice thickness until year 3000 in the simulations A1B-on and A1B-off is extremely different. A1B-on shows a similar pattern than the simulation B1, with reduced ice thickness in the margins of the ice sheet and increased thickness in part of the northern half of the ice sheet, with high elevation. The reduction of thickness is strongest in the east of the ice-sheet, where a big area becomes ice-free, and in the western margin. A vast area in the west at height of more than 2000 m experience a reduction of thickness. This is due to the non-zero summer surface melting over areas higher than 2000 m and to increased horizontal transport of ice from the interior to the margins. This increased flux of ice is due to an increase in the gradient of topography created by increased melting rates on the margins of the ice sheet and increased accumulation in the interior. Thus surface mass balance and the dynamics of the ice are strongly connected: the changes in the surface mass balance (accumulation minus surface melting) are the cause of changes in the topography, which cause changes in the dynamics, and the changes in the dynamics modify the surface mass balance via the height-effect. This height-effect influences both melting and accumulation rates: a) at lower heights higher melting rates take place, b) accumulation rates depend on the height via the height-desertification effect -less precipitation falls in higher areas- and changes in the fractionation of precipitation into rain and snow.

During the period 2801-3000, accumulation changes in A1B-on are positive everywhere over the ice-sheet. Surface melting is high over all areas lower than 2000 m, except over the southern tip of Greenland, where the increase of temperatures is very low due to the regional negative temperature anomalies associated with the weakened NAMOC. Maximum additional melting rates occur close to 70°N, on the east and west margins. Non-zero melting rates occur over the Greenland plateau at heights of more than 2000 m, in the central east part of the ice sheet. The changes in topography induce a stronger horizontal flux of ice from the interior of the ice sheet to the margins with respect to the fluxes in control. This increase occurs everywhere in the ice sheet.

The changes in the surface mass balance of the simulation A1B-off are very different to those in A1B-on. Surface melting increases only in the northern half

of the ice sheet, while the rest experiences an important reduction. The increase in the northern half is much lower than in A1B-on. Here melting rates are usually not higher than 0.5 m/yr compared to those from CTRL. Accumulation rates are lower than in control over more than half of the ice sheet. The reduction in snowfall is stronger at the east. Only the northwest and the low areas of the souther tip receive more accumulation than in control. At the southern tip this increase is due to a higher rate of precipitation falling as snow than in control. This is caused by lower temperatures there. Higher thickness of the ice at these low-elevation areas contribute to the decrease of temperatures via the height-effect. The changes in the gradient of topography and distribution of thicknesses caused by the changes in the surface mass balance produce a reduction of the horizontal flux of ice from the interior to the margins in the southern half of the ice-sheet.

As a result of the important differences between the terms in the mass balance of A1B-off and A1B-on, the changes in the pattern of ice thickness also differ very much. In A1B-off, the central and north-east part of the Greenland ice sheet experience a reduction of the thicknesses which is due, in the high areas, to decreased accumulation, and in the margins, to decreased accumulation combined with higher melting rates than in the control run. Only an area in the northwest and the southern tip experience an increase in the ice thickness. In the northwest, it is driven by enhanced accumulation. In the south, it is driven by increased snowfall (due to the reduction of the ratio of precipitation falling as rain) and by reduced melting rates. The ice sheet advances to new grid-points at the south of Greenland.

A2

The pattern of ice thickness changes in A2 by year 3000 shows a similar distribution to that of A1B-off. Reduced accumulation rates over the central part of the ice sheet around 70°N produce a reduction of thickness there. Over the rest of the ice-sheet, accumulation rates are higher than in control. Thus the area of reduced accumulation is smaller in A2 than in A1B-off, and does not include, for instance, the north-east of the ice sheet.

Surface melting rates are quite high over most of the low-elevated areas, except the southern tip (south of 65°N), where lower temperatures than in CTRL cause a reduction of surface melting. The area of positive surface melting rates extends very far into the Greenland plateau in some places at the northern half of the ice sheet. The melting rates in the central part of the ice-sheet are lower than in A1B-on, and the reduction of thickness there is consequently lower as well. Some grid points become ice free, although its number is smaller than in A1B-on. Over the northern third part of the ice sheet, however, the temperature forcing is

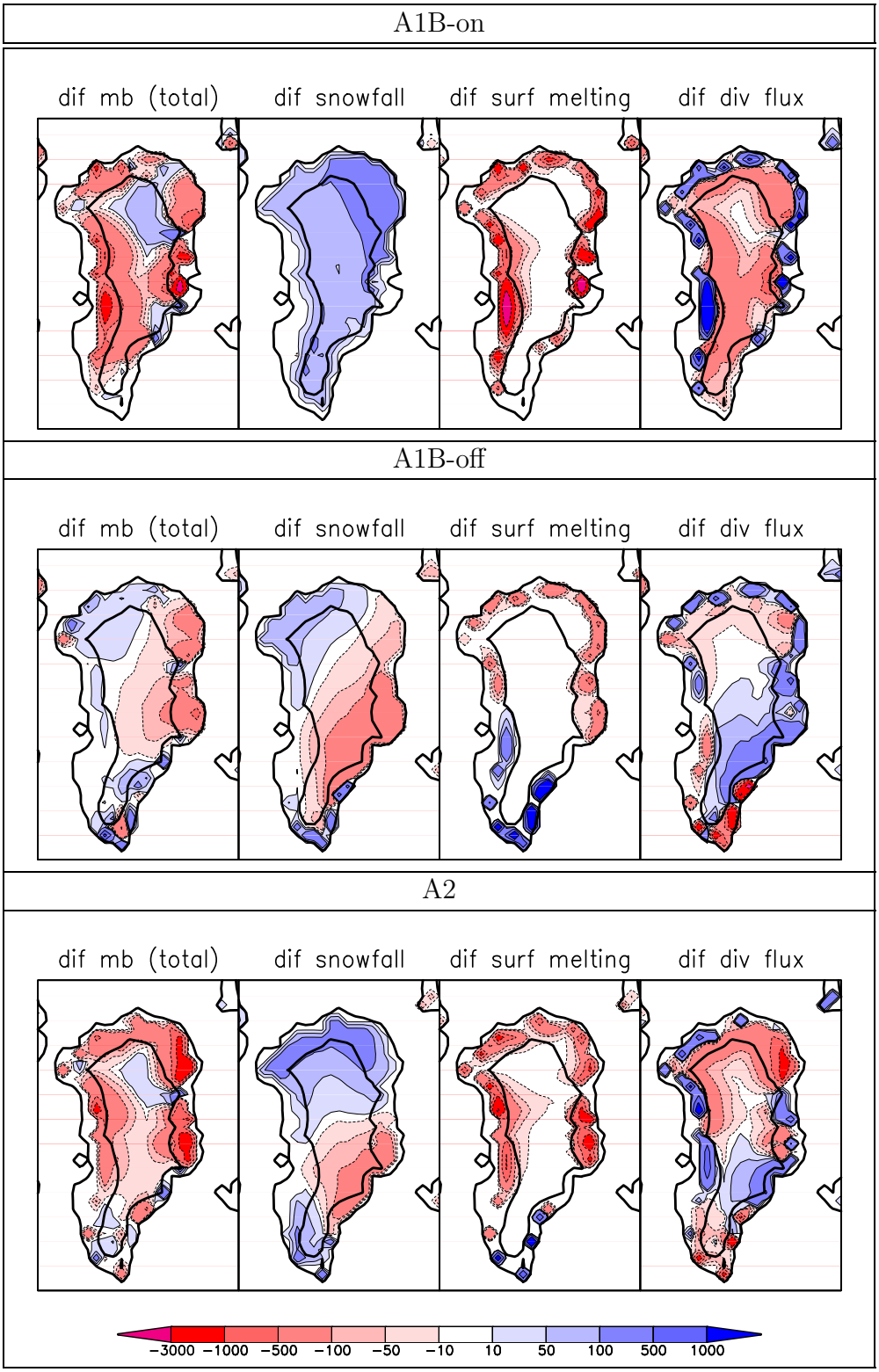

Figure 5.8: Comparison of changes in the mass balance [mm WE/yr] of Greenland for simulations A1B-on, A1B-off and A2 averaged over the period 2801-3000 and compared to CTRL: a)total mass balance change in the column of ice (net sum of all positive and negative terms including advection), b) surface accumulation (snowfall), c) surface melting, and d) changes in the horizontal transport.

stronger in A2 than in A1B-on, and so are the melting rates. Most of the original north-east margins of the ice sheet become ice free in the year 3000. Several grid points become ice-free also in the north and north-west.

The pattern of changes in the horizontal flux of ice varies spatially very much. Over the northern third of the ice sheet, increased accumulation in the interior and increased ablation in the margins drive an increase of the transport from the interior to the margins. The increase of thicknesses in the southern tip drives a stronger flux also. In the central part around 70°N, the flux decreases due to the reduction of ice thickness.

To conclude, the reason for the stronger decay of the volume of the ice sheet in the simulation A1B-on than in A2, where the global warming signal is significantly stronger but the NAMOC collapses, are the stronger melting rates in the central part of the ice-sheet. The changes in the northern third of the ice sheet are stronger in A2, but they do not surpass the magnitude of the strong loss of mass in the eastern margin of the central part of the ice sheet of A1B-on.

After year 3000

By the year 4000, the loss of volume of the ice sheet in the simulation for the scenario B1 is only 30 cm. The loss of mass occurs mainly at the east of the ice sheet, around 70°N. The distribution of ice thickness is essentially unchanged with respect to that at year 3000, except for this area in the east. In the simulation A1B-off, the distribution of ice thickness is similar to that in 3000 as well, but with stronger amplitude. The changes in the area of the ice sheet are also small. Surface melting rates are lower than in 3000, especially in the northwest (fig. 5.9). Accumulation rates are similar to those at year 3000, and also the horizontal fluxes of ice are similar.

While in 3000 the strongest loss of volume took place for the simulations A1B with active NADW formation, in 4000 the volume change is maximal for A2, with a loss of 2.7 m SLE, which represents roughly 1/3 of the original volume of the ice sheet. From year 3000, an acceleration of the loss of mass takes place in A2. Most of the loss of ice takes place in the northeast of the ice sheet. At the easternmost part of Greenland, the whole area at height lower than 2000 m has become ice-free. The area of the ice sheet with more than 2000 m height is considerably reduced in the northern half. The drainage of ice from the interior to the margins of the ice sheet has increased strongly in the northern half of the ice sheet, especially in the northeast. There this increased flux brought more ice to the ablation area, where it was melted, and lowered the originally high areas of the interior. The area with positive surface melting rates expanded into the interior in the north of

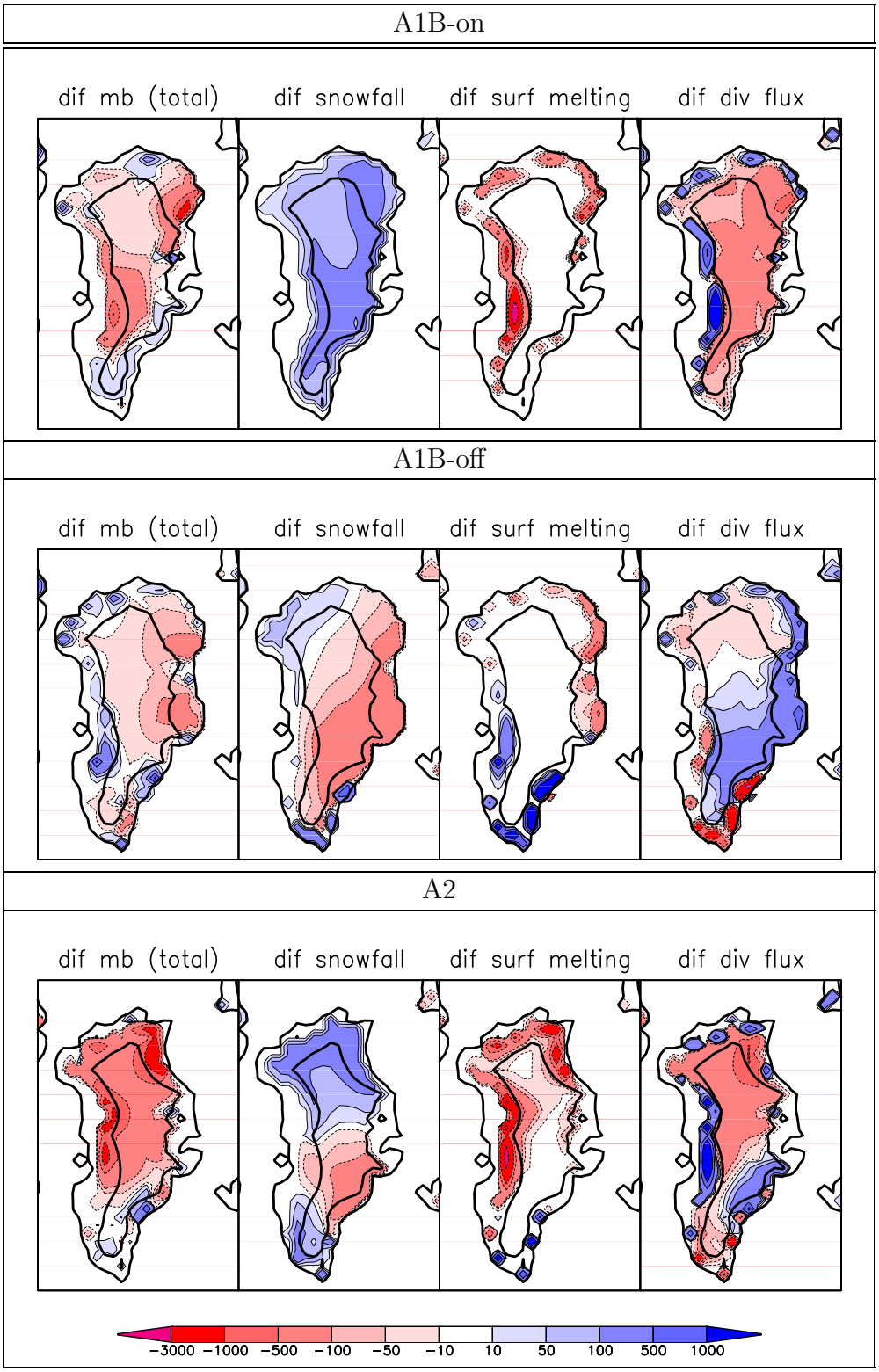

Figure 5.9: Comparison of changes in the mass balance [mm WE/yr] of the GrIS for simulations A1B-on, A1B-off and A2 averaged over the period 3600-4000: a) total mass balance change in the column of ice (net sum of all positive and negative terms including advection), b) surface accumulation (snowfall), c) surface melting, and d)changes in the horizontal transport.

the ice sheet. Accumulation rates are similar in year 4000 to those in 3000.

The rate of decay of the Greenland ice sheet in the simulation A1B-on is reduced strongly from after 3000. By 4000, the loss of mass is 70 cm SLE more than what was lost in 3000. The loss of ice takes place mainly in the east and west margins of the central part of the ice sheet. In the central part on the plateau, most of the area is more than 100 m lower than in CTRL. Accumulation rates are higher than in 3000. Surface melting rates are lower than at year 3000, specially in the northern part. There is no surface melting over most of the area higher than 2000 m.

5.4.3 Feedbacks between the Greenland ice sheet and climate

It will be distinguished here between the feedbacks between the Greenland ice sheet and the ocean (via increased freshwater fluxes from the decaying ice sheet) and feedbacks between the Greenland ice sheet and the atmosphere.

Feedbacks between the GrIS and the ocean

The freshwater fluxes from the Greenland ice sheet to the ocean do not exceed 0.01 Sv before the year 2200 in any of the simulations (fig. 5.10). Between the years 2200 and 2500, the highest fluxes are those of the simulations A1B in which the NAMOC remains active, with values between 0.01 and 0.02 Sv. From years 2500 to 3000 the fluxes of these simulations A1B and the simulations A2 reach the highest values (approximately 0.03 Sv). The freshwater fluxes from the ensemble simulation with scenario A1B where the NAMOC collapses between 2600 and 2750 are drastically reduced from year 2600 and they stay at low levels afterwards. The freshwater fluxes from the simulations A1B-off where the NAMOC collapses are very low.

The total freshwater fluxes into the North Atlantic basin begin to rise very quickly from year 2000, the additional fluxes being more than 0.1 Sv in the simulation A2 by year 2200. The values corresponding to the simulations A1B are approximately 0.08 Sv. The anomaly fluxes continue rising until reaching a maximum approximately by year 3000: 0.2 Sv in the simulations A2, 0.18 Sv for A1B-off, and 0.1 Sv for A1B-on. From year 3000, freshwater fluxes either stabilise or begin a slightly negative trend.

The comparison of the magnitude of the freshwater fluxes from the Greenland ice sheet with the magnitude of the total freshwater fluxes into the North Atlantic basin show that Greenland contributes only to approximately 10% of the total

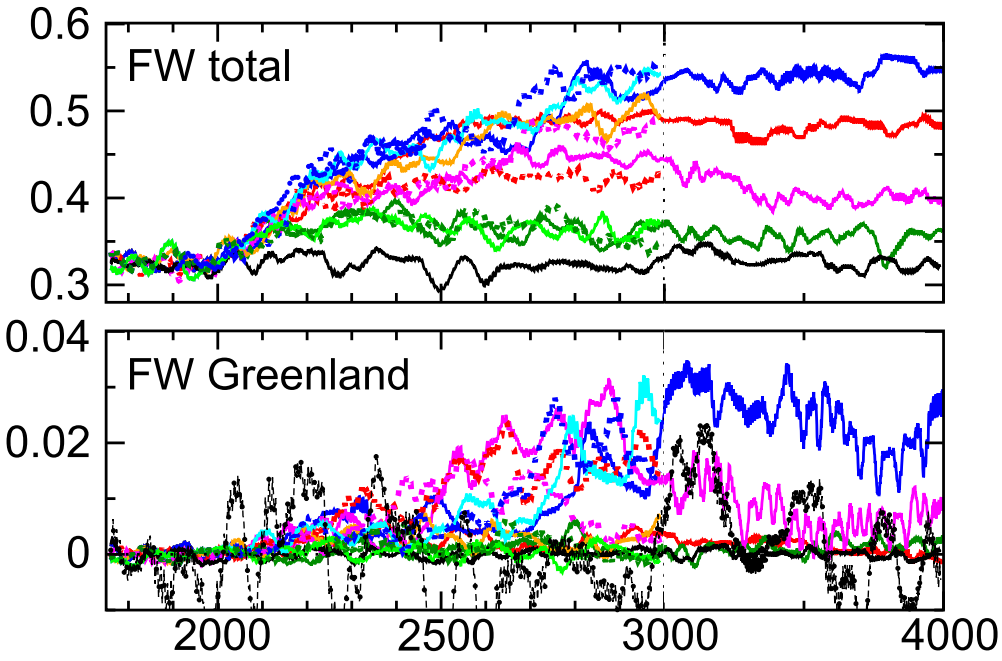

Figure 5.10: Total freshwater fluxes [Sv] into the North Atlantic (upper panel) and freshwater fluxes from the GrIS (lower panel). Note the different time scale from year 3000. Colours as in fig. 5.2. In the lower panel the variability of the CTRL total freshwater fluxes has been also plotted (dashed-dotted black line) in order to compare the signal from the ice sheets to the noise.

change. The signal of enhanced freshwater fluxes is thus dominated by the atmospheric moisture transport. The contribution from the Greenland ice sheet in the simulations is usually smaller than twice the standard deviation of the freshwater fluxes in the control simulation (approximately 0.02 Sv).

The strength of the overturning shows no major differences in the simulations A2 and the simulation A2_1w where the feedbacks from the ice sheets are not included (fig. 5.11). This confirms the minor role played by meltwater fluxes from Greenland in the changes in the ocean circulation that take place in the simulations A2. Nevertheless, in the A1B experiments, which are close to the bifurcation point, the contribution of meltwater from Greenland could have played a role in the transition to the collapsed NAMOC.

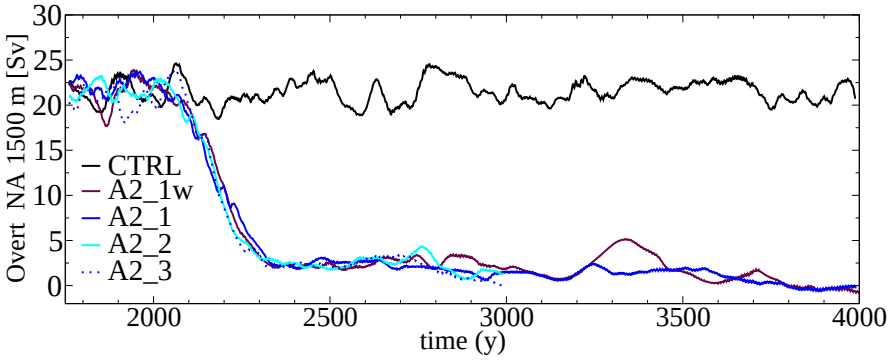

Figure 5.11: Strength of the North Atlantic overturning stream function at 30°N at 1500 m depth for CTRL (black), the three-ensemble simulation of the scenario A2 (blue lines), and for the simulation A2_1w (maroon) where the additional meltwater fluxes are ignored by the ocean model.

Reduction of Greenland meltwater fluxes due to cooling associated with changes in the NAMOC

The reduction of the strength of the overturning in the North Atlantic has been shown to play a very important role for the climate of Greenland and the mass balance of its ice sheet. This tight link between the ocean circulation and the freshwater fluxes from Greenland via changes in the surface melting over the ice sheet was proposed in the previous chapter dealing with stabilisation scenario simulations as *a potential stabilising feedback for the ocean circulation.* The five-member ensemble simulations for the scenario A1B-on have provided an optimal frame to study in more detail this suggested mechanism. freshwater fluxes from the GrIS have been shown to be very weak in three of the ensemble members from the time when the ocean circulation experience the transition to a collapsed NAMOC. In the ensemble member A1B-on where the overturning substantially weakens and

then recovers from year 2500, a drastic increase of the meltwater fluxes is seen. This shows, at least in this Earth System Model, the *high sensitivity of the mass balance of the Greenland ice sheet to the regional climate change caused by changes in the North Atlantic Meridional Overturning Circulation.*

Feedbacks between the GrIS and the atmosphere

In order to evaluate the role of the feedbacks between the Greenland ice sheet and the climate in the mass balance of the ice sheet, a simulation where those feedbacks are not included was performed (A2_1w). This simulation will be analysed in detail in the next chapter. For the simulations B1 and A1B no similar simulation was performed. A proper analysis of the impact of the ice sheets on climate is not possible without reference simulations not including this impact. Nevertheless, a simple analysis will be done here regarding the changes in the albedo of the Greenland ice sheet due to the changes experienced by the ice sheet in these simulations (fig. 5.12).

The albedo over the Greenland ice sheet can change due to changes in the surface temperature and to changes in the glacier mask. This dependence of the albedo of the atmospheric model on changes in the surface temperature is meant to account for the presence of meltwater, which lowers the albedo. The albedo of the ice sheet from the control simulation has small variations due to the variability of the simulated control climate.

In B1, the albedo of the area of the reference GrIS slightly decreases until year 3000. This decrease is due to the increase in surface temperatures. Shortly after year 3000, one of the points in the atmospheric grid becomes ice-free. This lowers the mean albedo further.

The albedo of the simulation A1B-off decreases during the first centuries of the simulation, but from 2100 onwards, following the collapse of the NAMOC, it begins to increase. From year 2200 onwards, the albedo is higher than in the control run. No changes in the glacier mask occur in this simulation.

In simulations A1B-on, the albedo first decreases in both simulations. In A1B_1, it slightly increases during the period 2300-2400 due to regional cooling associated to substantial weakening of the NAMOC (fig. 5.2). Between 2450 and 2600, when local temperatures in Greenland rise until reaching maximum values (fig. 5.4), the albedo decreases substantially. One grid point becomes ice-free between years 2500 and 2600. From year 2600 onwards the albedo does not experience substantial changes. During this period another change in the glacier mask takes place. The albedo of the simulation A1B_4, with a "late" collapse of the NAMOC, behaves similarly to the albedo of A1B-on until year 2500, when the

NAMOC from A1B_4 begins to weaken abruptly. After 2500, the albedo increases substantially, reaching values similar to CTRL by year 3000.

The mean albedo of the simulations A2 does not differ substantially from the albedo of control until year 2900. After 2900, the albedo decreases almost steadily. By 4000, the albedo of A2 is the lowest of all the simulations. Several glacier mask transitions take place between years 2900 and 4000. The albedo of the simulation A2_1w is very similar to the albedo of A2 until 2900. From that year and until year 4000, the albedo of A2_1w increases slightly. Since the changes in glacier mask, topography and freshwater fluxes caused by changes in the ice sheets are not given to the rest of the ESM in the simulation A2_1w, the changes in albedo are only caused by changes in surface temperature which do not include the signal due to topographic changes (height-signal). This indicates that, in A2, most of the change in albedo taking place after year 2900 is dominated by changes in topography and area of the ice sheet. After 3000, the summer near-surface temperature anomaly in A2 has equal or stronger magnitude than the winter near-surface temperature anomaly (fig. 5.4). This is not the case in A2_1w. The changes in albedo are probably playing a role in this intensification of the summer warming signal in A2 from year 3000. Nevertheless, a more detailed analysis would be needed to isolate the contribution of albedo from the contribution of other processes, e.g. changes in the general circulation of the atmosphere caused by topographic changes of the GrIS.

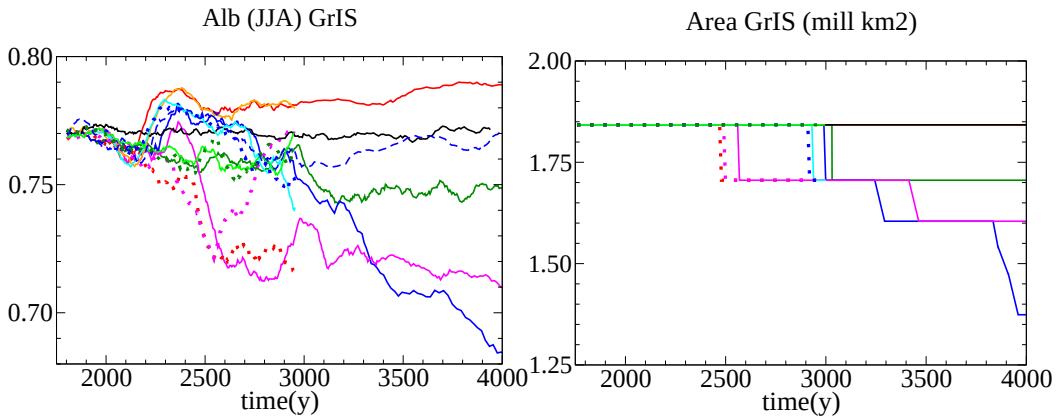

Figure 5.12: (a) Changes in the albedo for the area of the reference Greenland ice sheet for CTRL and the SRES scenarios B1, A1B and A2 until year 4000. (b) Changes in the area [millions km^2] of the Greenland ice sheet in the atmospheric grid for the same simulations of (a). Colours as in fig. 5.2.

5.5 The evolution of the Antarctic Ice Sheet (AIS)

5.5.1 Regional climate change over the area of Antarctica

The temperatures over Antarctica increase in all the simulations (fig. 5.13). The magnitude of the temperature changes with respect to CTRL averaged over the reference AIS from CTRL is stronger in winter (JJA) than in summer (DJF), which is the season which is important regarding changes in the surface melting.

The AIS-mean summer temperature increase by the year 2300 is 2-3 K in all the simulations. From then, the AIS-mean summer temperature does not change much in the simulation B1. After 3000 it begins to decrease slightly. By the year 4000, it is close to 1 K. In the simulation A2, the AIS-mean summer temperature increases strongly after 2300, reaching 6 K by the year 3000. From then, it remains more or less unchanged. In the simulations A1B, the AIS-mean summer temperature increases from year 2300 until 3.5 K in A1B-on and 4 K in A1B-off. The slightly stronger warming in the case of the simulation with a collapsed NAMOC is related to enhanced convection in the Southern Ocean. In 4000, the temperature anomaly is close to 4 K.

Precipitation rates increase in all the simulations.

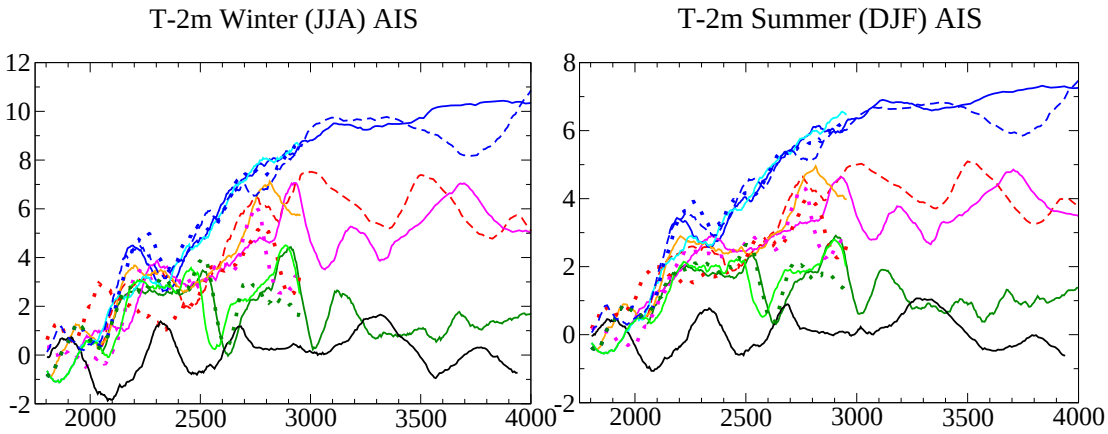

Figure 5.13: (a) Time series (20-year running means) of near-surface winter and summer temperature changes averaged over the area of the AIS in CTRL. The temperature change has been reduced to the standard topography of CTRL by applying a height correction with a lapse rate of -6.5°C/km. Colours as in fig. 5.2.

5.5.2 Changes in the mass balance of the Antarctic ice sheet

The Antarctic ice sheet gains mass in all the simulations (see fig. 5.14). The control simulation is showing a slight drift of 0.2 m SLE in 1000 years. By the year 4000, the mass gain is 0.7 m SLE in B1, between 2 and 2.2 m in the A1B simulations, and 3.2 m SLE in A2.

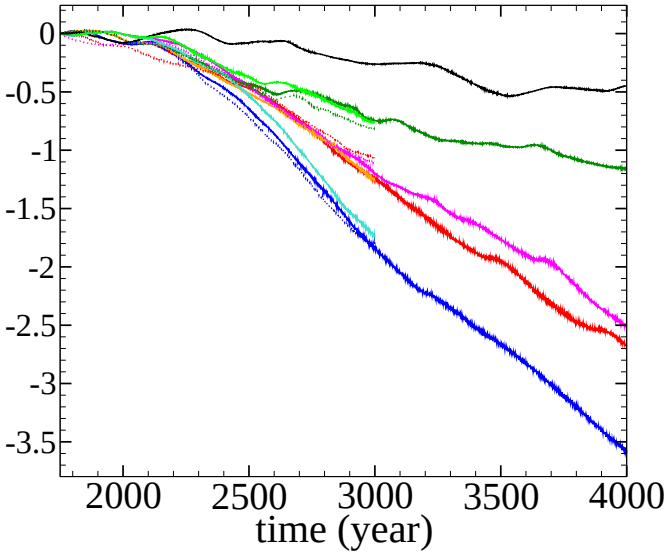

Figure 5.14: Time series of the changes in the volume of the AIS (units: contribution to sea level rise, in m; negative values indicate sea level drop). Colours as in fig. 5.2.

In 3000, the pattern of changes in ice thickness shows increased thickness everywhere except for some low areas at the margins (fig. 5.15). Some points become ice-free at the margins as well. The increase in thickness of most of the area is clearly stronger in A2 than in A1B.

By 4000, the thickness of most of the areas in the Antarctic ice sheet has increased with respect to the thickness one thousand years before. More points have become ice-free, specially in the Antarctic Peninsula. In A2, the loss of ice volume and area in the Antarctic Peninsula is particularly strong.

The changes in the mass balance (fig. 5.16) are dominated by changes in the accumulation. Surface melting increases at some points at the margin of the ice sheet in the A1B and A2 simulations. No melting occurs at heights of more than 2000 m, since the temperatures are well below zero during the summer season in the perturbed climates. No important changes occur in the horizontal flux of ice

in the interior of the East Antarctic Plateau. Most of the changes occur close to the isoline of 2000 m height. Increased thickness and increased topographic gradients due to the slight increase of surface melting at same low areas drive a slight increase in the horizontal transport of ice to the margins.

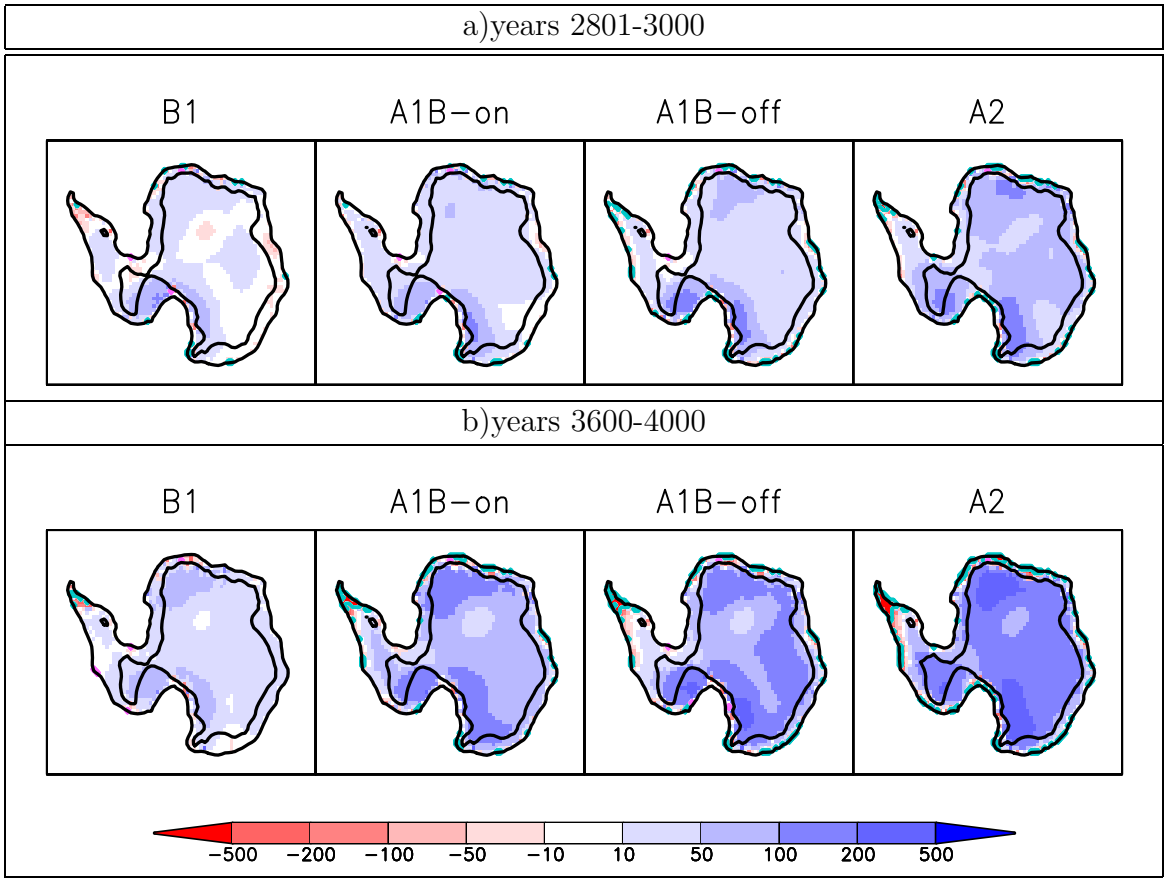

Figure 5.15: Changes in ice thickness [m] and grounding line position (blue line: area becoming ice free; pink line: area becoming iced) in the Antarctic ice sheets for the period (a) 2801-3000 and (b)3600-4000 for the simulations B1, A1B-on, A1B-off and A2 minus CTRL. In black: contour lines for heights z=0 m and z=2000 m.

5.6 Conclusions

The main conclusions that can be drawn from this study are summarised in the following:

- As in the stabilisation scenario simulations performed with this ESM, the contribution of meltwater fluxes from the Greenland ice sheet to the changes in

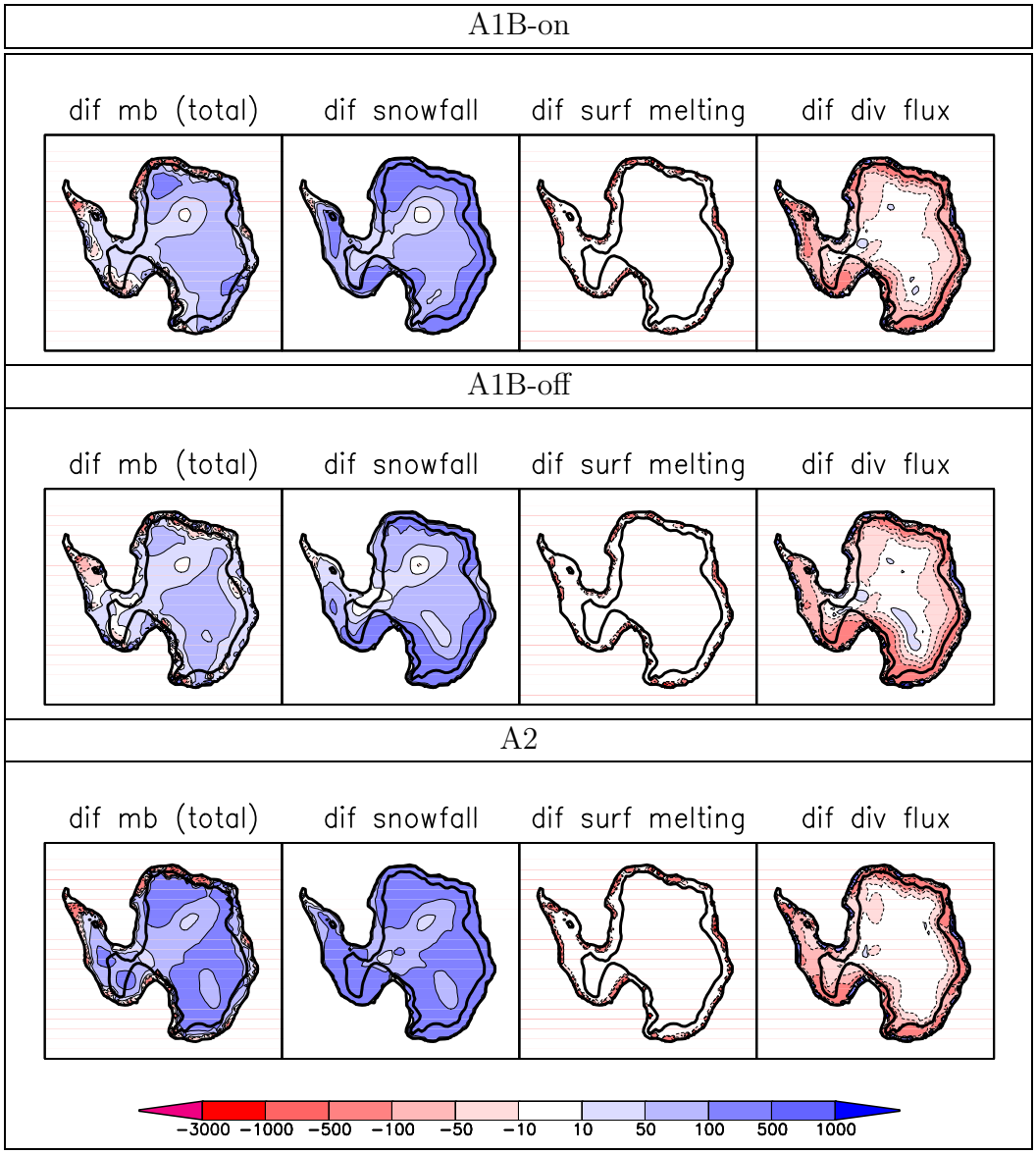

Figure 5.16: Comparison of changes in the mass balance [mm WE/yr] of the AIS for simulations A1B-on, A1B-off, and A2 averaged over the period 3600-4000 and compared to CTRL: a) total mass balance change in the column of ice (net sum of all positive and negative terms including advection), b) surface accumulation (snowfall), c) surface Melting, and d) changes in the horizontal transport.

the NAMOC have been shown to be small in comparison with the atmospheric moisture fluxes. Thus the main driver of the strong changes in the NAMOC in the simulations forced with SRES scenarios A2, A1B and B1 is the enhanced atmospheric moisture transport into the North Atlantic Basin.

- Nevertheless, the melting of Greenland could be playing a role in the fate of the NAMOC in the A1B scenario simulations, where the ocean is close to the bifurcation point.

- The surface melting of the Greenland ice sheet is much weaker in the A1B-off (collapsed NAMOC) simulations than in the A1B-on (with active NAMOC). ***The mass balance of the Greenland ice sheet shows a strong sensitivity to changes in the strength of the NAMOC.*** The reduction of meltwater fluxes from Greenland due to the regional climate change associated with a weakening of the NAMOC can be identified as a *negative feedback for the decay of the Greenland ice sheet* and a *potential stabilising mechanism for the NAMOC,* as suggested in the previous chapter.

- Storage of water by the Antarctic ice sheet compensates or exceeds the sea level rise due to the Greenland contribution. The dynamics of outlet glaciers, ice streams and ice shelves are not modelled in this approach, but they could potentially play an important role in the future mass balance of the Antarctic ice sheet. Therefore the results shown here should be interpreted carefully. The wet bias of the atmospheric model caused by the course resolution of this model approach (T21) also play a role in the strong storage of water in Antarctica, since precipitation rates are corrected with anomalies instead of ratios.

Chapter 6

Disintegration of the Greenland ice sheet and interactions with the climate system

This chapter addresses two main questions: 1) the modifications, if any, that potential changes of the Greenland ice sheet due to anthropogenic climate change can produce in the climate system and 2) how these modifications could alter the mass balance of the Greenland ice sheet. The second question leads to the identification of feedbacks between the Greenland ice sheet and the climate system.

In the previous chapters, special emphasis was placed on the feedbacks between the Greenland ice sheet and climate via changes in the meltwater fluxes. This chapter will focus mainly on processes related to the atmosphere.

In order to address the previously formulated questions, mainly two simulations will be analysed. The first is a multi-millennia simulation corresponding to the SRES scenario A2 described in the previous chapter. By (calendar) year 7000 the Greenland ice sheet has almost disappeared in this simulation. A second simulation is analysed for the same scenario. In this simulation the modifications of freshwater fluxes, glacier mask and topography by the Greenland ice sheet are ignored by the rest of components of the ESM. These two simulations will be compared in order to identify the presence and importance of feedbacks for the evolution of the GrIS, and in order to explore the impact of changes in the Greenland ice sheet onto the climate system.

The structure of this chapter is as follows. In the first part 1) the evolution of the Greenland ice sheet until its almost complete disappearance under the SRES scenario A2 will be shown, 2) this evolution will be compared to the evolution of the Greenland ice sheet in a simulation where the feedbacks between the ice sheet

and the climate system are not included, 3) the feedbacks between the ice sheet and the atmosphere will be analysed as well as the importance of its contribution to the mass balance budget of the GrIS. In the second part the impact of the disappearance of the Greenland ice sheet on the climate system will be explored. This impact will be compared with pre-industrial climate and the warm climate of the simulation A2.

6.1 Disintegration of the GrIS under scenario A2 and associated feedbacks

6.1.1 Set-up

One of the ensemble simulations for the scenario A2 described in the previous chapter has been prolonged until reaching calendar year 9000. Another simulation A2_1w (1w meaning one-way coupling) has been performed, where the feedbacks between the ice sheets and the atmosphere as well as ocean have been ignored. This simulation reaches steady-state by year 7000, and it was stopped at this time. The atmospheric data from the period 6000-7000 are repeated until year 9000 for the forcing of the ice sheet model in A2_1w. This is done under the assumption that the climate of A2_1w will be stable during the period 7000-9000, which is a reasonable assumption.

6.1.2 Global climate change: atmospheric carbon dioxide, atmospheric changes

The highest atmospheric concentration of CO_2 in the simulation A2 (approximately 1680 ppmv) is reached approximately at year 2500 (see figure 6.1a). Maximum global warming occurs around year 3000, when the global mean temperature is about 5°C higher than in CTRL (see figure 6.1b). This time difference between the maximum of the atmospheric concentration of carbon dioxide and the temperature maximum is related to the time-scales of the deep ocean, where the heat is stored and then progressively released. During the period 4000-6000 the global mean temperature decreases by 1.5°C, and afterwards remains stable until the end of the simulation.

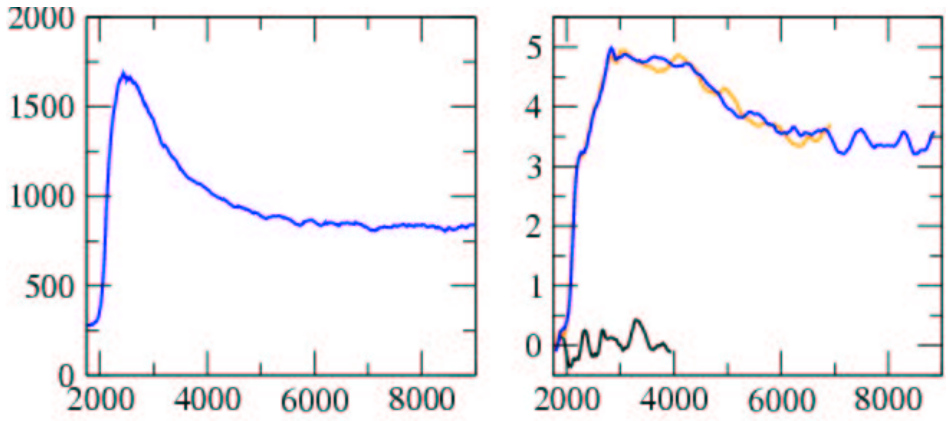

Figure 6.1: Time series of a) CO_2 atmospheric concentration [ppmv] and b) anomalies of global mean temperature to CTRL for the simulations A2(blue) and A2_1w (orange). The black line represents 2250 years of CTRL.

6.1.3 Decay of the Greenland ice sheet

The volume and area of the GrIS (fig. 6.2) evolve similarly in the simulations with two-way coupling (A2) and one-way coupling (A2_1w) until year 3600. From this time onwards, the rate of decay of the ice sheet diminishes significantly in the simulation A2_1w, while it remains unchanged in A2. This happens close to the beginning of the negative trend in the global mean temperature. Until year 3600, in both simulations, area and volume changes decay at a similar pace. After 3600, the area of the ice sheet decays at a slower rate.

Differences in the mass balance around year 3600

The stronger reduction of the Greenland ice sheet in the simulation A2 compared to A2_1w from year 3600 until 4000 is mainly due to differences in the mass balance at the western and northwestern margins of the ice sheet (compare the fig. 6.3 with fig. 5.9 from the previous chapter). The stronger reduction of thickness in the simulation A2 is caused by higher surface melting rates. The area with non-zero surface melting at the northern half of the ice sheet is larger in A2. The melting rates is particularly stronger at the west and north-west margins. The area with negative surface mass balance extends to some parts of the ice sheet at the north-west with heights between 2000 and 2500 m, while the equilibrium line in A2_1w is mostly placed at heights lower than 2000 m (compare the time slices for the years 3500 and 4000 in the figures 6.6 and 6.7).

The changes in the atmospheric forcing leading to this differentiation of the

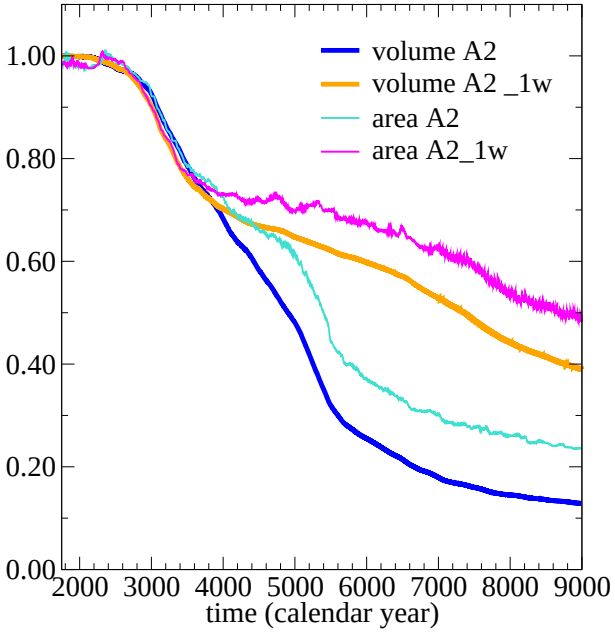

Figure 6.2: Comparison of the GrIS volume and area changes expressed as percentage of the initial ones for the simulations A2 (volume: blue, area: turquoise) and A2_1w (volume: orange, area: magenta).

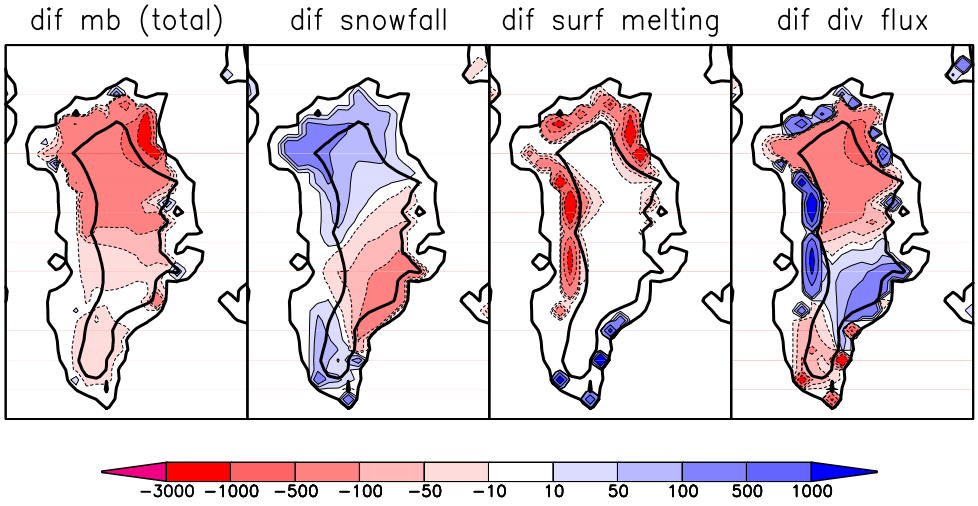

Figure 6.3: Changes in the mass balance of the GrIS [mm WE/yr] for simulation A2_1w averaged over the period 3600-4000: a)total mass balance change in the column of ice (net sum of all positive and negative terms including advection), b) surface accumulation (snowfall), c) surface Melting, and d) changes in the horizontal transport.

surface mass balance by year 3600 will be analysed in the following. Averaged over the period 3450-3950, summer near-surface temperatures over Greenland are higher in A2 than A2_1w (fig. 6.4a). After correcting for the differences in height of both simulations with a lapse rate of -6.5 °C/km, the summer near-surface temperatures of A2 are higher than those of A2_1w by more than 1 K over most of Greenland. Maximum differences of more than 2 K occur at the east coast, because of the high differences in albedo (more than 0.20, see fig. 6.4b) due to the transition of two points in the atmospheric grid from glacier to non-glaciated. Averaged over the area covered by the ice sheet in both simulations, the differences of the albedo of A2 and A2_1w are approximately 0.04.

No signal of increased advection of heat to the ice sheet is seen during this period (not shown), which discards the hypothesis of changes in the atmospheric circulation as the main cause of the extra-warming of the ice sheet in the simulation A2. Thus three main processes could explain the temperature differences:

1) Differences in surface albedo.

2) Underestimation of the height-effect.

3) Other atmospheric processes triggered by the topographic and area changes that have occurred.

Although an extra simulation would be needed to isolate the effect of the albedo from the other processes, albedo changes seem to be the main motor of the differences in the near-surface temperatures between A2 and A2_1w. The mean albedo of the glaciated areas of A2 and the mean albedo of the Greenland ice sheet of A2_1w begin to diverge from each other approximately in the year 3200 (fig. 6.5f). This occurs with similar timing to the differentiation of the summer near-surface temperatures. These facts reinforce the assumption that albedo changes are the main mechanism responsible for the different evolution of the ice sheet in A2 and A2_1w.

The changes in the albedo over the glaciated points of the atmospheric model ECHAM3 are due to the increase of temperatures associated with the reduction of height (see Chapter 2, where the parameterisation of albedo in ECHAM3 is described). This dependence of the albedo with the near-surface temperature averaged over the grid cell aims to account for the low albedo of sub-scale areas at melting point.

The evolution of the Greenland ice sheet between years 4000 and 9000

Between the years 4000-5000, the Greenland ice sheet in A2 decays at approximately the same pace as the previous thousand years. The height of the equilibrium line (separating the areas with net positive surface mass balance from the

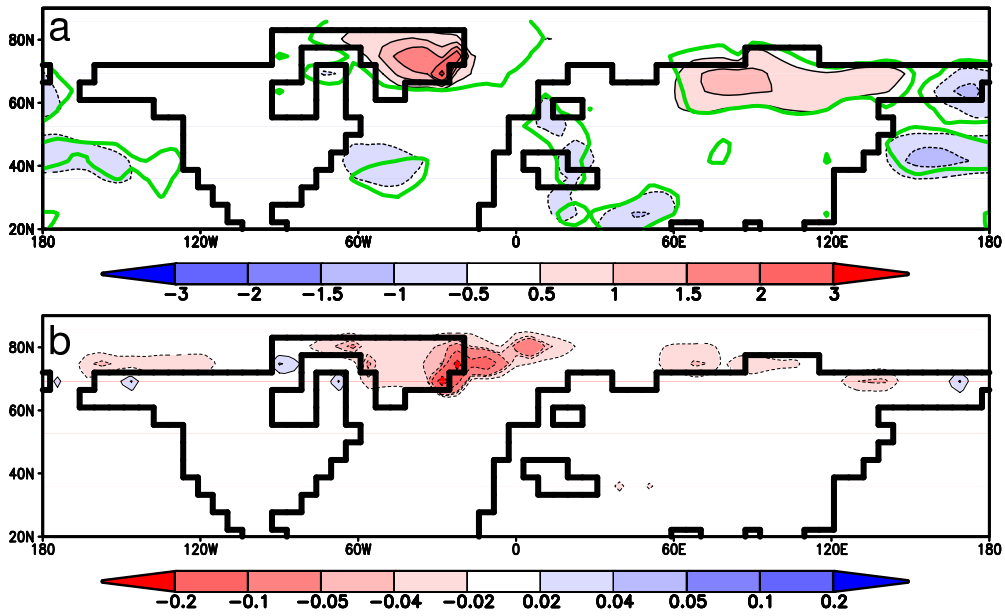

Figure 6.4: Average over years 3450-3950 of: a) Summer (JJA) surface temperature anomaly [K] corrected at the height of the reference ice sheet through a lapse rate of -6.5°C/km and b) summer albedo differences between the simulations A2 and A2_1w. The green line in the first and third panels delimits the areas where the signal is higher than 2.8 times the standard deviation of summer temperature in the control simulation.

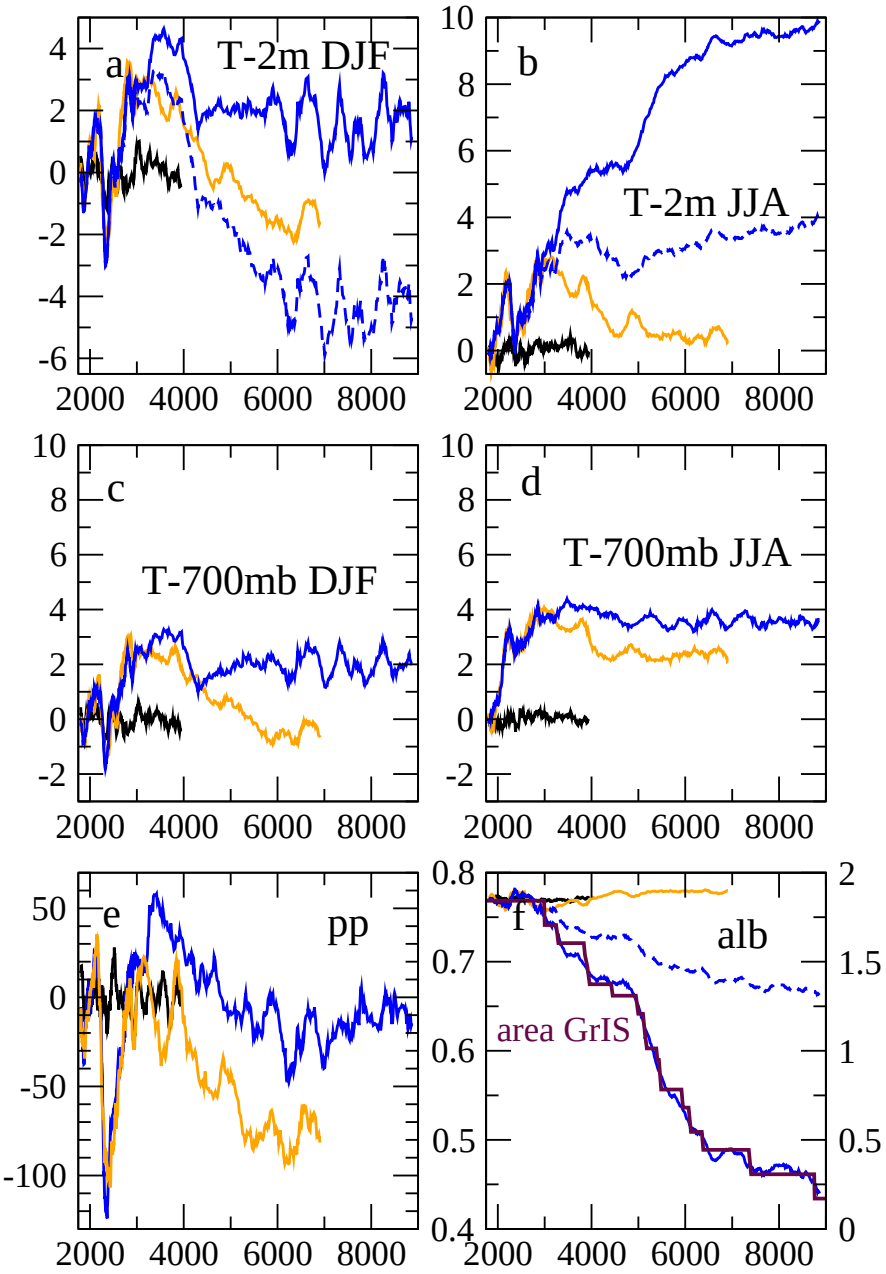

Figure 6.5: Evolution of the anomalies with respect to the CTRL mean for several atmospheric variables integrated over the area of the CTRL GrIS for the simulations CTRL (black), A2 (blue) and A2_1w (orange). Dashed blue lines in a) and b) represent the near-surface temperature corrected at the reference height of control with a lapse rate of 6.5 K/km. a)Mean winter near-surface temperature [K], b)Mean summer near-surface temperature [K], c)Winter 700-hPa temperature [K], d) Summer 700-hPa temperature [K], f)Annual precipitation [mm/yr], h) Mean albedo, ice sheet area in the atmospheric line (maroon line) [mill km^2], and changes of the mean albedo of glaciated points of A2 (dashed blue line).

areas with net negative surface mass balance) is considerably higher in the northern half of Greenland in the simulation A2 than in A2_1w (see figures 6.6 and 6.7). These differences in the position of the equilibrium line are due to higher surface melting melting rates in A2 than in A2_1w.

A period with strong melting rates occurs in A2 between the years 5000 and 5500. During this time, several points of the ice sheet deglaciate on the atmospheric grid. The marginal points of the ice sheet model close to those atmospheric grid points experience increased melting rates due to the warming associated with the changes in surface albedo.

By 5500, the area of the ice sheet is reduced to 1/2 of the original area. Most of the northern half of the ice sheet is ice-free, but the central-east margin, where the bedrock is highest.

By 7000, the ice sheet is reduced to 1/5 of its original volume. The small ice sheet is located at the southern tip and at the south-east coast. There the summer temperatures are lower than in the control simulation, due to the regional climate change associated with the collapsed NAMOC. The topography of the ice sheet at the southern tip of Greenland has stayed almost unchanged since the beginning of the simulation, with its dome being always higher than 2500 m. In 7000, the area of the ice sheet in A2_1w has fallen to 62% of the initial extent and its volume is reduced to 52%.

6.1.4 Ocean-GrIS feedbacks

The feedbacks between the ocean and the ice sheet during the two first millennia of the SRES scenario simulations and during the stabilisation scenario simulations have been discussed in the previous chapters. The evolution of the strength of the NAMOC in the simulations A2 and A2_1w without feedbacks was analysed until calendar year 4000 in the previous chapter. No significant differences in the strength of the NAMOC were found between those two simulations. From year 4000, the NAMOC remains collapsed (not shown) in both simulations A2 and A2_1w. Therefore the meltwater fluxes from Greenland do not play any role in a potential recovery of the strength of the NAMOC from year 4000.

6.1.5 Atmosphere-GrIS feedbacks

The evolution of the global mean temperature is similar in the simulations A2 and A2_1w (fig. 6.1). This indicates that the changes in the mass balance of the global ice sheets do not have a strong impact on global climate.

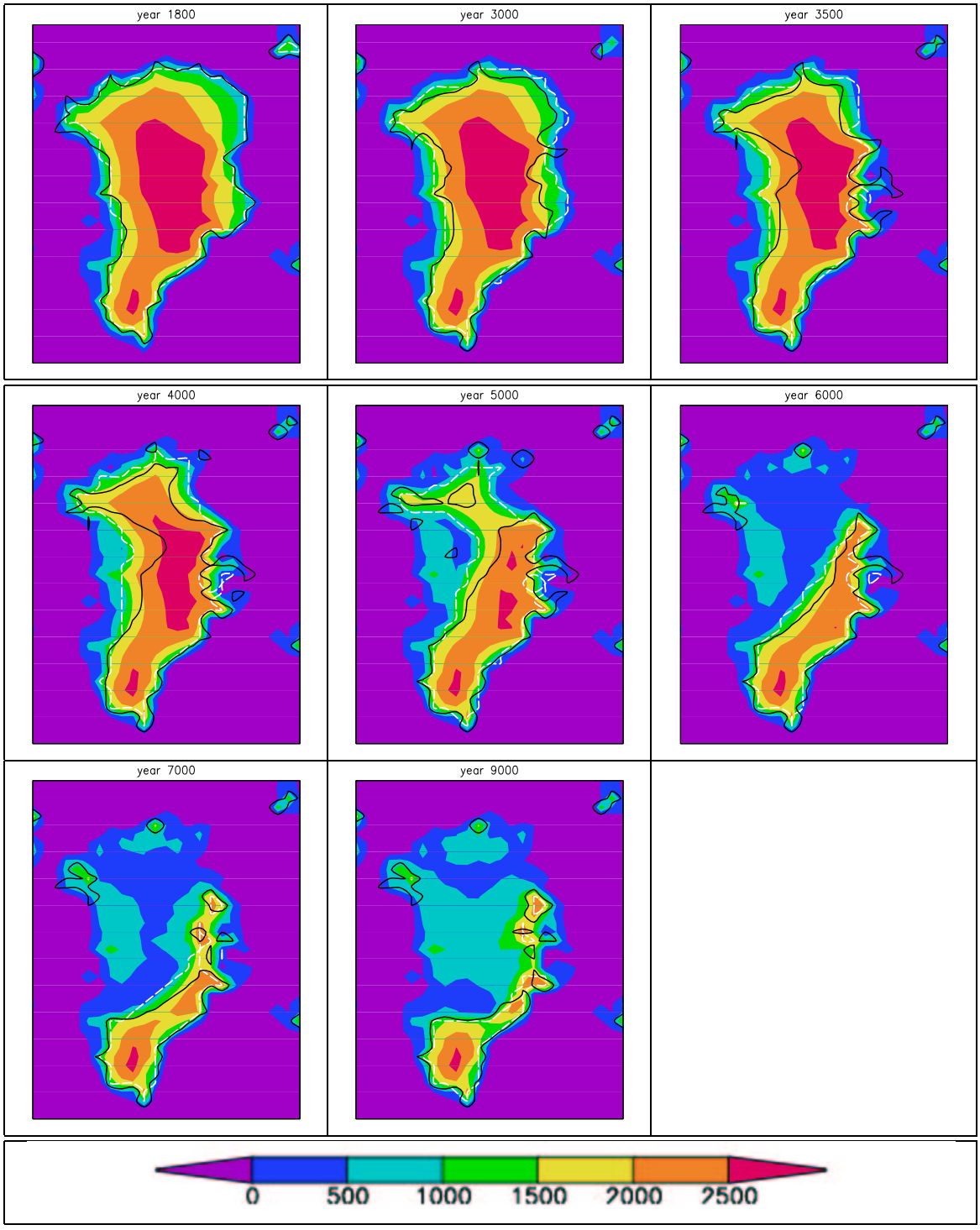

Figure 6.6: Evolution of the GrIS in simulation A2. The colour bar corresponds to the topographic height in m. The dashed white line indicates the grounding line (limits of the grounded ice) and the solid black line, the equilibrium line (limiting the regions where accumulation exceeds ablation). The years 1800, 3000, 3500, 4000, 5000, 6000, 7000 and 9000 have been taken for the topographic heights and the position of the grounding line. For the equilibrium line the mean of the mass balance terms of the previous 50 years has been taken.

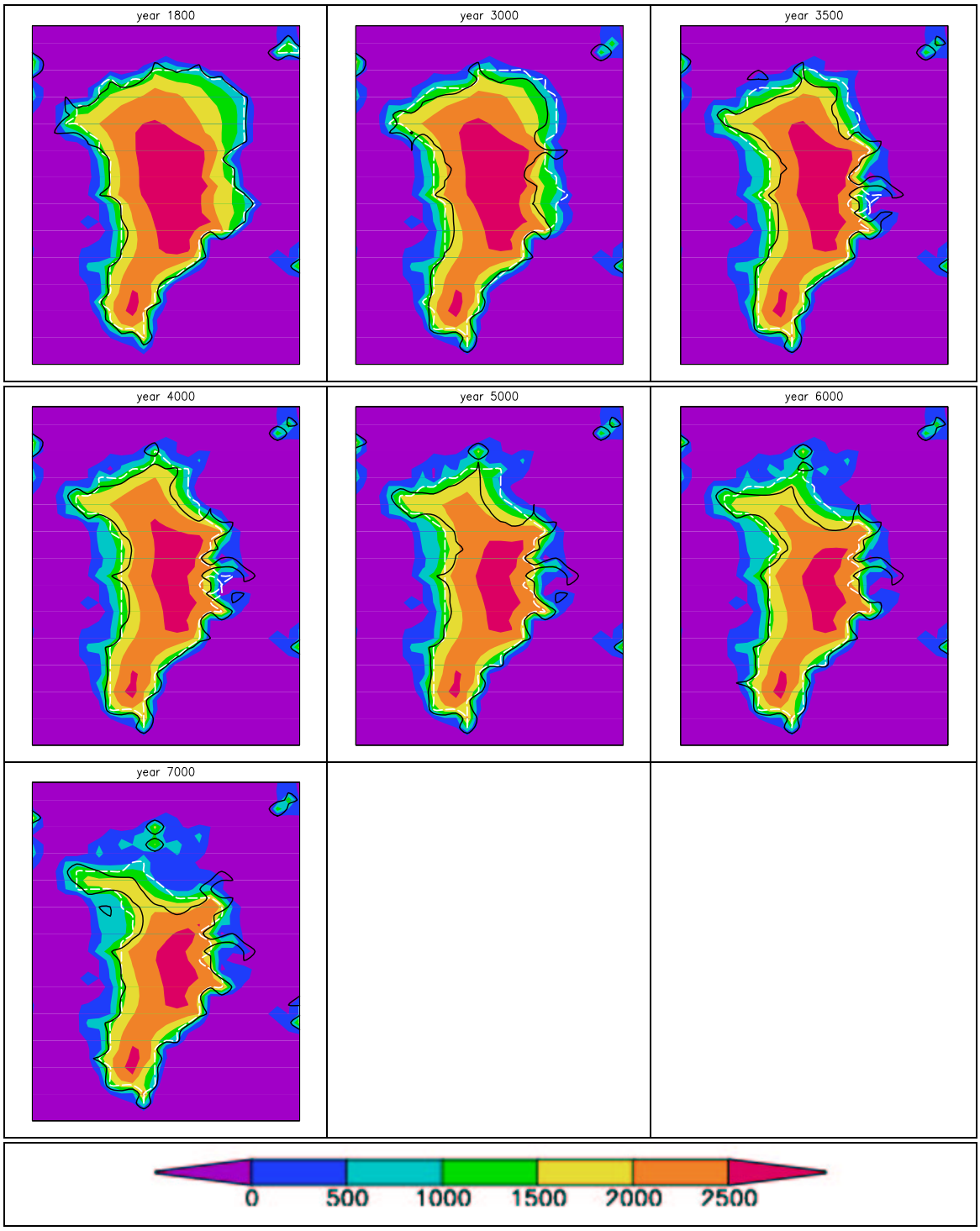

Figure 6.7: The same as in fig. 6.6, but for the simulation A2_1w.

The regional climate over Greenland, though, is strongly modified by the changes in the Greenland ice sheet. These changes begin to be important for the climate of the Greenland ice sheet approximately at the time when the mean height of the ice sheet in the atmospheric model has been reduced by 250 m (see fig. 6.8a). Until year 3200, the climate over Greenland is similar in the simulations A2 and A2_1w (fig. 6.5). From this year, both summer and winter temperatures at the 700 hPa level, representing in both simulations the free atmosphere over Greenland, are higher in the simulation A2 where the feedbacks from the ice sheet are included (fig. 6.5c and d). This increase of temperatures grows with time for the winter season. In summer the difference is always close to 2 K from approximately 3500 until the end of the simulation.

The winter near-surface temperatures reduced to the topography of the reference Greenland ice sheet are lower in the case of A2 from year 4000 onwards. Since the temperatures at higher levels are higher in the case of A2, this indicates a strengthening of the surface inversion layer.

Summer near-surface temperatures are higher in A2 than in A2_1w. By the end of the simulation, the difference is approximately 9 K. Almost 2/3 of this anomaly can be explained by the height-effect assuming a lapse rate of -6.5°C/km (fig. 6.8b). The rest of the signal must be explained by atmospheric circulation changes and albedo changes. It will be shown later in the second part of this chapter, that the anomalies of heat export are negative in summer when the Greenland ice sheet is absent. This indicates that the increase in albedo over Greenland produces a net export of heat to other areas. Thus it can be assumed that the warming signal not explained by the height-effect can be attributed to the changes in the albedo.

The disappearance of the Greenland ice sheet decreases the mean albedo over the original area of the ice sheet by approximately 0.40 (fig 6.5f). The decrease during the simulation A2 is due to two phenomena: the decrease of the glaciated area and the increase of surface temperatures. The evolution of the mean albedo over the original area of the GrIS is mainly controlled by the changes in the glacier mask. Nevertheless, the reduction of albedo via changes in the surface temperature is also strong during the simulation, as it can be observed from the analysis of the changes of albedo of the glaciated points. An albedo reduction of 0.15 is associated with this effect.

The decay of the Greenland ice sheet produces an increase of the precipitation rates over Greenland (fig 6.5e). This increase in precipitation rates does not necessarily represent an increase in snowfall, because the decay of the ice sheet also produces a warming over the area. This warming could potentially increase

the fraction of precipitation falling as rain. During the period between 3600-4000, snowfall rates are nevertheless higher in the simulation A2 than in A2_1w (compare the map of snowfall from fig. 5.9 in the previous chapter and fig. 6.3). Thus, at the time when the decay rate of the GrIS in the simulation A2 begins to be substantially different from the rate in A2_1w, *the increase in accumulation following the reduction of height of the ice sheet acts as a negative feedback* for the decay of the ice sheet. Anyway, the differences in the mass balance between A2 and A2_1w at that time are dominated by the differences in surface melting. The *increase in melting rates caused by the decay of the ice sheet via changes in the surface albedo acts as a positive feedback* for the decay of the ice sheet. This effect dominates over the one by increased accumulation rates.

To summarise, in this model approach, the atmospheric feedbacks associated with the decay of the Greenland ice sheet are not relevant for the mass balance of the ice sheet until sufficient changes in the topography and area of the ice sheet have taken place. A threshold has been found at 3/4 of the original volume and area of the ice sheet. In Ridley *et al.* (2005), with an ice sheet model bi-directionally coupled to the HadCM3 AOGCM for a multicentury simulation with $4xCO_2$ greenhouse forcing, this threshold was found to be at 2/3 of the original volume. They found that the processes associated with the decay of the ice sheet act as a negative feedback for its decay. This reduction of the decay rate takes place via the development of atmospheric convection due to the strong thermal contrast in their model between the deglaciated margins and the glaciated areas. They suggest that the development of these circulation cells may be a function of GCM resolution. These convective cells do not develop in the ESM of this study, where the resolution is lower and where the thermal contrast between deglaciated and glaciated model points is substantially weaker than in the results from Ridley *et al.* (2005).

6.2 Climatic impact of the disappearance of the Greenland ice sheet

The impact on the climatic system of the disappearance of the Greenland ice sheet will now be explored for two cases: 1) Absence of GrIS from a simulation of pre-industrial climate and 2) absence from a simulation with the climate of A2, where the NAMOC collapses.

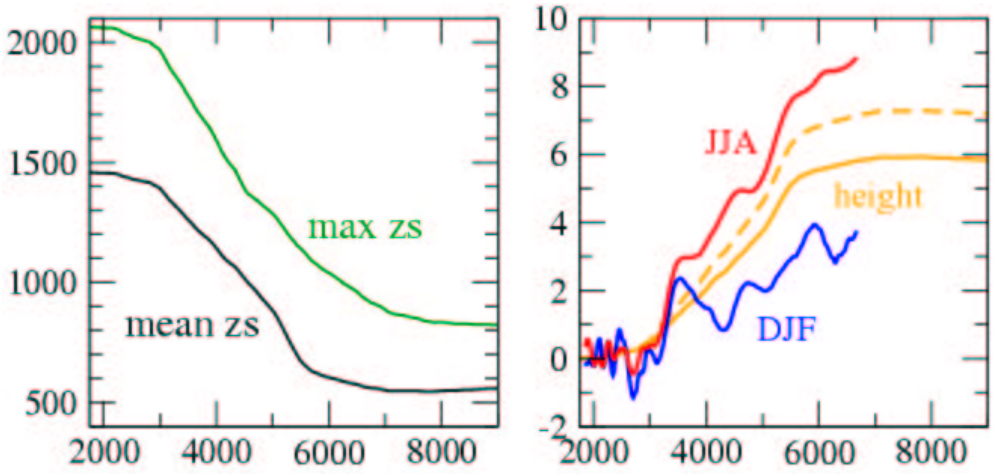

Figure 6.8: a) Evolution of the maximum and mean height over the CTRL GrIS in simulation A2. b) Comparison of the (averaged over the area of the CTRL GrIS) T-2m temperature anomaly A2 - A2_1w (DJF=blue, JJA=red) and the magnitude of the height-effect assuming lapse rates of -6.5 (solid orange) and -8°C/km (dotted orange).

6.2.1 State of the art

Several studies have been performed with General Circulation Models in order to evaluate the impact of the removal of the Greenland ice sheet on climate. Most of them have been performed with a present or pre-industrial climate as reference, in order to evaluate the role of the ice sheet in the general circulation of the atmosphere. Junge *et al.* (2005) performed two simulations with the model ECHAM4 with resolution T42 and T106 and prescribed climatological sea surface temperatures (SSTs). The topography of the Greenland ice sheet was set to sea level but the glacier mask was not modified. They compared the effect of the model resolution in the results and found similar results for the near-field changes and significant differences in the pattern far from the Greenland ice sheet.

Toniazzo *et al.* (2004) used 40 and 60-year simulations with the AOGCM HadCM3 for pre-industrial climate with a horizontal resolution in the atmospheric model of 2.5° latitude x 3.75° longitude. One simulation was performed with the Greenland orography at the level of the present bedrock, and another with relaxed (rebounded) bedrock. The surface characteristics over Greenland were prescribed as bare soil. The removal of the Greenland ice sheet increased the mean summer temperature by 15°C. They found, similarly to Junge *et al.* (2005), a decrease in the strength of the North Atlantic storm track when the ice sheet was absent.

Crowley and Baum (1995) used the climate model GENESIS1.02.A with a horizontal resolution of 4.5° (latitude) x 7.5°(longitude) and found summer temperatures on the ice-free Greenland of about 10 °C. This number varied between 6 and 14°C depending on specification of vegetation type, elevation of Greenland, and orbital forcing.

Lunt *et al.* (2004) used the Institut Pierre Simon Laplace AOGCM (IPSLCM4). The spatial resolution of the atmospheric model in this study is 5° in longitude and 4° in latitude. In the simulations without Greenland, with a length of 40 years, the orography in the Northern Hemisphere was set to the orography of the bedrock after isostatic rebound, and the ice sheet was replaced by barren tundra vegetation. The CO_2 concentration was set to present levels. They found an annual mean temperature increase over Greenland of +5.7°C and a cooler winter in the Barents Sea area, with a substantial increase in sea ice. They related the cooling over the Barents Sea to the decreased poleward heat transport due to weaker storm activity. 40% of the JJA temperature increase over Greenland was attributed to the decreased altitude, and 60% to the change in surface type (from an ice sheet with albedo 0.85 to snow-free bare soil with albedo 0.20). They found increased East Greenland precipitation and decreased West Greenland precipitation due to the reduced height of Greenland.

Petersen *et al.* (2004) performed a 10-years-length simulation with the NCAR Community Model (CCM3) at T106 horizontal resolution (approximately 1.1° x 1.1°) forced with climatological sea surface temperatures, and with the Greenland orography set to sea level. They found increased cyclonic activity over the North Atlantic in the absence of Greenland, in contrast to Toniazzo *et al.* (2004) and Lunt *et al.* (2004).

Ridley *et al.* (2005) analysed the climatic impact of the decay of the Greenland Ice Sheet in a 4x CO_2 simulation with HadCM3 coupled bi-directionally to an ice-sheet model of the GrIS. This is a transient simulation, while the studies cited before are based on steady-state simulations. The convection in the North Atlantic weakens only slightly in this simulation. They did not find a significant impact of the melting of Greenland in the ocean circulation. Their results for the regional impact of the absence of the GrIS are similar to those of Toniazzo *et al.* (2004).

A study of the impact of the absence of the Greenland ice sheet in a climate with higher concentration of greenhouse gases where the Meridional Overturning Circulation has collapsed is missing from the literature. In this chapter such a case will be studied.

6.2.2 Climatic impact of the disappearance of the GrIS under pre-industrial climate conditions

Set-up

Two simulations will be compared: the control simulation CTRL, representing pre-industrial climate, with a length of 2250 years, and a simulation CTRL_NOGr where the Greenland ice sheet has been almost completely removed. For this simulation, the topography and glacier mask of the northern hemisphere from the year 9000 of A2 have been taken as initial conditions. The southern hemisphere ice sheets are the same as in CTRL.

Only a small area remains glaciated in Southern Greenland. The bedrock is almost completely rebounded in the ice free regions. Figure 6.9 shows the glacier mask and topography in the atmospheric grid (T21) corresponding to the simulations CTRL and CTRL_NOGr. The Greenland ice sheet of the control simulation is represented by 19 atmospheric grid points. Due to the spectral smoothing, only the main dome of the GrIS is captured at the T21 resolution, the secondary one in the south is missing. The main dome has a height of 2000 m in the atmospheric grid.

The simulation CTRL_NOGr has a length of 1000 years. A periodically synchronous coupling has been performed. Periods of 2 years of fully coupled simulation are followed by 8 years where the slow components (all but the atmosphere) are forced with an archive of atmospheric data of previous atmospheric years. For the analysis of the results of this simulation, the first 100 years of simulation will be regarded as spin-up, and only the period 200-1000 will be considered.

Results

For the analysis of climate anomalies, the control climate CTRL will be used as reference, since the approach taken in this study is the analysis of the impact of the disappearance of the GrIS. Note that in some other studies the present/pre-industrial simulation was used as reference (for instance, in the study by Junge *et al.* (2005), since their approach was the study of the impact of the presence of the GrIS in the current climate).

The temperature patterns for near-surface and at 700 hPa are compared for the climates of both simulations (fig. 6.10). The near surface temperatures in winter (DJF) are slightly warmer in most of Greenland in the simulation where the ice sheet is absent, but some areas at the east and north-west margins show a slight cooling. A cooling is simulated in the North Atlantic around 70°N, with maxi-

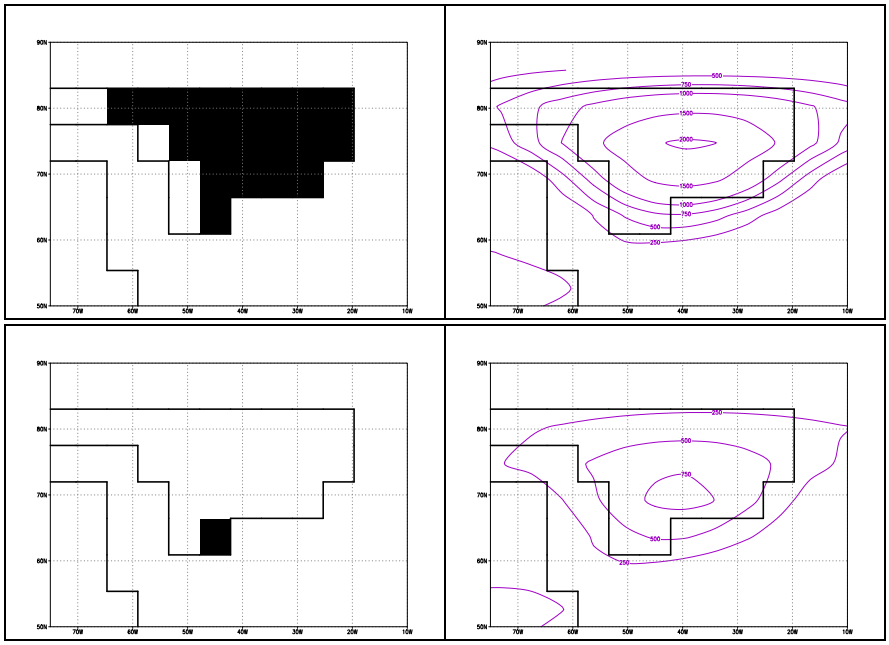

Figure 6.9: Glacier mask (black=ice sheet, first column) and topography (second column) in the atmospheric grid (T21) corresponding to the simulations CTRL (first row) and CTRL_NOGr (second row). Countour lines for the topography are shown at the levels 250, 500, 750, 1000, 1500 and 2000 m.

mum in Scandinavia, and in Hudson Bay (this signal is not visible at 700 hPa). Higher temperatures are seen in the Bering Sea when the GrIS is absent. In the 700 hPa level (fig. 6.10, second panel), higher temperatures over Greenland can be seen, with a maximum in the northwest. The winter surface inversion is stronger in CTRL_NOGr than in CTRL (see the difference between the temperature at 700 hPa and the near-surface temperature in fig. 6.11a), explaining the differences in the pattern and sign of temperature anomalies over Greenland at 2-m and 700 hPa.

The winter cooling over Scandinavia is a strong feature of the 700 hPa temperature anomalies. Associated with this cooling, and acting as a positive feedback, there are changes in the albedo of sea ice, snow, and land vegetation. The forest fraction is reduced by more than 50% in this area (not shown). The cooling over Scandinavia is also one of the main results of the studies from Toniazzo *et al.* (2004) and Junge *et al.* (2005).

Without the ice sheet, near-surface summer temperatures over Greenland are on average 10°C warmer (fig. 6.10, third panel). Maximum warming occurs during the month of June (fig. 6.11a). The warming is found both in Greenland and in the surroundings. A slight cooling is simulated over Scandinavia and Hudson Bay. At 700 hPa (fig. 6.10, fourth panel) only the warming over Greenland is captured.

The albedo over Greenland reaches a maximum difference in the month of July, when it is 35% lower than in CTRL (fig. 6.11b). Most of the change in the albedo is explained by the transition from glaciated to ice-free. The minimum albedo of a glacier point in ECHAM3 is 0.60, corresponding to a melting surface. The equivalent minimum albedo for snow-covered surfaces on ice-free land is 0.40. The increase of temperatures plays also a role in the decrease of albedo (if the surface temperature is far from melting point, the albedo of the snow approaches 0.60). The cold bias of the ECHAM3/LSG/LPJ/HAMMOC/SICOPOLIS ESM at high latitudes (for details see Mikolajewicz *et al.* (accepted)) does not allow the appearance of snow-free areas in Greenland during the summer season, which would decrease the albedo to values of approximately 0.15, corresponding to the parameterisation for bare soil. The cold bias does not allow either the establishment of vegetation on the Greenland area, which would further increase the warming over Greenland, or the occurrence of snow-free areas in summer, as it would be expected.

The anomalies CTRL_NOGr-CTRL of the heat flux export integrated over the whole atmospheric column show an opposite pattern over Greenland for the winter and summer seasons (fig. 6.12). During winter, the atmosphere over Greenland imports more heat from other regions when the ice sheet is removed. During sum-

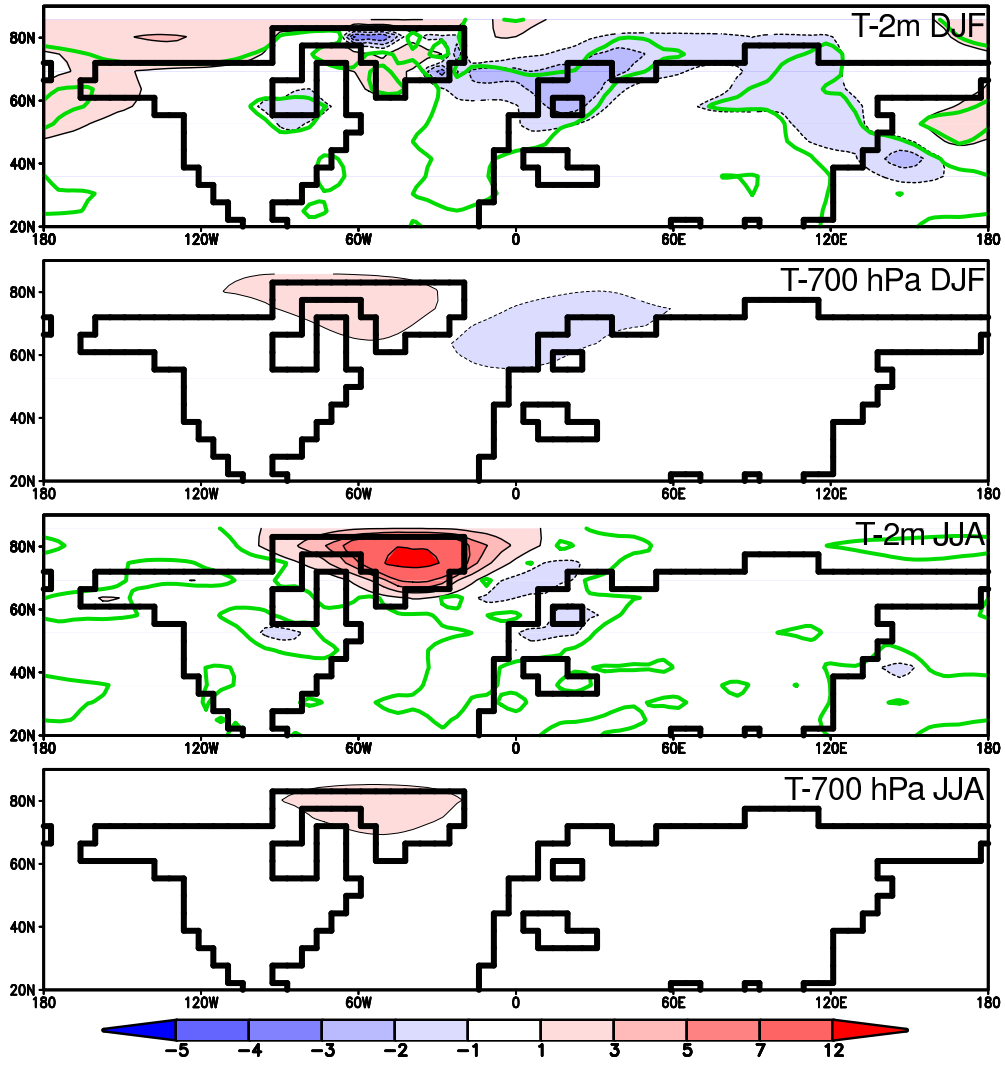

Figure 6.10: Anomalies of the near-surface and 700 hPa temperature [K] pattern between the simulations CTRL_NOGr and CTRL for winter (DJF, first and second panels) and summer (JJA, third and fourth panels). The green line in the first and third panels delimits the areas where the signal is higher than 2.8 times the standard deviation of summer temperature in the control simulation.

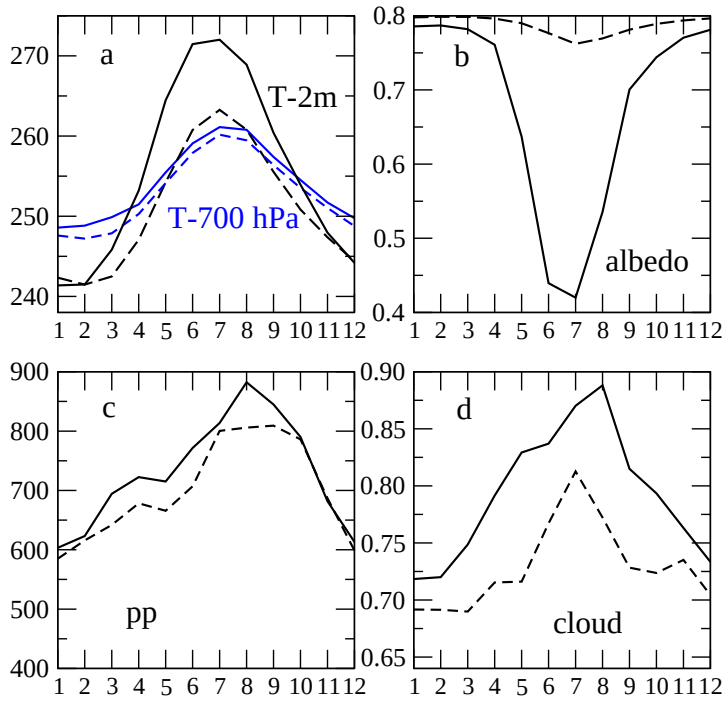

Figure 6.11: Seasonal cycle of a) near-surface and 700 hPa (blue) temperatures [K], b) albedo, c) precipitation [mm/yr], and d) cloud cover for the simulations CTRL (dashed line) and CTRL_NOGr (solid line) averaged over the area of the CTRL GrIS. X-axis: 1=January, 2=February, ... 12=December.

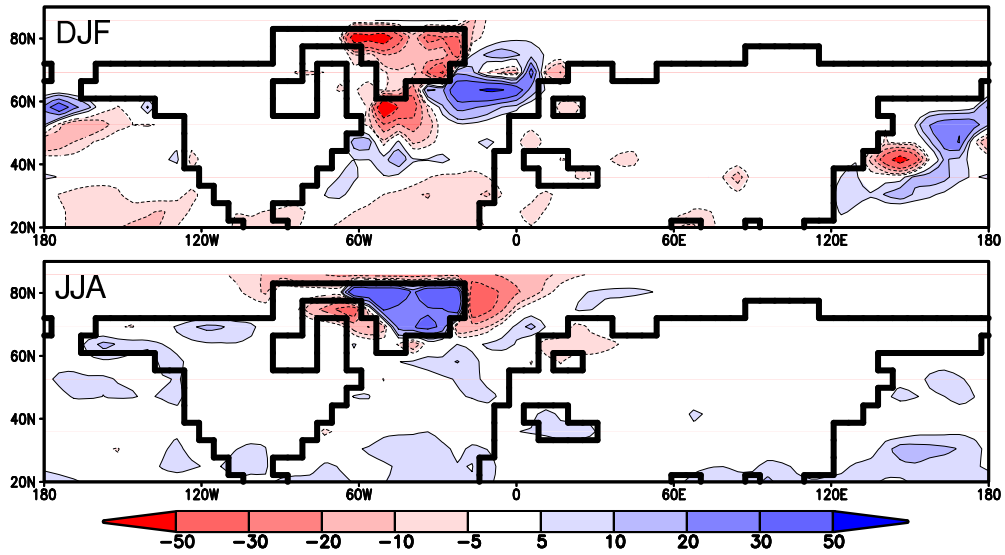

Figure 6.12: Heat divergence anomalies [Wm^{-2}] CTRL_NOGr-CTRL for winter (upper panel) and summer (lower panel).

mer, the anomalies of heat divergence over Greenland are positive. Warm air is exported from the Greenland area, which is warmer due to the albedo changes, to the neighbouring regions. This explains the warming in the surroundings of Greenland seen in fig. 6.10, third panel. During winter, the North Atlantic atmosphere imports less heat in the simulation without Greenland, with maximum changes at 70°N. This is consistent with the atmospheric cooling in this region, which is also reflected in ocean surface temperatures, which are cooler than in CTRL by approximately 0.4°C. These results are consistent with those of Toniazzo *et al.* (2004) regarding changes in the heat import/export.

The absence of the Greenland ice sheet weakens the climatological winter ridge east of Greenland (fig. 6.13). Therefore, the mean winter circulation is more zonal if the topographic obstacle created by the ice sheet is removed. This was also found by Junge *et al.* (2005)and Petersen *et al.* (2004).

The pattern of the storm track is plotted for both simulations together with the anomalies in figure 6.14. The technique applied for the analysis of the storm track is from Blackmon (1976). The removal of the Greenland ice sheet produces a reduction of the storm track north of 50°N over the North Atlantic, Eurasia and North America. The maximum of cyclonic activity is shifted southwards. As an exception to this pattern, a small increase of the activity occurs in Northern Greenland. The storm track intensifies over the Mediterranean region and the Pacific Ocean between 30 and 40°N.

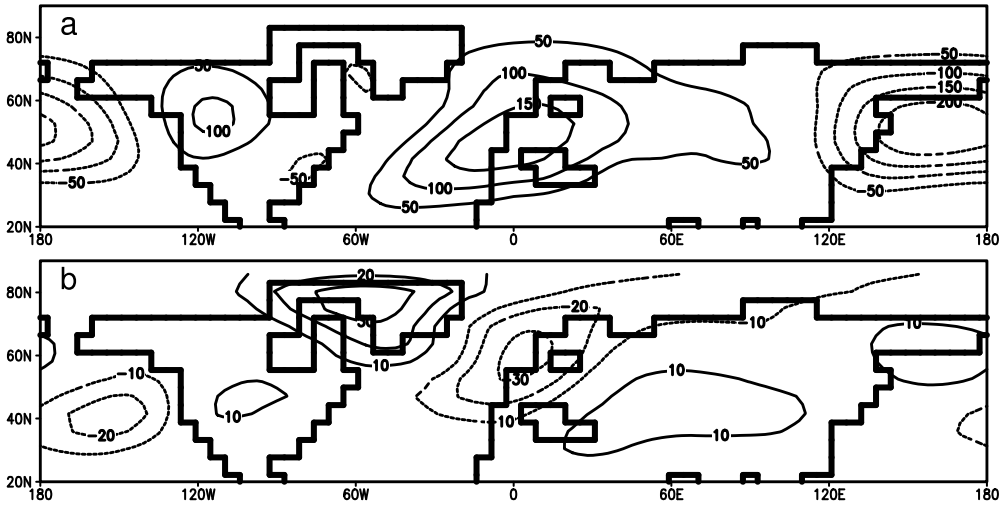

Figure 6.13: Winter geopotential height anomalies [gpm] with respect to the zonal mean: (a) in CTRL, (b) anomalies CTRL_NOGr-CTRL.

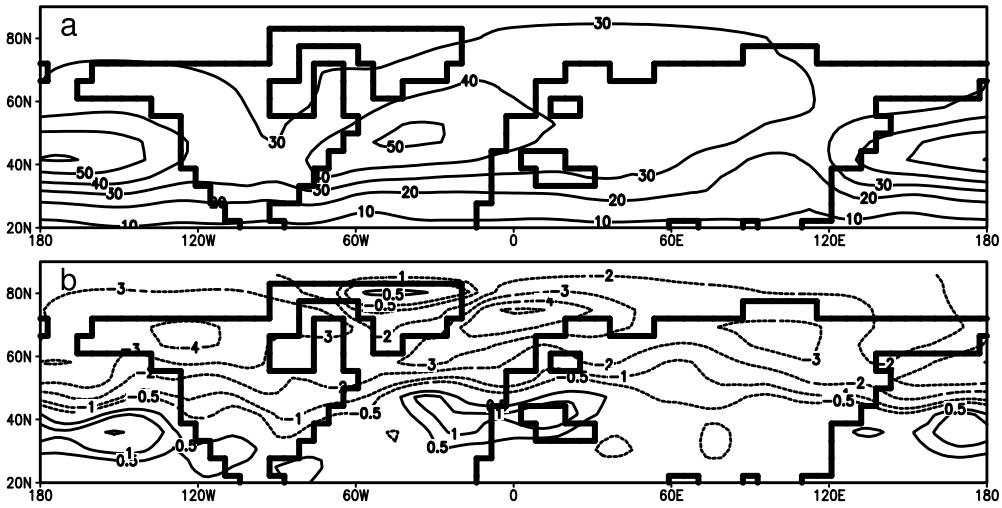

Figure 6.14: The winter (DJF) 500-hPa geopotential height 2.5-6 days bandpass statistics [gpm]: (a) in CTRL, (b) anomalies of CTRL_NOGr with respect to CTRL.

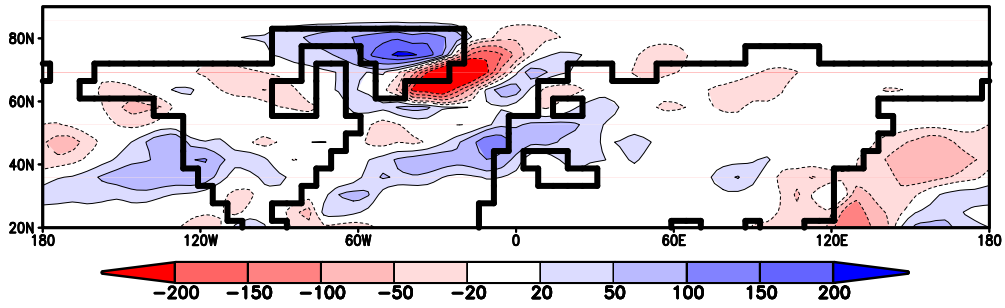

Figure 6.15: Annual precipitation anomalies [mm/yr] CTRL_NOGr minus CTRL.

The removal of the Greenland ice sheet produces a decrease of precipitation in the southeast of Greenland and an increase in the rest of Greenland (figure 6.15). Precipitation rates increase over central and southern Europe, and the North Atlantic and Northeast Pacific close to 40° N. Part of the precipitation anomaly in the southeast of Greenland is due to changes in convective precipitation. The changes over Europe and southeast Greenland are stronger in winter than in summer. The increase of precipitation in central and northern Greenland is stronger in summer (not shown). The reduction in precipitation in southeast Greenland can be explained by the decrease in the storm-track and by reduced orographic forcing. The increase in the Pacific and Atlantic at approximately 40° N follows the pattern of changes in the storm track.

Summary

According to this modelling results, the main effects of the removal of the Greenland ice sheet in a pre-industrial climate are: 1) a more zonal winter circulation in the northern hemisphere, due to removal of the topographic obstacle, 2) a southward shift of the storm track, 3) a cooling over Scandinavia during winter, 4) an increase of precipitation in central and southern Europe, 5) an increase of precipitation over most of the Greenland ice sheet due to smoother orography, and 6) a summer warming of 10°C over Greenland.

Is the Greenland ice sheet bi-stable under pre-industrial/present climate conditions of CO_2 and insolation?

Crowley and Baum (1995) answered "Yes". Lunt *et al.* (2004) obtained the opposite answer, since the Greenland ice sheet regrows in their model if the initial conditions are an ice-free Greenland. Calov *et al.* (2005) performed a long-term equilibrium run with the Intermediate Complexity Model CLIMBER-2 coupled to

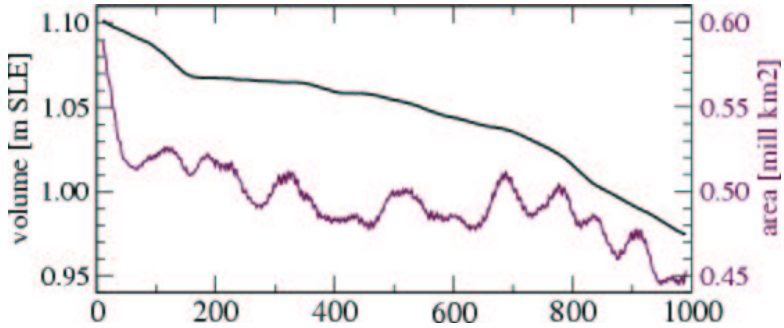

Figure 6.16: Northern Hemisphere ice sheet volume (black) and area (maroon) evolution during the simulation CTRL_NOGr. The x-axis corresponds to time (model years).

the ice-sheet model SICOPOLIS for the present-day orbital parameters and found two different equilibrium states: the glaciated and the non-glaciated Greenland.

In this Earth System Model, *the Greenland ice sheet is bi-stable under pre-industrial conditions of insolation and greenhouse forcing*: it cannot be formed if the initial conditions are an ice sheet-free Greenland. Figure 6.16 shows the evolution of the volume of the Northern Hemisphere ice sheets along the 1000 years of the simulation CTRL_NOGr, where only a small ice sheet exists as initial condition and most of Greenland is ice-free (see section 6.2.2). Even with this little seed which could favour the growth of the ice sheet, the volume of the ice sheet does not increase. Instead, it decreases. This is due to the fact that the initial ice sheet was taken from the end of the simulation A2, where the cold conditions at the southeast of Greenland associated with the collapsed NAMOC supported the ice sheet there. With the change to a climate forced with pre-industrial levels of CO_2 the NAMOC activates and the regional climate in the south and south-east of Greenland is warmer. Due to this warming, the small ice sheet decays.

6.2.3 Climatic impact of the disappearance of the GrIS under anthropogenic climate change conditions

It was shown before that the Greenland ice sheet is reduced to a small ice sheet in the south and south-east of Greenland by year 9000 of the simulation A2, with a volume of approximately 1.1 m SLE. The climate of the last thousand years of this simulation (i.e. from years 8000 to 9000) will be used for the analysis of the impact of the removal of the Greenland ice sheet on the climate of A2. As reference climate, the climate of the last thousand years of the simulation A2_1w,

where the topography and glacier mask of the ice sheet are unchanged during the simulation, will be taken. Since the climate of this simulation is approximately at steady-state during this period (years 6000 to 7000), it will be assumed that the climate of A2_1w would be the same during the years 8000 to 9000. Therefore the climate of the simulation A2_1w during years 8000 to 9000 will be approximated by the climate between years 6000 and 7000.

The dimensions and extension of the Greenland ice sheet do not change much from years 8000 to 9000 (fig. 6.2 and 6.6). Therefore the topography and glacier mask of the Greenland ice sheet in the atmospheric grid during this period are similar to the topography and glacier mask of the simulation CTRL_NOGr. In order to establish a parallel nomenclature with the simulations shown in the previous section, the climate of the years 6000-7000 of A2_1w will be labelled as A2_REF, while the climate between the years 8000 to 9000 of A2 will be labelled as A2_NOGr. The nomenclature of the simulations analysed in this chapter is summarised in table 6.1.

Results

Before analysing the impact of the absence of the GrIS in the climate of A2, the climate of A2_REF will be described and compared to the pre-industrial climate of CTRL.

1) The Reference climate of A2_REF

The mean and transient features of the atmospheric circulation of A2_REF are different from those of CTRL. The decreased latitudinal gradient of temperatures associated with the global increase of temperatures produce a more zonal mean atmospheric circulation over the North Atlantic, Arctic and Europe. This was shown in simulations with the AOGCM ECHAM3/LSG for stabilisation scenarios of 2x and 4x pre-industrial CO_2 (Voss and Mikolajewicz, 2001). The cooling of the North Atlantic area associated with the collapse of the NAMOC have also the same effect of a shift into a more zonal circulation than for the present climate. This phenomenon was shown also in some water-hosing experiments with ECHAM3/LSG (Schiller *et al.*, 1997). The anomalies of the winter geopotential heights to the zonal mean show this structure of a more zonal circulation (compare fig. 6.13a and 6.17a). The ridge over Europe is shallower and has a smaller area in the northern boundary. The ridge is significantly weaker over Scandinavia and the North Atlantic north of 55°N. The trough west of Greenland in A2_REF is not visible when only anomalies of more than 50 gpm are plotted. The trough with centre in the western North Pacific is also slightly weaker.

The storm track has also a more zonal structure in A2_REF than in CTRL

Name	*Length*	*Description*
A2	Calendar years 1750-9000	
A2_1w	Calendar years 1750-7000 (-9000 ice sheet model run offline with atmospheric forcing 6000-7000)	As A2, but changes in freshwater fluxes, glacier mask and topography from ice sheets are not passed to other components (one-way coupling).
CTRL	Model years 0-1000	Control simulation pre-industrial CO_2
CTRL_NOGr	Model years 0-1000	As CTRL, without Greenland ice sheet
A2_REF	Years 6000-7000 from A2_1w	Topography and extent of the Greenland ice sheet as in CTRL
A2_NOGr	Years 8000-9000 from A2	Without Greenland ice sheet

Table 6.1: Nomenclature of the simulations analysed in this chapter

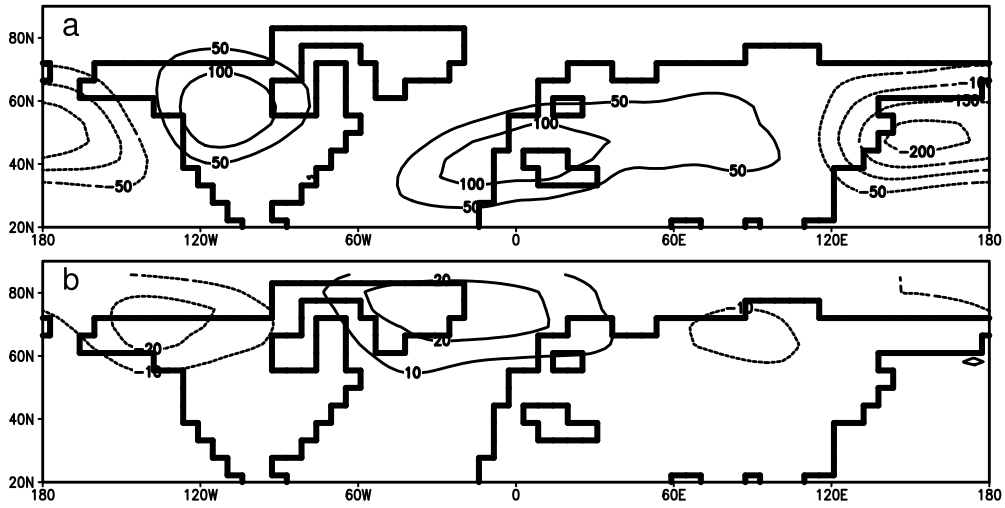

Figure 6.17: Winter geopotential height anomalies to the zonal mean [gpm]: (a) from A2_REF; (b) anomalies A2_NOGr - A2_REF.

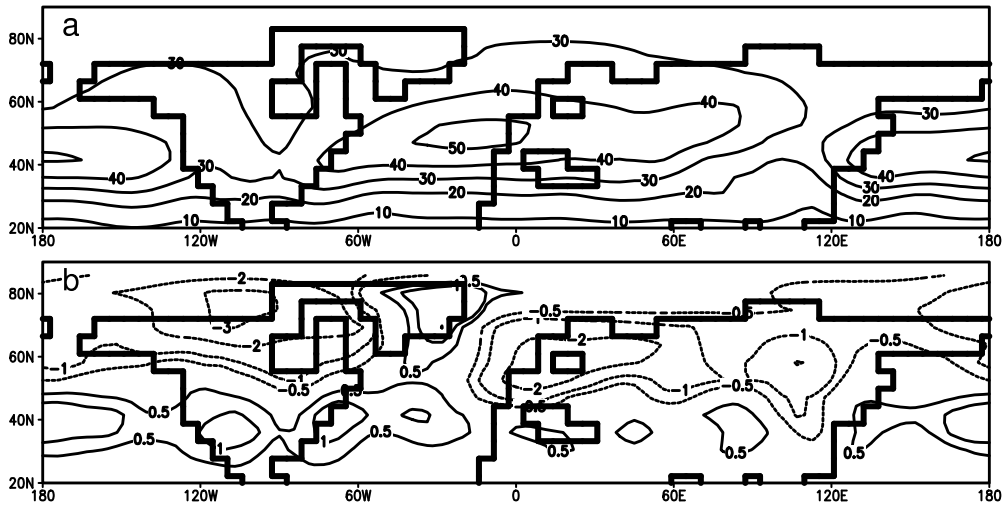

Figure 6.18: The winter 500-hPa geopotential height 2.5-6 days bandpass statistics [gpm]: (a) from A2_REF ; (b) anomalies A2_NOGr-A2_REF.

(fig. 6.14a and 6.18a). The storm track is more intense than in CTRL for central Europe around 50°N and significantly weaker in the North Atlantic, East of Greenland, and the central North Pacific.

2) Climatic impact of the absence of the GrIS

The disappearance of the GrIS produces an increase of 7°C in the near-surface temperature in the interior of the Greenland ice sheet during winter (fig. 6.19, first panel). The positive anomaly extends eastwards of Greenland over the ocean

at 70 to 80°N. Similarly to the case for present climate, a cooling is observed over the area of Hudson Bay in A2_NOGr. Lower temperatures are located over northern Eurasia, with a temperature minimum over Central Siberia instead of the minimum located over Scandinavia in CTRL_NOGr - CTRL. The cooling over northern Asia can be observed in the 700-hPa anomalies as well (fig. 6.19, second panel).

The summer temperature change over Greenland presents no significant differences either on area or intensity with the one observed for CTRL_NOGr - CTRL (fig.6.19, third and fourth panels). The mean increase of near-surface summer temperatures is also approximately 10°C.

Positive feedbacks of snow, vegetation and sea-ice albedo act during winter (not shown), when the surface albedo of the Labrador Peninsula and north of Hudson Bay increases by more than 20%. An increase of albedo of similar magnitude is located over the central Siberian Plateau. An increase of sea ice cover in the Baltic and Norwegian Seas acts also as a positive feedback. During summer, a positive albedo-temperature feedback occurs in the Barents Sea and for Hudson Bay.

The absence of the GrIS extends the climatological ridge east of Greenland into the North Atlantic north of 50°N, Scandinavia and Greenland itself (fig. 6.17b). Thus, the disappearance of the ice sheet reduces the zonality of the flow.

When the Greenland ice sheet is absent, the storm track is stronger over most of the North Atlantic, except the Norwegian and the North Sea, where it is substantially weaker (fig. 6.18b). The storm track increases also over most of Greenland as well. The storm track is weaker over northern Canada and most of Europe and northern Asia. It shifts southwards in the North Pacific. Thus the removal of the ice sheet produces a less zonal pattern over the high latitudes of the North Atlantic due to the increase over Greenland and a southwards shift.

The pattern of changes in precipitation over Greenland (fig. 6.20) associated with the absence of the ice sheet for the A2 scenario are similar to those for present climate: a decrease of precipitation in the southeast and an increase in the rest of Greenland. The decrease in precipitation in the southeast is weaker than in CTRL_NOGr-CTRL, possibly due to the strengthening of the storm track over Greenland. Consistently with the winter storm-track changes, there is a negative anomaly of precipitation during winter in northern Eurasia.

Summary and discussion

Substantial differences have been found for the impact of the disappearance of the GrIS in the perturbed climate of A2 when compared to the the impact in the pre-

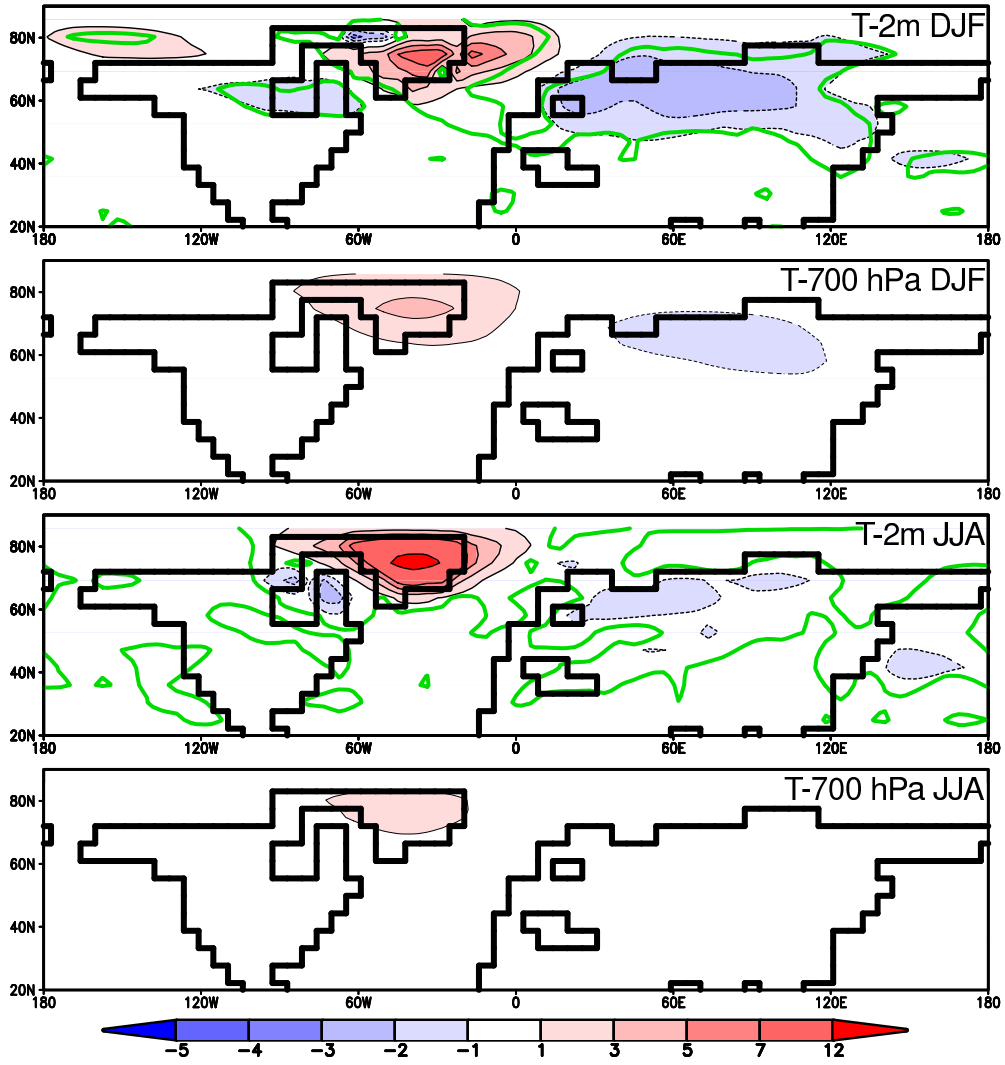

Figure 6.19: Anomalies of the near-surface and 700 hPa temperature pattern [K] between the simulations A2_NOGr and A2_REF for the winter (first and second panels) and summer (third and fourth panels). The green line in the first and third panels delimits the areas where the signal is higher than 2.8 times the standard deviation of summer temperature in the control simulation.

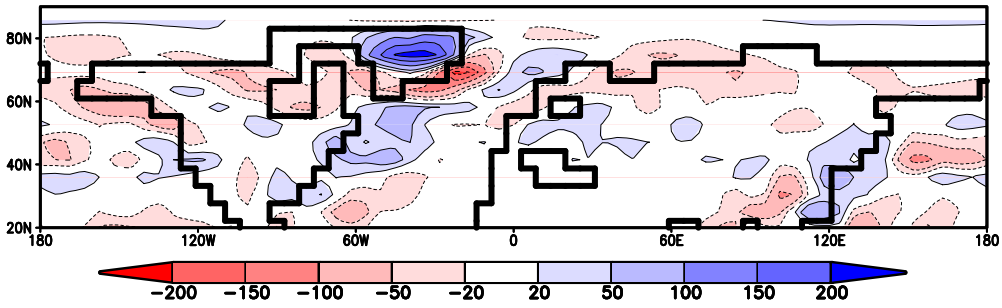

Figure 6.20: Anomalies of annual precipitation [mm/yr] between A2_NOGr and A2_REF.

industrial climate. For instance, the maximum cooling is simulated over northern Asia instead of Scandinavia, and the zonality of the storm track and the mean circulation is reduced in the simulation without the ice sheet. Ridley *et al.* (2005) found a similar impact of the disappearance of the GrIS in a 4xCO_2 simulation and in the pre-industrial climate simulated with the same model (Toniazzo *et al.*, 2004). In their 4xCO_2 simulation the NAMOC weakens but does not collapse. The differences between their results and the results shown here could possibly be due to the collapse of the NAMOC, which causes substantial differences between the pattern of atmospheric circulation in the pre-industrial and A2 climates.

6.3 Conclusions

The main conclusions of the study shown in this chapter are the following:

- The feedbacks between the Greenland ice sheet and the climate are not relevant for the mass balance of the ice sheet until a certain threshold is reached in the decay of the ice sheet. In this ESM, these feedbacks begin to be relevant from the time when the ice sheet has been reduced to approximately 75% of the original volume.

- The feedbacks associated with the decay of the Greenland ice sheet are ***positive*** in this modelling approach, hence they accelerate the rate of decay of the Greenland ice sheet.

- The acceleration of the decay of the ice sheet by the feedbacks is due to ***increased surface melting.*** This increased surface melting seems to be caused by enhanced warming due to a ***reduction of the summer albedo***. However an additional simulation separating the albedo contribution to the total changes in the climate of Greenland would be needed in order to quantify more rigorously the role played by the albedo.

- The height-effect explains approximately two thirds of the increase of summer temperatures caused by the disappearance of the Greenland ice sheet in a climate with high concentration of greenhouse gases and a collapsed NAMOC. The rest of the increase is due to albedo and atmospheric circulation changes.

- The decay of the Greenland ice sheet, at least in this ESM, has a local impact on the climate of Greenland and other areas at northern high latitudes, but not a global impact.

- The disintegration of the Greenland ice sheet in a climate with high concentration of greenhouse gases and a collapsed NAMOC has a *different impact on the general and transient circulation of the atmosphere than for a disintegration in a pre-industrial climate.*

- The collapse of the NAMOC in the simulation A2 makes the survival of a stable small ice sheet in the south of Greenland possible.

- In this modelling approach, the Greenland ice sheet is bi-stable under present conditions of insolation and greenhouse forcing.

Chapter 7

Model description: ECHAM5/-MPI-OM/LPJ/SICOPOLIS

In the previous chapter the multi-century response of global ice sheets to climate change under anthropogenic greenhouse gas forcing has been studied with the model ESM1. Because of the periodically synchronous coupling technique used and its course resolution, the ESM1 was suitable for such long-term studies. In this and next chapter a new ESM (ESM2) will be introduced and applied to the study of the evolution of ice sheets under anthropogenic climate change forcing. This new study will benefit from an improved modelling of the atmospheric component (ECHAM5 includes several improved parameterisations and it simulates a current climate closer to observations than the version 3 of ECHAM) and the ocean component (MPI-OM instead of the model LSG), and from increased horizontal resolution (T31). As in ESM1, the model LPJ is coupled to ESM2 for the modelling of land vegetation. The modelled present climate from the coupled ECHAM5/MPI-OM/LPJ is closer to observations than the climate from ESM1 and the coupling of an ice sheet model can be performed without any flux corrections. The response of the GrIS to anthropogenic climate change modelled with ESM1 was found to be relatively modest due to the low climate sensitivity of the model compared to other models. The magnitude of the ice sheets response could be different when modelled with ESM2, due to the higher climate sensitivity of the coupled ECHAM5/MPI-OM. Because of all reasons given here, a parallel study to the previous with ESM1 will be performed with ESM2.

In this chapter the new Earth System Model ECHAM5/MPI-OM/LPJ/-SICOPOLIS (also referred to as ESM2) will be described. The coupling between the atmospheric component and the ice sheet model does not need flux corrections. Although a coupling without flux corrections was performed with Earth System

Models of Intermediate Complexity (e.g. Calov *et al.* (2005)), this is a step forward with respect to previous studies with bidirectional coupling of AOGCMs and ice-sheet models (Ridley *et al.*, 2005). Besides, the melting rates in this ESM2 are calculated with an energy balance scheme, which is a more physical approach than the use of the parameterisations from the temperature-index methods. The calculation of surface melting, though, is performed via temperature-index methods in many studies of future mass balance of ice sheets performed with a dynamical ice sheet (Fichefet *et al.* (2003), Ridley *et al.* (2005), Huybrechts *et al.* (2004)). The scheme presented here does not have the problems inherent to empirical formulations. For instance, the parameterisations of degree-day methods are calibrated via present-day measurements. It is not clear whether the empirical relationships between the current climate and mass balance of the ice sheets would still be valid in other climate regimes.

The structure of this chapter is as follows. In the first section the atmospheric, ocean and land vegetation components of the model and their coupling are described. In the next section, the coupling between the ice sheet model and the other components is explained. The scheme used for the calculation of the mass balance of the ice sheets is explained in Section 3.

7.1 The ESM ECHAM5/MPI-OM/LPJ/-SICOPOLIS

The core of this Earth System Model (ESM) is the AOGCM ECHAM5/MPI-OM. The model needs no flux adjustments and has been tested for applications under present day conditions (Jungclaus *et al.*, 2006).

The atmospheric component of the ESM is the Atmospheric General Circulation Model ECHAM5.2 (Roeckner *et al.*, 2003). In this ESM it is used with a horizontal resolution of T31 (approximately 3.75°x 3.75°) and a vertical resolution of 19 vertical (hybrid) levels on a hybrid sigma-pressure coordinate system up to a pressure level of 10 hPa. Prognostic variables are vorticity, divergence, surface pressure, temperature, water vapour, cloud water, cloud ice, cloud droplet and ice crystal number concentrations. The prognostic variables, except water and chemical components, are represented by spherical harmonics with triangular truncation at wavenumber 31 (T31). For the advection of water vapour, cloud liquid water, cloud ice and tracer components, a semi-Lagrangian transport scheme (Lin and Rood, 1996) is applied. Cumulus convection is based on the mass fluxed scheme after Tiedke (1989) with modifications from Nordeng (1994). The cloud micro-

physics scheme of Lohman and Roeckner (1996) consists of prognostic equations for cloud liquid water and cloud ice. The transfer of solar radiation is parameterised after Fouquart and Bonnel (1980) and the transfer of longwave radiation after Morcrette *et al.* (1998).

The OGCM MPI-OM (Marsland *et al.*, 2003) is used with a horizontal resolution of 4° on a curvilinear grid with 40 vertical levels. The grid poles are placed on Greenland and Antarctica in order to avoid the pole-singularity problem at the North Pole and in order to obtain higher resolution in the deep water formation regions of the Labrador Sea, the Greenland Sea, and the Weddell Sea. The topography was interpolated from the ETOPO5 (ETOPO5, 1988). Specific topographic features, such as the important conduits of overflows and throughflows, were adjusted to observed sill depths. The primitive equations for a hydrostatic Boussinesq fluid are formulated for a free surface. The vertical discretisation is on z-levels and the bottom topography is resolved by partial grid cells (Wolff *et al.*, 1997). Using the formulation of Arakawa and Lamb (1977) the spatial arrangement of scalar and vector variables is formulated on a C-grid.

The dynamic and thermodynamic sea ice model is similar to the one in the HOPE model (Wolff *et al.*, 1997). The dynamics of sea ice are formulated using viscous-plastic rheology following Hibler III (1979). The changes in sea ice thickness are calculated from the balance of radiative, turbulent, and oceanic heat fluxes. The effect of snow accumulation on sea ice is included. The transformation from snow to ice when the snow-ice interface sinks below sea level due to snow loading is modelled. The effect of ice formation and melting is accounted assuming a sea ice salinity of 5 psu.

The atmosphere and ocean models are coupled via the OASIS coupler (Valcke *et al.*, 2003). The ocean passes the sea surface temperature (SST), sea ice area, sea ice thickness, snow depth, and the ocean surface velocities to the atmosphere. River runoff and glacier calving are treated interactively in the atmosphere model and the freshwater fluxes are given to the ocean as part of the atmospheric freshwater flux field. The land hydrology model includes a river routing scheme (Hagemann and Dümenil-Gates (1998) and Hagemann and Dümenil-Gates (2003)). This coupling has a time-step of 1 day.

Land vegetation is modelled with the dynamical model LPJ (Sitch *et al.*, 2003). The model set-up and its coupling to the atmospheric component are basically the same as those in the ESM1 ECHAM3/LSG2/LPJ/HAMOCC/SICOPOLIS described in Chapter 2. The horizontal resolution of the model is the same as the atmospheric model (T31).

The three-dimensional thermodynamic ice sheet model SICOPOLIS simulates

the ice sheets of both hemisphere. The model is used with a horizontal resolution of 80 km and 21 vertical levels in the ice domain. The set-up of the model is the same as in the ESM1.

The (fully synchronous) coupling between the atmosphere-ocean and the land vegetation and ice sheet models takes place with a time-step of 1 year. The time step of the atmospheric model is 40 minutes. The time step of the ocean component is 8640 seconds. The land vegetation model and the ice sheet model are run with a time step of 1 year.

7.2 Coupling between the ice sheet model and other components

The coupling between the climate model and the ice sheet model is bi-directional. The surface mass balance is calculated with a time-step of six hours from the output of the previous timestep from the atmospheric model. The feedbacks from the ice sheet model (meltwater fluxes, glacier mask and topography) are given to the climate model at the end of each simulated year.

The atmospheric forcing of the ice sheet model consists of 6-hourly radiation fields (downward shortwave and longwave radiation), near surface (2-m height) temperature and dew-point, precipitation rates, and wind speed at 10 m height. An additional field of surface pressure is taken in order to calculate the near-surface air density.

The changes in sea level due to the changes in storage of water by the modelled ice sheets are passed to the atmospheric model, where they are added to the orography. The sea level change is given as forcing to the ice sheet model in the next model year.

7.2.1 Downscalling of atmospheric forcing fields

The atmospheric fields mentioned before are bi-linearly interpolated from the atmospheric grid (horizontal resolution T31) onto the ice sheet model grid (horizontal resolution 80 km).

To account for the height differences between the topography of the atmospheric model and the ice sheet model, several height corrections have been applied. For the near-surface temperature and dew point, the environmental lapse rate (-6.5°C/km) has been applied. Precipitation rates have been corrected from the height-desertification effect (reduction of precipitation rates with increasing

topographic height). For that, it was assumed that the precipitation rates do not change with height between 0 m and a height h_0, and that for heights $> h_0$ they decrease at an exponential rate. A halving of the precipitation rates is prescribed for every km over zs_{thresh} (Budd and Smith, 1979):

$$P_{ISM} = P_{ISM}(h_{ref}) = \begin{cases} exp\left(\gamma_p \left[max(h, h_o) - h_0\right]\right) & h_{ref} \leq h_0 \\ exp\left(\gamma_p \left[max(h, h_o) - h_{ref}\right]\right) & h_{ref} \geq h_0 \end{cases} \tag{7.1}$$

with $\gamma_p = -0.6931$ km^{-1}

For the downward longwave radiation a decrease of 2.9 W/m^2 is assumed for every 100 m of height increase (Marty *et al.*, 2002).

The near-surface air density is also corrected when height changes. The change of near-surface air pressure with height is calculated first and then converted into density change.

7.2.2 Fields given by the ice sheet model to the ocean and atmospheric models

The ice sheet model provides freshwater fluxes to the ocean every year. The freshwater flux is given to the ocean at the ocean grid point closest to the ice sheet grid point.

Topography and glacier mask are provided from the ice sheet model to the atmospheric model. The glacier mask of the ice sheet model is interpolated onto the atmospheric grid. If more than 40% of the area of the atmospheric grid point is ice-covered, then the atmospheric grid point is considered to be glaciated, otherwise it is completely ice-free.

7.3 Surface mass balance calculation

As already explained, the surface mass balance is calculated with an energy-balance scheme from several 6-hourly fields of the atmospheric model. The mass balance is calculated at the resolution and surface height of the ice-sheet model. The surface mass balance scheme is applied after the simulation of 1 year of the atmospheric model. The calculated accumulation, surface melting rates and surface temperatures are passed to the ice sheet model and then the ice sheet model is run with these boundary conditions of the surface mass balance and temperature of the uppermost layer of the ice sheet.

7.3.1 Calculation of snowfall rates

Snowfall rates are derived from precipitation rates with a time step of 6 hours. Precipitation is converted into snow if the near surface temperature is lower than 0°C.

7.3.2 Calculation of surface melting

Melt rates are calculated from the balance of the radiative fluxes (shortwave and longwave), latent and sensitive heat fluxes, heat conduction to/from inner snow layers, and the heat released/absorbed due to the fall of precipitation on the ice surface.

A snowpack of thickness 20 m has been discretised into several layers for the calculation of the heat conduction through the uppermost (snow) layers of the ice sheets. The uppermost layer has a thickness of 0.33 m. The thickness of the layers increases with depth. The density and thermal conductivity of the snow vary with depth. For the dependence of snow density on depth, the empirical relation from Schytt (1958) is used

$$\rho(z) = \rho_{ice} - (\rho_{ice} - \rho_s) \cdot \exp(-C \cdot z) \tag{7.2}$$

where z represents the depth, ρ_{ice} is the density of ice (917 kg m^{-3}) and C is a constant for a given site. The mean value from measurements at two stations in central Greenland, C=0.024 m^{-1} (Paterson, 1994), is used.

The thermal conductivity of the snow K is assumed to depend on the ice density through the formula of Schwerdtfeger (1963):

$$K(z) = \frac{2K_{ice}\rho(z)}{(3\rho_{ice} - \rho(z))} \tag{7.3}$$

where K_{ice} =2.10 W m^{-1} K^{-1} (Yen, 1981) is the thermal conductivity of ice.

To calculate the melt rates, first the temperature of the uppermost layer of the snowpack in contact with the atmosphere T_S is calculated from the energy balance at the snow surface through the equation:

$$-\rho_s c_p \frac{\partial T_s}{\partial t} = \frac{\partial F}{\partial z} \tag{7.4}$$

where ρ_s is the density of the uppermost layer of the snowpack in contact with the atmosphere, c_p is the specific heat capacity of snow and F is the sum of the radiative, latent, sensible and precipitation heat fluxes:

$$F = S_{abs} - L\uparrow + L\downarrow + E + H + H_p + H_{cond} \tag{7.5}$$

In the previous equation S_{abs} is the absorbed shortwave radiation flux, $L\uparrow$ is the upwards longwave radiation flux, $L\downarrow$ is the downwards longwave radiation flux, E is the latent heat flux, H is the sensible heat flux, H_p is the heat either released or lost by precipitation falling on the snow surface, and H_{cond} is the heat flux conducted from/to the next snow layer. Details about the calculation of the heat fluxes are given later in this chapter.

If the temperature T_s calculated from equation 7.4 exceeds the melting point temperature T_{melt}=273.15 K, T_S is set to T_{melt} for the recalculation of the heat fluxes and the equation 7.4 is solved again for T_s. The energy needed to warm the surface from the melting point to the new solution for T_s over the melting point is the energy available for melting. Melting rates are calculated assuming a latent heat of fusion of 3.65 x10^5 kJ kg.$^{-1}$

Calculation of the heat fluxes

In the following the calculation of the terms of equation 7.5 will be described.

The absorbed wave shortwave radiation S_{abs} is calculated from the downward shortwave radiation $S\downarrow$ according to:

$$S_{abs} = (1 - \alpha) \cdot S\downarrow \tag{7.6}$$

The albedo α of the surface depends on several factors, like the presence of meltwater, dust, vegetation, and the time since the last snowfall (aging factor). A parameterisation for snow and ice albedo similar to the parameterisation from the atmospheric model has been used here. α is set to a minimum value $\alpha_m = 0.55$ for the case of the surface being at pressure melting point. A maximum value α_{max} =0.825 is used for cold surfaces ($T_S \leq T_0$=268.15 K). In the temperature range $T_0 < T_S < T_{melt}$, α is obtained by linear interpolation

$$\alpha = \alpha_{max} - (\alpha_{max} - \alpha_m) \cdot \frac{T_S - T_0}{T_{melt} - T_0} \tag{7.7}$$

The longwave radiation emitted by the surface $L\uparrow$ is calculated from the surface snow temperature Ts as the radiation emitted by a black body

$$L\uparrow = -\sigma \cdot T_s^4 \tag{7.8}$$

where σ is the Stefan's constant σ =5.67 x 10^{-8} Wm^{-2}K^{-4}.

The absorbed longwave radiation $L\downarrow$ is taken directly from the (interpolated and height-corrected) output of the atmospheric model.

The sensible heat flux H is calculated via a bulk-formula from the 10-m wind speed and the difference between the screen (2 m-height) air temperature T_{air} and the prognostic variable T_s (temperature of the snow surface)

$$H = C_d \cdot \rho_{air} \cdot u_{10} \cdot (T_{air} - T_s) \tag{7.9}$$

where ρ_{air} is the air density and C_d is the drag coefficient C_d=1.515 J kg^{-1}K^{-1} (Ambach and Kirchlechner, 1986).

The latent heat flux E is calculated as well via bulk-formula from the 10-m wind speed and the vapour pressure at screen height (2 m) e and at the surface e_s (where the air is assumed to be saturated)

$$E = 22.2 \cdot A \cdot u_{10} \cdot (e - e_s) \tag{7.10}$$

from (Paterson, 1994), where A is the adimensional transfer coefficient A=1.5 x 10^{-3}(Ambach and Kirchlechner, 1986).

The heat flux from/to the next snow layer H_{cond} is calculated from

$$H_{cond} = K \cdot \frac{\partial T}{\partial z} \tag{7.11}$$

where K is the thermal conductivity of the snow.

The heat released/absorbed during precipitation falling on the snow surface H_p is calculated from the precipitation rates p and the temperature of the raindrops/snowflakes. This temperature is approximated by the near-surface air temperature T_{air}. The formula used for the calculation of H_p is

$$H_p = p \cdot c_p \cdot (T_{air} - T_{melt}) \cdot \rho_w \tag{7.12}$$

where p is the precipitation rate, ρ_w is the density of water, and c_p is the conductivity of snow/water (depending on the occurrence of precipitation as snow or rain).

7.3.3 Calculation of the profile of temperatures in the snowpack

The profile of temperature in the snow pack is modified every time-step according to the heat fluxes caused by differences of temperature between each layer and the layer immediately above. These temperatures can be modified by the heat released by the refreezing of percolated meltwater.

7.3.4 Refreezing of meltwater

If melting occurs, the surface meltwater can percolate and be refrozen at inner layers of the snowpack at temperatures lower than the pressure melting point. The potential amount of meltwater that can be refrozen at each layer is calculated from the energy absorbed by the snow layer when its temperature is raised from its initial temperature to the melting temperature T_{melt}. The actual amount of refrozen meltwater at each layer is the minimum of the potential amount that can be refrozen and the amount of meltwater that reaches the layer.

7.3.5 Surface temperature

The ice sheet model needs a surface boundary condition for the temperature of the uppermost ice layer of the vertical grid (with 21 levels). The boundary condition at the bottom of the ice column is given by the geothermal heat flux.

Daily and seasonal variations of the near-surface air temperature over a glacier propagate approximately only until a snow depth of 10-15 m. The temperature measured at a depth of 10 or 15 m of a glacier is equal to the mean annual air temperature, except if the maximum air temperature is higher than 0°C (Paterson, 1994). In this case, the refreezing of meltwater should raise the firn temperature above the mean annual air temperature. On the other hand, the glacier temperature surface cannot rise above 0°C.

The temperature of the uppermost ice layer of the surface is calculated within the energy balance scheme shown here from the temperature of the snowpack at depth 15 m.

7.3.6 Calculation of sublimation.

Sublimation rates are calculated from the latent heat fluxes, with a sublimation heat value of L_{sub}=2.834 x 10^6J/kg.

Chapter 8

Evolution of global ice sheets under greenhouse stabilisation scenarios modelled with ESM2

The Earth System Model ECHAM5/MPI-OM/LPJ/SICOPOLIS (ESM2) has been used to study the evolution of global ice sheets under anthropogenic climate change. This ESM2 has a higher climate sensitivity than ESM1, and consequently the response of the global ice sheets to the increased concentration of greenhouse gases is expected to be different from ESM1.

The bi-directional coupling of the ice sheets has been performed without flux corrections. This represents a step forward in the studies of the response of the global ice sheets to anthropogenic climate change.

8.1 Initialisation of the model

The ice sheet model was initialisated with a simulation of the two last glacial cycles, similarly as described in Chapter 3 for the Initialisation of the model for the simulations with ESM1. After that, the ice sheet model and the vegetation model as well were spun-up with the climatology of a control climate simulation with the AOGCM ECHAM5/MPI-OM.

The ice-sheet model and the vegetation model were coupled to the ocean and atmospheric components simultaneously. The coupled model was run for 300 years with pre-industrial concentration of greenhouse gases (control simulation CTRL), and from year 300 the greenhouse simulations were started. The first simulated year with perturbed concentration of CO_2 will be the year 1 of the simulations.

8.2 Set-up

A set of simulations have been performed in order to validate the new Earth System Model ECHAM5/MPI-OM/LPJ/SICOPOLIS and in order to study the response of the global ice sheets to two different stabilisation scenarios. A control simulation CTRL of length 500 years with prescribed CO_2 concentration of 280 ppmv was run. Two simulations where the atmospheric CO_2 concentration rises by 1% per year until reaching 2 times and 4 times the pre-industrial level have been performed. These experiments will be referred to as 2x and 4x, respectively. In 2x, the stabilisation level is reached at year 70; in 4x, at year 140. The simulation 2x has a length of 200 years. The simulation 4x has a length of 300 years.

An additional set of three experiments has been performed with the coupled model ECHAM5/MPI-OM/LPJ. The ice sheet model was not coupled. These simulations will be compared to the simulations CTRL, 2x and 4x in order to investigate the impact of the ice sheets onto the climate system. They will be referred to as CTRL_noism, 2x_noism, and 4x_noism.

In table 8.1 an overview of the simulations analysed in this chapter is given.

Name	Description
CTRL	Control simulation with prescribed CO_2 concentration of 280 ppmv
2x	1% increase of CO_2 /year until stabilisation at 2x pre-industrial level
4x	1% increase of CO_2 /year until stabilisation at 4x pre-industrial level
*_noism	Simulations without the ice sheet model (only ECHAM5/MPI-OM/LPJ)

Table 8.1: Simulations analised in this chapter.

8.3 Control ice sheets

The ice sheets from the control simulation CTRL will be described here.

8.3.1 Northern hemisphere control ice sheets

The simulated northern hemisphere ice sheets have a total area of 2.56±0.04 x 10^6 km^2. These glaciated areas are placed on Greenland, the Canadian Archipelago (Baffin Island, Ellesmere Island), in the Rocky Mountains and the Alaska Range, on high elevated areas of East Siberia, Svalbard and Novaya Zemlya (fig. 8.1). These glaciated areas are simulated at the location of actual glaciers and ice caps (see figure in chapter 3). The simulated ice sheets have a volume of 9.3 m SLE. The simulated Greenland ice sheet has a volume of 8.7 m SLE, which is 20% larger than the volume of the measured ice sheet (7.2 m SLE, Church *et al.* (2001)). Most of the extra-ice is placed in northeast Greenland, extending onto the shelf, similarly as shown for the control Greenland ice sheet from ESM1. The simulated glaciers in the Rocky Mountains and the Alaska Range have a volume of 0.48 m.

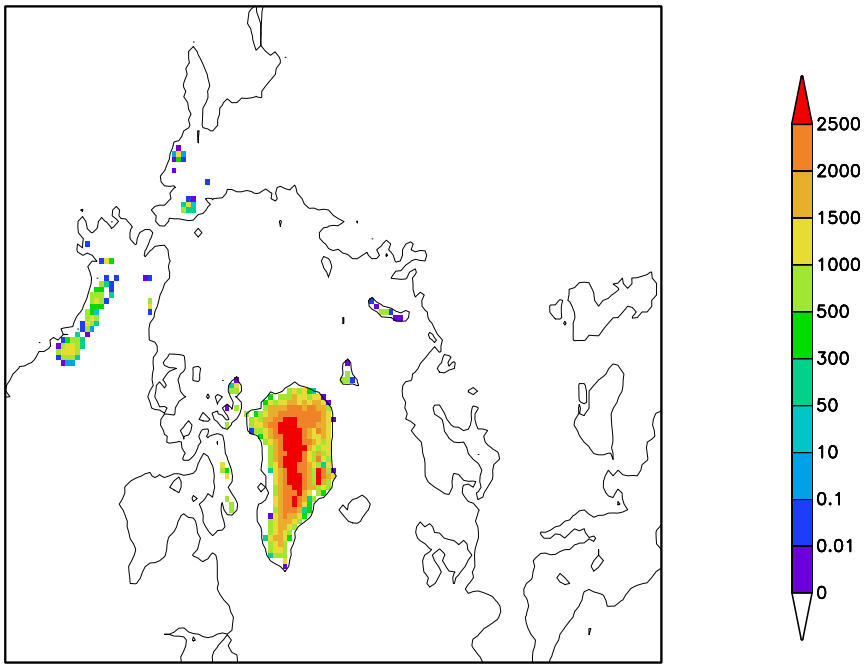

Figure 8.1: Mean thickness [m] of the northern hemisphere ice sheets from the control simulation in the ice-sheet model grid. The black contour line corresponds to the model isoline for the topographic height=0 m. The refined scale for thickness < 50 m is given to separate ephemeral (snowcover surviving at least one melting season but disappearing afterwards) from permanent glaciers.

8.3.2 Southern hemisphere control ice sheets

In the southern hemisphere, the simulated ice sheets are placed only on Antarctica. The Antarctic ice sheet of CTRL has a mean volume of 66.9 m SLE, with a growing trend of 0.4 mm/yr. This trend is due to the overestimation of precipitation rates by the atmospheric model. This overestimation is caused by the coarse resolution (T31) of the model: the orographic barrier effect of the ice sheet is reduced due to the smooth topography at this model resolution.

The simulated volume is 9% bigger than the available measurements (Church *et al.*, 2001). The area of the CTRL Antarctic ice sheet is 12.55±0.01 x 10^6 km^2, very close to the measurements (12.37 ±0.01 x 10^6 km^2). Main differences with the ice sheet model simulated with ESM1 are found on the Antarctic Peninsula (not shown). In the ice sheet from ESM2 the grounding line is closer to observations in this area.

8.4 Global changes in the atmosphere and ocean

The mean global temperature increases in all the greenhouse simulations (fig. 8.2, upper graph). In 2x, the increase in the mean global near-surface temperature is approximately 2.8 K one century after the stabilisation of the CO_2 concentration in the model year 70. In 4x, the increase in the mean global near-surface temperature is approximately 7.5 K one century after the stabilisation of the CO_2 concentration in the model year 140.

In simulation 2x, averaged over the period between years 155-185, the annual temperatures over the world oceans increase by 1-3 K (fig. 8.3, upper panel). Over most of the continents, the temperature increases by 3-5 K. The warming is strongest in the northern high latitudes (more than 5 K over the Arctic and Northern Siberia). The lowest temperature increase occurs in the North Atlantic, due to reduced strength of the Meridional Overturning Circulation (MOC). In this region the increase in the annual temperature is less than 1 K.

In simulation 4x, averaged over the period between years 255-285, most of the world oceans experience an increase of the annual temperature between 5 and 7 K (fig. 8.3, lower panel). Temperature increases more than 7 K in the tropical Pacific. In the Arctic temperature increases by more than 13 K. Over land, temperature increases by 7-10 K. Maximum warming takes place in the high northern latitudes, desert areas (Sahara, Arabian Peninsula), in Tibet, and Australia. Northern Eurasia and Northern North America experience an increase of more than 10 K. In the interior of Antarctica temperature increase by more

than 13 K. The lowest increase of temperature takes place in the North Atlantic, where it increases only 1-3 K.

The hydrological cycle is enhanced in both simulations 2x and 4x. One hundred years after the stabilisation of CO_2 concentration in 2x, in the year 170, the annual global mean precipitation has increased by 5%. By year 270, the increase in 4x is approximately 14%.

The strength of the North Atlantic Meridional Overturning Circulation (NAMOC) is strongly reduced in all the perturbed climate simulations, whether the additional freshwater from the ice sheets are included or not (fig. 8.2, lower graph). Both in 2x and 2x_noism, the maximum strength of the NAMOC at 30° N decreases from the mean value of 13 Sv from CTRL to 7 Sv in year 150. The reduction is stronger in the simulations 4x and 4x_noism, where the strength of the overturning shrinks to approximately 5 Sv in year 200.

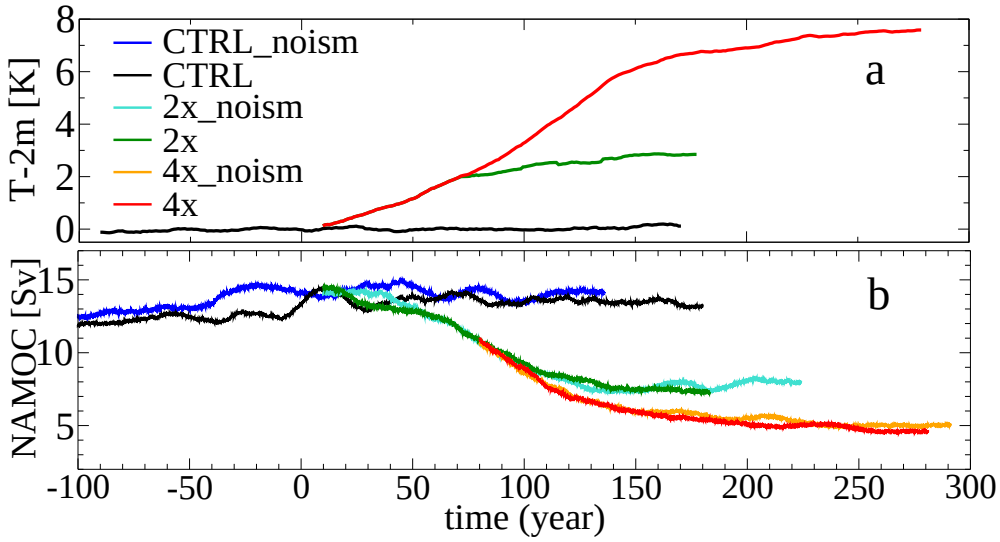

Figure 8.2: (a) Changes in the near surface (2-m height) temperature [K] and (b) strength of the north Atlantic meridional overturning at 30°N and at 1500 m depth [Sv] for 2x (green), 2x_1w (light green), 4x (red), and 4x_1w (yellow) relative to CTRL (black); 20-year running means.

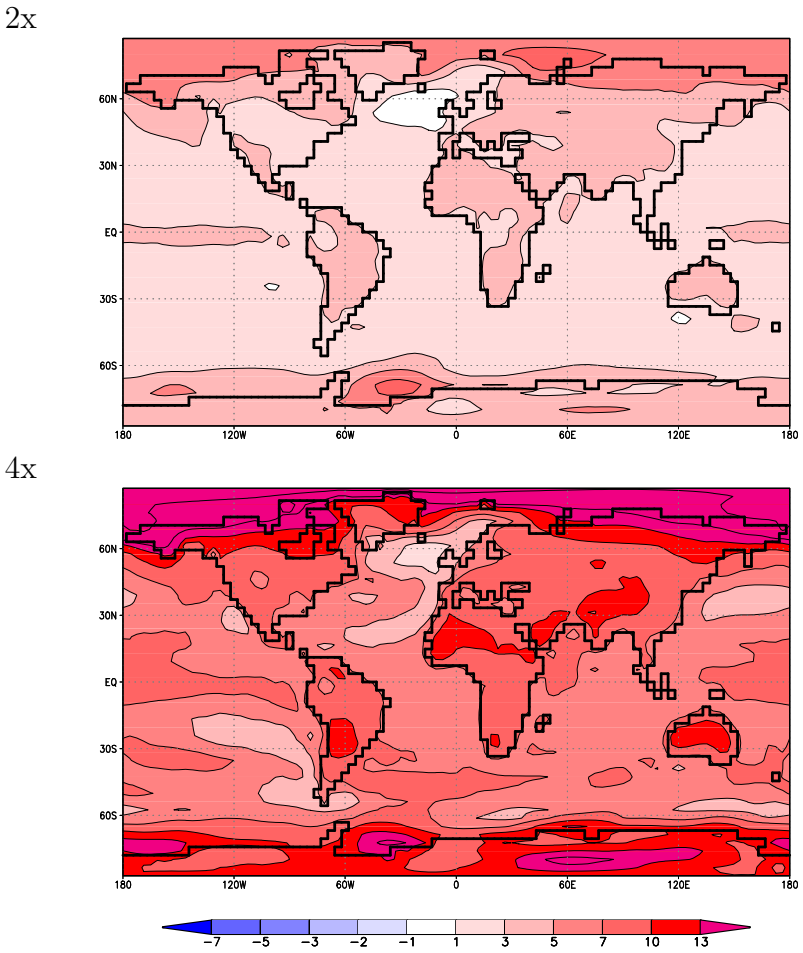

Figure 8.3: 2-dimensional distribution of changes in the mean annual near-surface air temperature [K] in the simulations 2x (years 155-185) and 4x (years 255-285) compared to CTRL.

8.5 Evolution of the Greenland ice sheet

8.5.1 Regional climate change over Greenland

The regional climate change over Greenland is weaker than in other places at similar latitude in the high northern latitudes. This is due to the reduction of northward heat transport by the ocean associated with the weakening of the NAMOC. While in the simulation 4x with ESM1 this reduction of heat transport produced negative anomalies in the pattern of summer temperature change over parts of Greenland, the temperature change is positive in ESM2 over entire Greenland (fig. 8.4). This is caused by the higher climate sensitivity of ESM2. Hence, the global warming signal associated with the increased concentration of greenhouse gases is stronger than the regional cooling signal associated with reduced ocean transport.

As in the simulations with ESM1, the temperature anomalies are higher in the northern part of Greenland and lower in the southern part. One hundred years after the stabilisation of the atmospheric CO_2 concentration, the summer (JJA) near-surface temperature has increased between 3 and 5 K over the northern half of the ice sheet. Almost no temperature change occurs at the southern tip of the island.

Averaged over the years 255 to 285, the summer temperature change has a strong north to south gradient in the simulation 4x. Temperature increases between 1 and 3 K in the southermost part of the island. An average increase of 5 K occurs between 70 and 73°N, in the centre of the ice sheet. Temperatures increase between 7 and 10 K over the northern half of the ice sheet.

8.5.2 Changes in the mass balance of the Greenland ice sheet

The area and volume of the northern hemisphere ice sheets decreases in all the simulations (fig. 8.5). By year 200, the volume reduction is equivalent to a sea level rise of 15 cm in 2x, and 55 cm in 4x. By year 300, the ice loss in 4x is equivalent to a sea level rise of 1.2 m. Most of this reduction is due to the decay of the Greenland ice sheet, whose contribution to the sea level rise is 1.1 m SLE.

In 2x, by year 170, the ice thickness in most of areas with less than 2000 m height is reduced (fig. 8.6). The strongest reduction takes place at the eastern central margin. In the interior there are no strong changes. Melting rates are stronger than in CTRL in all areas lower than 2000 m (fig. 8.7). Non-zero melting rates exist for a large area with more than 2000 m height in the western half of the

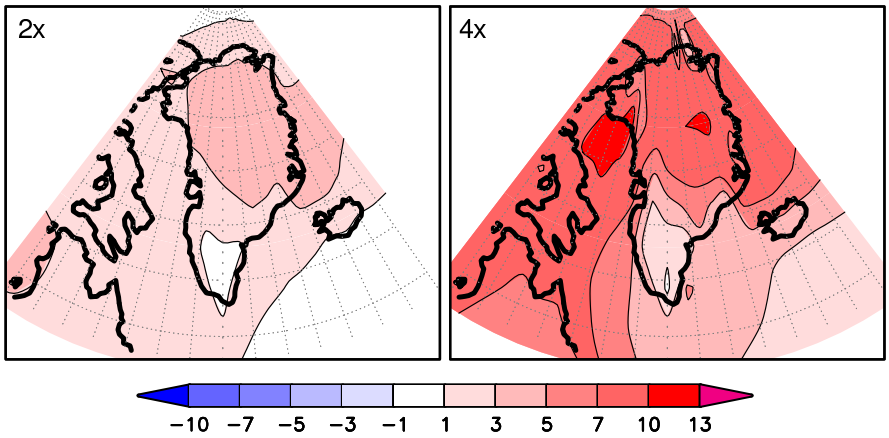

Figure 8.4: Changes in the summer (JJA) temperature [K] over Greenland with respect to CTRL in 2x (average years 155-185) and 4x (average years 255-285). Note that the temperature anomaly has not been corrected for the different reference topography of CTRL and the greenhouse simulations.

ice sheet. Accumulation rates increase over most of the ice sheet, except some low areas at the southern half of the island where the ratio of rain to snow increases.

In 4x, by year 170, the ice thickness in most of areas with more than 2000 m height decreases by several tens of meters. By year 270, the ice thickness is several tens of meters thinner than in CTRL in all areas in the interior and hundreds of meters in the margins. The only exception is the southern tip, where there is no surface melting and snowfall rates increase (fig. 8.7). Except in this area, surface melting occurs *everywhere over the ice-sheet,* even at the top of the ice sheet. Melting rates exceed 500 mm/yr for most of the Greenland Plateau. Accumulation rates are stronger than in CTRL and 2x, except in some marginal areas where the fraction of precipitation falling as rain is higher than in CTRL.

8.6 Evolution of the Antarctic ice sheet

8.6.1 Regional climate change over Antarctica

Antarctica is one of the regions experiencing a stronger than average warming in these greenhouse simulations. In 2x, by year 170, the summer temperatures have increased by 3-5 K over the ice sheet (fig. 8.8). In 4x, by year 270, most margins of the ice sheet experience an increase of 7-10 K. The increase is stronger in the ice shelf areas. At some areas in the interior and close to the Weddell Sea, the increase is even stronger than 13 K.

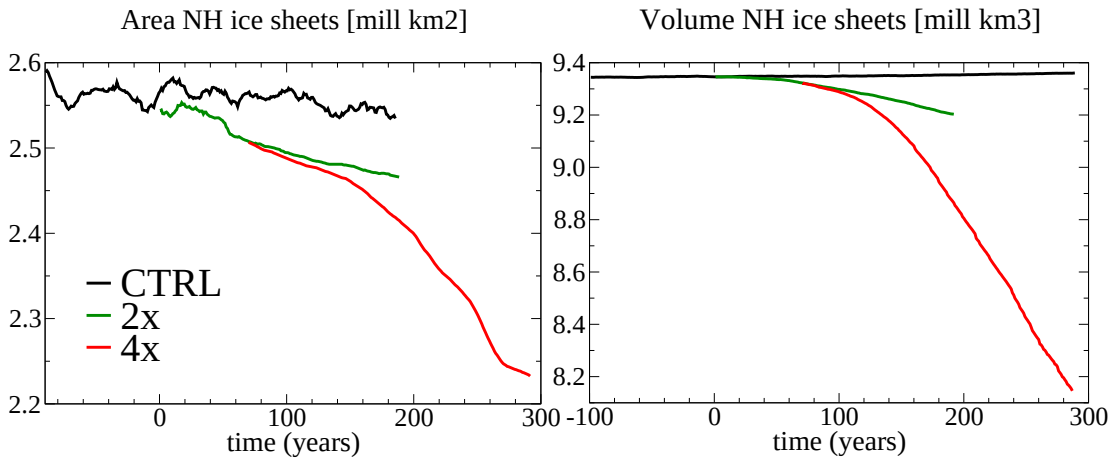

Figure 8.5: Changes in the area and volume of the northern hemisphere ice sheets in 2x (green), 4x (red) and CTRL (black); 20-year running means.

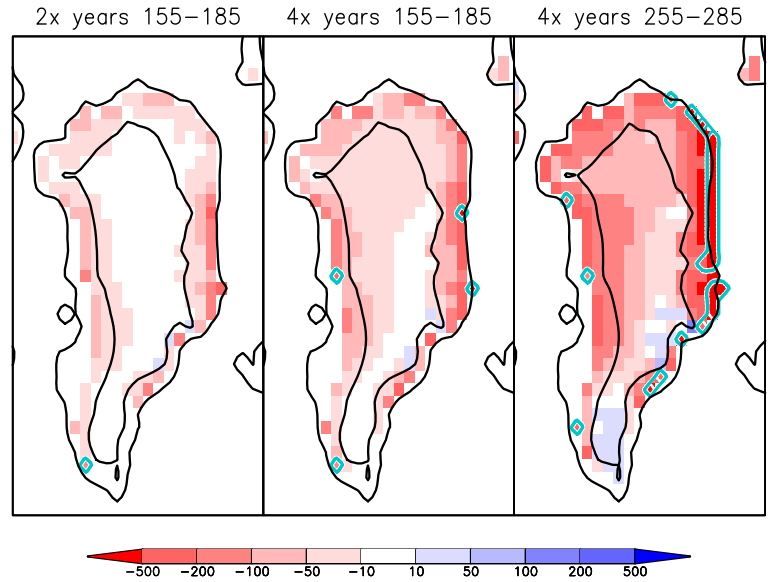

Figure 8.6: Changes in ice thickness [m] and grounding line position (blue line: area becoming ice free) in the GrIS for the period 900-1000 for the simulations 2x, 3x and 4x minus CTRL. In black: contour lines for heights z=0 m and z=2000 m.

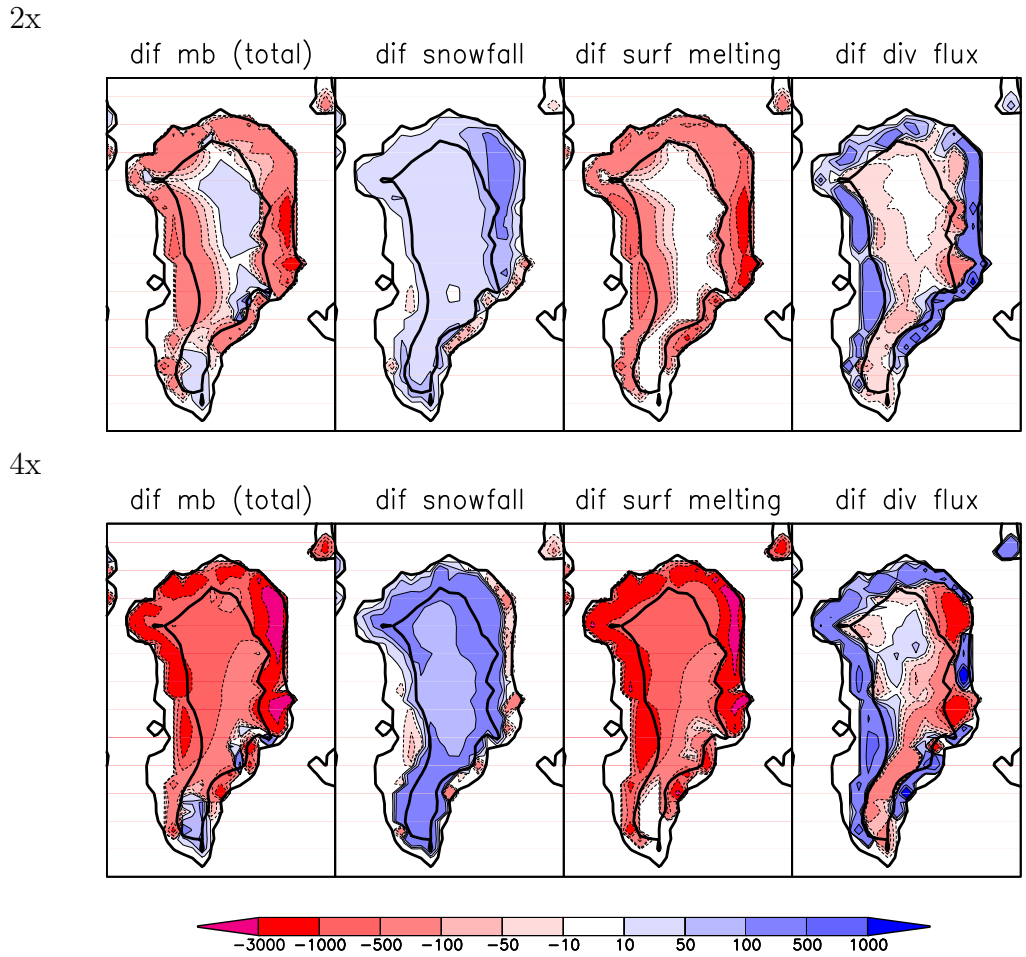

Figure 8.7: Two-dimensional changes in the mass balance [mm WE/yr] of Greenland between simulations 2x (years 155-185) and 4x (years 255-285) and CTRL: first column: total mass balance; second column: surface accumulation (snowfall); third column: surface melting; fourth column: changes in horizontal transport. In black: contour lines for heights z=0 m and z=2000 m.

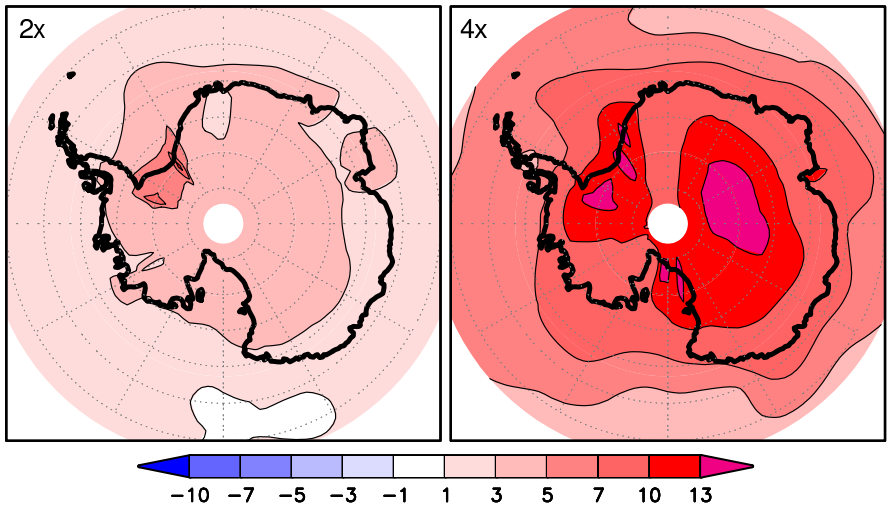

Figure 8.8: Changes in the summer (DJF) temperature [K] over Antarctica with respect to CTRL in 2x (average years 155-185) and 4x (average years 255-285). Note that the temperature anomaly has not been corrected for the different reference topography of CTRL and the greenhouse simulations.

8.6.2 Changes in the mass balance of the Antarctic ice sheet

The area of the grounded ice of the Antarctic ice sheet decreases in both simulations 2x and 4x (fig. 8.9). By the year 300, the grounded ice area is reduced by 0.4 x 10^6 km^2 in 4x. In 2x the ice sheet gains mass due to increased accumulation rates. The storage of water by the year 200 is equivalent to a sea level lowering of 7 cm. In 4x, the ice sheet grows until approximately year 140. From then, it begins to decay. The contribution to sea level rise is 30 cm by the end of the simulation.

The ice thickness of many areas of the ice sheet increases by several tens of meters by year 300 in simulation 4x (fig. 8.10). The thickness of marginal areas decreases. The strongest reduction of the volume of the ice sheet takes place in West Antarctica, mainly in the Antarctic Peninsula and the Amundsen Sea Coast. The two-dimensional pattern of ice thickness changes is similar in the simulation 2x, although with a lower amplitude. The area of the Antarctic Peninsula also experiences the strongest reduction of volume.

Accumulation rates increase in both simulations 2x and 4x (fig. 8.11). A modest increase of surface melting rates takes place in some low areas in 2x. In 4x, the increase of surface melting takes place over most of the areas below 1000 m height. A very strong increase occurs in the Antarctic Peninsula. The ice flux

accelerates in this area, contributing to the mass loss.

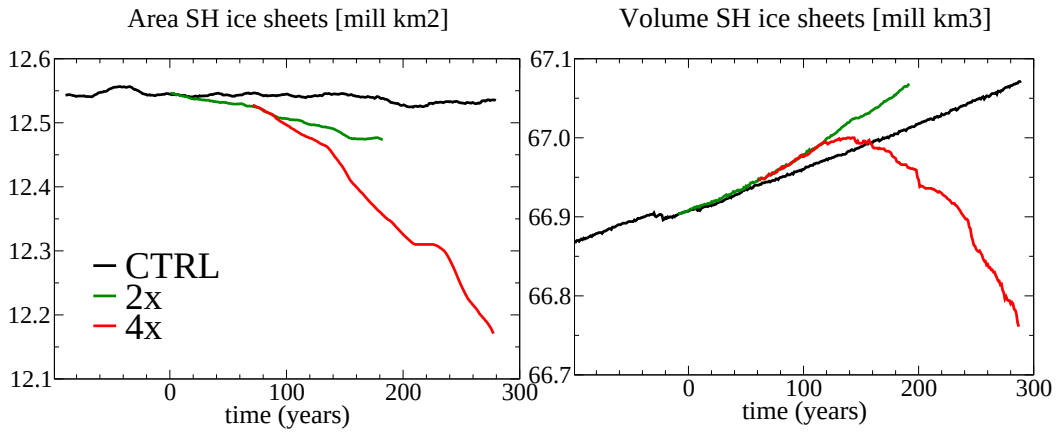

Figure 8.9: Changes in the area (20-year running means) and volume of the southern hemisphere ice sheets in 2x (green), 4x (red) and CTRL (black).

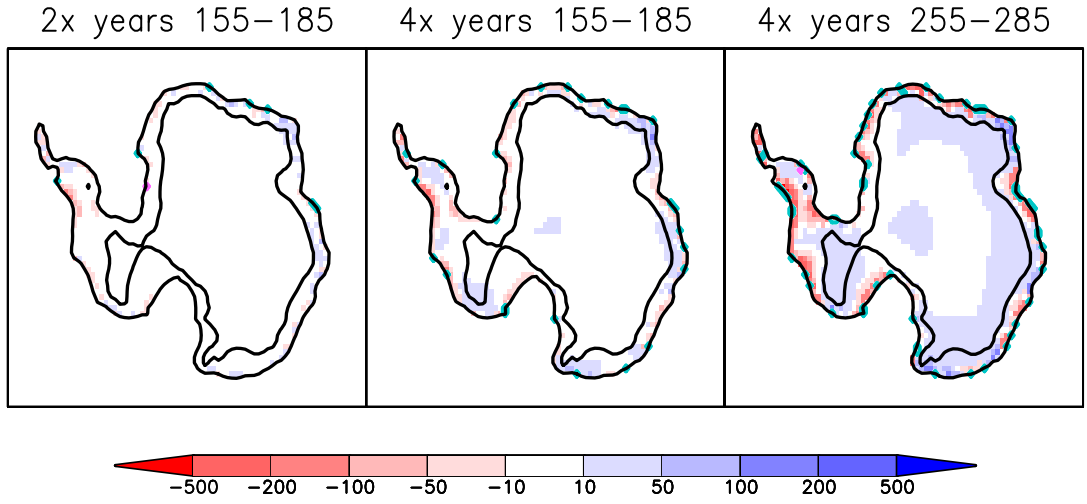

Figure 8.10: Changes in ice thickness [m] and grounding line position (blue line: area becoming ice free; pink line: area becoming iced) in the AIS for the simulations 2x (years 155-185) and 4x (years 255-285) minus CTRL (same period of time as in the respective greenhouse simulation). In black: contour lines for heights z=0 m and z=2000 m.

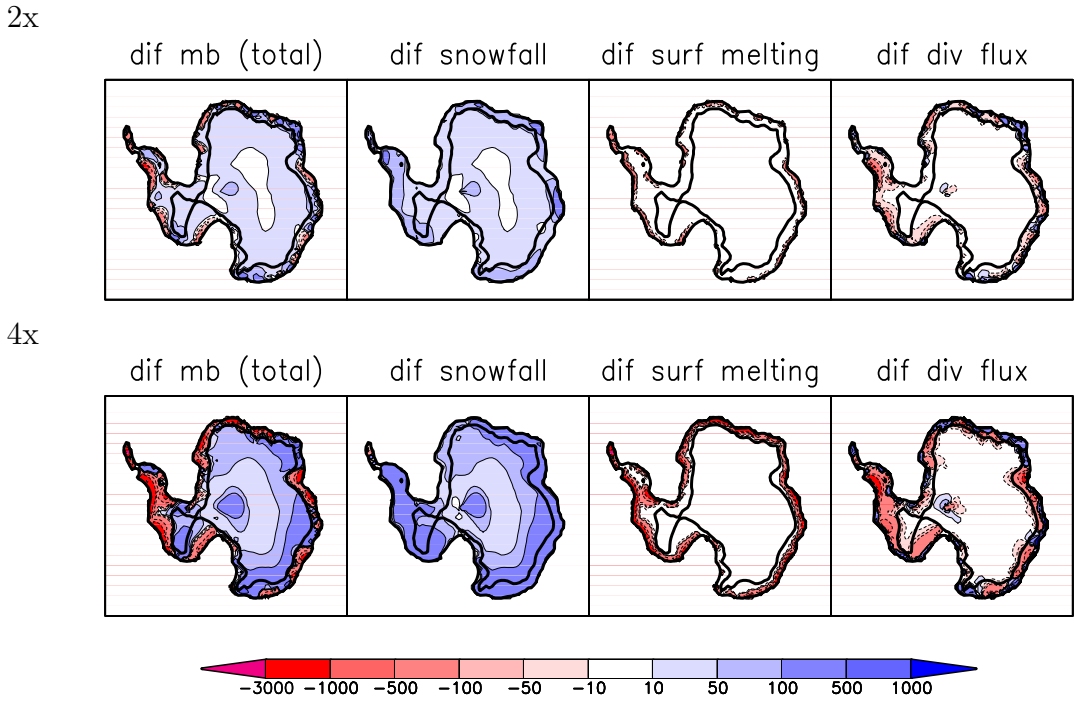

Figure 8.11: Two-dimensional changes in the mass balance [mm WE/yr] of Antarctica between simulations 2x (years 155-185, upper panel) and 4x (years 255-285, lower panel) and CTRL: first column: total mass balance; second column: surface accumulation (snowfall); third column: surface melting; fourth column: changes in horizontal transport. In black: contour lines for heights z=0 m and z=2000 m.

8.7 Freshwater fluxes from ice sheets and ocean circulation

The meltwater fluxes from both the Greenland and Antarctic ice sheets are relatively strong in these greenhouse simulations. By the year 200, the meltwater fluxes from the Greenland ice sheet are approximately 0.015 Sv in 2x and 0.08 Sv in 4x (fig. 8.12c). In the southern ocean, the meltwater fluxes from the Antarctic ice sheet (fig. 8.12d) are positive in both simulations 2x and 4x. The positive sign of 2x in spite of the negative contribution to sea level rise is due to the loss of non-grounded ice (the floating ice shelves do not contribute to sea level changes but do contribute to the balance of freshwater fluxes). The meltwater fluxes from the Antarctic ice sheet from CTRL are slightly negative due to the negative trend explained in 8.3.2. Maximal meltwater fluxes from the AIS for 2x are approximately 0.005 Sv. Maximal meltwater fluxes from the AIS for 4x are approximately 0.04 Sv.

The difference in the freshwater fluxes into the North Atlantic and Southern Ocean between the simulations with bi-directional coupling of the ice sheets (2x, 4x) and the simulations with ice sheets passively coupled (2x_1w, 4x_1w) are not exactly identical to the magnitude of the meltwater fluxes from the ice sheets. Other factors related to the bi-directional coupling of the ice sheets can contribute to these differences. For instance, differences in the topography and extension between the prescribed ice sheets of the simulations *_1w and the interactive ice sheets can produce some differences in the orographic forcing of precipitation. The different orography could also affect evaporation rates via differences in surface temperature.

8.7.1 NAMOC

In the simulation 4x the North Atlantic Meridional Overturning Circulation (NAMOC) weakens very strongly (fig. 8.2b). The evolution of the NAMOC in the simulation 4x_noism, where the ocean does not receive the additional freshwater fluxes from the ice sheets, is very similar to the evolution in 4x. The anomalies with respect to CTRL of total freshwater fluxes into the North Atlantic in this simulation 4x_noism (fig. 8.12a) are very high at the time of the strong weakening of the NAMOC (for instance, 0.08 Sv by year 100). The freshwater fluxes from Greenland begin to represent a substantial part of the total budget several decades after the period of strong weakening. Thus the increase of moisture transport by the atmosphere into the North Atlantic drainage basin combined with surface

warming are sufficient to cause a collapse of the NAMOC. Although the contribution of meltwater fluxes from Greenland to the total budget is approximately one half of the total budget from year 150, these fluxes from the ice sheet do not produce any further weakening in an already collapsed overturning circulation.

In 2x_noism, increased atmospheric water transport before year 100 causes a substantial weakening of the NAMOC (fig. 8.2). The evolution of the NAMOC is similar in 2x, with the additional freshwater flux of 0.01 Sv by year 100 from the northern hemisphere ice sheets. Thus the meltwater fluxes from the ice sheets do not change the process of weakening of the NAMOC. The continuation of the simulations 2x_noism and 2x_ism could potentially show an effect of the additional meltwater fluxes from Greenland on the recovery/non-recovery of the NAMOC, since the magnitude of these fluxes is not small.

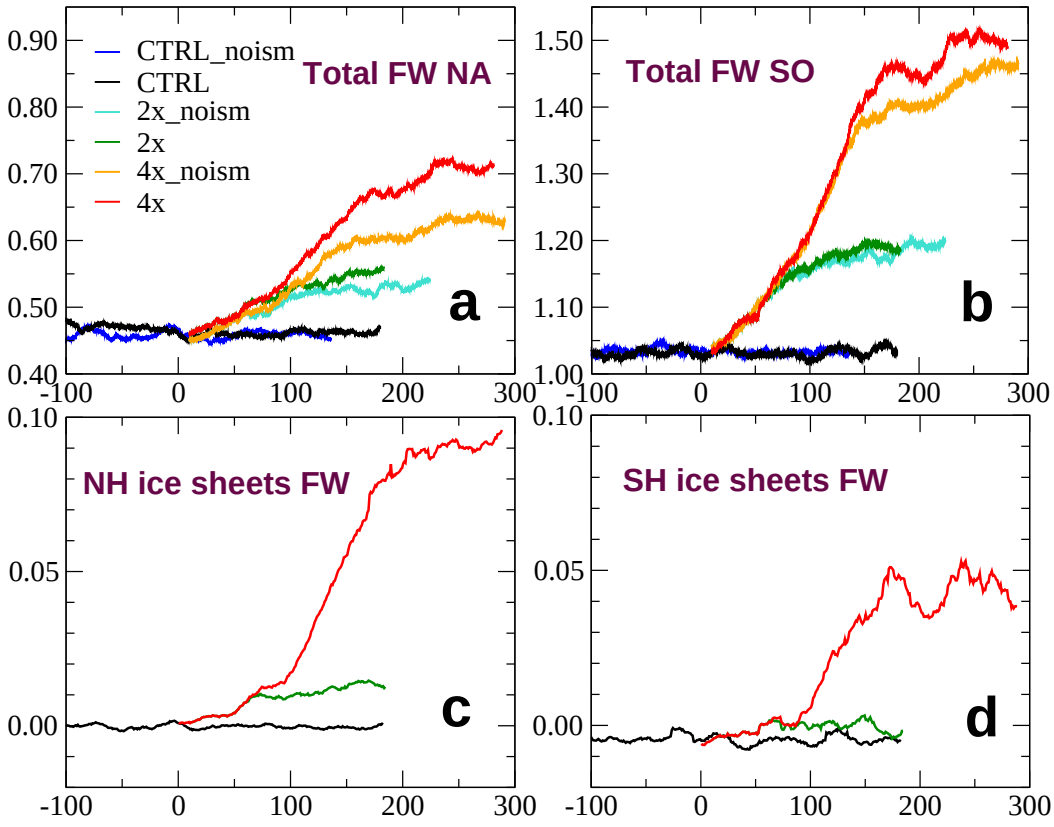

Figure 8.12: Total freshwater fluxes [Sv] into the North Atlantic and Arctic (a) and Southern Ocean (b), and freshwater fluxes from the northern hemisphere (c) and southern hemisphere (d) ice sheets for 2x (green), 2x_1w (light green), 4x (red), and 4x_1w (yellow) relative to CTRL (black); 20-year running means.

8.8 Conclusions

The main conclusions from the results of this study are summarised in the following:

- *An ice sheet model has been coupled to an AOGCM without flux corrections.* The simulated reference ice sheets from the control simulation corresponding to pre-industrial climate are relatively stable.

- The response of the Greenland ice sheet to the stabilisation scenarios of two times and four times pre-industrial CO_2 level is relatively strong compared to previous simulations with the ESM1 ECHAM3/LSG2/HAMOCC/LPJ/SICOPOLIS. This stronger response is due to the stronger climate sensitivity of the ESM2.

- Although the response of the ocean circulation to anthropogenic climate forcing is similar in ESM1 and ESM2, the change of temperature over the Greenland ice sheet is always positive in the simulations 2x and 4x with ESM2.

- Although the meltwater fluxes from the Greenland ice sheet are quite strong in the simulation with quadrupling of atmospheric CO_2 , they do not produce any strong effect in the ocean circulation because strong atmospheric moisture fluxes into the North Atlantic basin cause an early collapse of the NAMOC.

- Freshwater fluxes from the Greenland ice sheet could play a role in the recovering of the NAMOC in the simulation with doubling of atmospheric CO_2 .

- The warming over the Antarctic ice sheet in 4x surpasses the threshold from which the increase of surface melting exceeds the increase in snowfall. The mass balance becomes negative and the ice sheet looses mass.

Chapter 9

Conclusions and Outlook

9.1 General conclusions

Ice sheets are a physical component of the global climate system. They can modify the climate via changes in albedo and changes in topography, which can modify the general circulation of the atmosphere. Due to the location of the current ice sheets of Greenland and Antarctica close to the sites of deep water formation, increased freshwater fluxes from the ice sheets can potentially modify the strength of the ocean meridional overturning.

Climate change associated with anthropogenic emissions of greenhouse gases could cause important changes in the mass balance of the ice sheets of Greenland and Antarctica and therefore in sea level. Several studies of changes in the mass balance of ice sheets due to anthropogenic greenhouse forcing have been performed with the output of General Circulation Models. Most of these studies focus on the evolution of the ice sheets until the year 2100 (Church *et al.*, 2001). These studies do not include the contribution of changes in the dynamics of the ice sheets to the mass budget. However, changes in the topography of the ice sheets caused by the modification of the surface mass balance can potentially drive strong changes in the dynamics of the ice sheets. Besides, increased melt rates lower the topography and, as a consequence, surface temperatures increase, inducing further melting ("height-feedback"). In order to include the effect of changes in the topography in the mass balance calculations, a dynamical ice sheet model is needed.

The present study was performed in order to accomplish two main goals:

1. To study the evolution of global ice sheets behind the conventional screen of year 2100, that is, the long-term (multi-century) evolution of the ice sheets under anthropogenic greenhouse gas forcing.

2. To explore the effect of changes in the ice sheets on the climate and the

impact of these changes on the mass balance of the ice sheets as well (identification of feedbacks between the mass balance of ice sheets and the climate).

In order to achieve these two goals, a three-dimensional thermomechanical ice sheet model was coupled to two different Earth System Models (ESM1 and ESM2). Both ESMs include general circulation models of the atmosphere and ocean. This is the first study where global ice sheets are bi-directionally coupled to an AOGCM, with a closed global water budget. A previous study by Ridley *et al.* (2005) was performed with a model of only the Greenland ice sheet bidirectionally coupled to an AOGCM for a $4xCO_2$ simulation.

The ESM1 includes therefore the main components of the climate system (atmosphere, ocean, land vegetation, and ice sheets) and a closed carbon cycle. This fully coupled model permits a comprehensive study of climate changes due to anthropogenic greenhouse perturbation, with changes in carbon emissions as the only prescribed forcing for the system. The main conclusions from the results presented in this thesis achieved with several stabilisation and IPCC SRES scenarios are summarised in the following:

1. The Greenland ice sheet looses mass in all scenarios, in agreement with the studies of Gregory *et al.* (2004) and Greve (2000). Surface melting is modelled to exceed snow accumulation.

2. The freshwater fluxes from the Greenland ice sheet are moderate and do not play an important role in ocean circulation. The North Atlantic Meridional Overturning Circulation (NAMOC) weakens/collapses depending on the scenario, due to increased atmospheric moisture transport into the North Atlantic basin.

3. This weakening/collapse of the NAMOC produces a strong reduction of northward oceanic heat transport into the northern latitudes, which has important consequences for the regional climate of Greenland. The mass balance of the Greenland ice sheet (GrIS) is found to be very sensitive to the changes in heat transport due to changes in the NAMOC. This strong dependency is identified as a potential negative feedback for changes of the NAMOC due to freshwater fluxes from the GrIS. This dependency of the mass balance on the regional effect of a weakened/collapsed NAMOC was not studied explicitly in previous work about the evolution of ice sheets under anthropogenic forcing.

5. As in Ridley *et al.* (2005), it was found that the feedbacks between the ice sheets and the atmosphere are not important for the mass balance of the ice sheets until sufficient changes in the area and topography of the ice sheet are reached. With this model, and for the GrIS, this threshold was found at 3/4 of the original volume and area of the GrIS. The sign of these feedbacks was found to be positive, while in the study of Ridley *et al.* (2005) was found to be negative. Differences

are attributable to lower thermal contrast between ice-free and glaciated regions and to lower model resolution in this study with ESM1.

6. The impact of the disappearance of the GrIS in a climate with higher concentration of greenhouse gases and collapsed NAMOC was shown. A collapsed NAMOC was not considered in previous studies of the effects of the absence of the ice sheet. The results from this study show a different impact in the transient and mean features of the atmospheric circulation when the NAMOC collapses in the reference climate with respect to a reference climate with active NAMOC.

7. Accumulation rates are found to dominate the mass balance of the Antarctic ice sheet (AIS) in the simulations with ESM1. The AIS grows in all the simulations.

The coupling of the ice sheet model to the AOGCM from ESM2 was performed without flux corrections for the atmospheric forcing and with an energy balance scheme for the calculations of the melting rates, instead of the temperature-index method used in ESM1. This is the first study without flux corrections for the full coupling of an ice sheet model to an AOGCM. The control climate was shown to be relatively stable, except for a slight positive trend of the mass balance of the AIS due to overestimation of precipitation rates as a consequence of the smooth topography of the model. Nevertheless, the anthropogenic climate change signal is much stronger than this trend. The main results obtained with this ESM2 can be summarised as follows:

1. Confirming the results of previous studies (Huybrechts and de Wolde (1999), Church *et al.* (2001)), the sign of the AIS contribution to future sea level change was found to depend on the magnitude of the warming. For a $4xCO_2$ simulation, the warming over the ice sheet surpasses a certain threshold such that increased surface melting exceeds increased snowfall and the mass balance becomes negative.

2. Freshwater fluxes from the Greenland ice sheet are stronger in the simulations of 2x and $4xCO_2$ with ESM2 than in the simulations with ESM1 for the same stabilisation scenarios. This different magnitude of the response is due to the higher climate sensitivity of ESM2.

3. The freshwater fluxes from the GrIS are relatively high. In $4xCO_2$ the NAMOC collapses due to increased atmospheric moisture transport. Therefore the extra fluxes from the GrIS are not important for the evolution of the ocean circulation. In the simulation $2xCO_2$, however, the extra fluxes from the GrIS could potentially play a role in the recovery/non-recovery of the strength of the NAMOC.

9.2 Outlook

The study performed with the ESM1 and ESM2 has several limitations. These limitations will be classified in two groups: a) limitations due to the Shallow Ice Approximation (SIA) in the ice sheet model and b) limitations related to the resolution of the model.

9.2.1 Limitations of the Shallow Ice Approximation

Most ice sheet models are based on the SIA (Hutter, 1983), which is valid for an ice mass with a small aspect ratio ($H << L$, where H and L are the horizontal and vertical dimensions, respectively), where flow is dominated by internal shear deformation: ice flow is driven by gravity, and vertical shearing is concentrated close to the bedrock. The ice sheet model SICOPOLIS used in this study is based as well on the SIA. However, the SIA is not a good approximation at all places in the ice sheet, such as at the ice divide or near the ice margin (Baral *et al.*, 2001). At the margins of ice sheets (which comprises grounding lines, transition zones, outlet glaciers and ice streams), all forces in the mass balance become equally important, especially when basal sliding comes into play or even dominates the horizontal flow field. Longitudinal stretching and lateral shearing play an essential role in the dynamics of large outlet glaciers and major Antarctic ice streams.

Thermomechanical ice sheet models that solve the Stokes problem in three dimensions are not widely developed. Some examples of models including higher-order stresses are the models of Mayer (1996), Albrecht (2000), Saito (2002), and Pattyn (2003).

The dynamics of ice streams, outlet glaciers and ice shelves cannot be modelled with the ice sheet model used for this study. Recent measurements of acceleration of ice streams and outlet glaciers in Greenland and Antarctica (see Chapter 1) reveal that rapid dynamic changes can be important, contributing a notable fraction of the on-going sea-level rise and potentially becoming dominant over ice-sheet mass-balance changes in the future. Models including the full suite of physical processes implicated in the ongoing changes are needed to assess if these ongoing changes represent minor perturbations before stabilisation or a major change that may affect sea level notably.

Grounding line retreat along the major WAIS ice shelves is modelled for basal melting rates $>$ 5-10 m/year, causing the demise of WAIS ice shelves after a few centuries and retreat of coastal ice toward more firmly grounded regions after a few millennia (Huybrechts and de Wolde (1999), Warner and Budd (1998)). SICOPOLIS does not model ice shelves, therefore this process by which higher

ocean temperatures can affect the mass balance of the ice sheets cannot be modelled.

9.2.2 Limitations due to resolution

The resolution of the ice sheet model (80 km) and the lack of a complete formulation of the stresses explained before do not permit to resolve the fast-flowing features at the ice sheet margins (ice streams, outlet glaciers, glacier tongues, ...). But the resolution of the ice sheet model has an impact also on the calculation of the surface mass balance. Since the margins of the ice sheets are quite steep, higher resolution would resolve better the width of the ablation area (Wild *et al.*, 2003).

The resolution of the AGCM is critical for an accurate modelling of precipitation over the ice sheets (Ohmura *et al.*, 1996). The lower the resolution, the higher the overestimation of precipitation due to reduced orographic forcing. Nevertheless, the resolution T31 of ECHAM5 in ESM2, although not ideal, was shown to be a fair compromise between computational expenses and resolution for the purpose of the multi-century simulations performed.

Bibliography

Abe-Ouchi, A., 1993. Ice sheet response to climatic changes: a modelling approach. *Zuercher Geogr. Schr*, **54**, 134 pp.

Albrecht, O., 2000. *Dynamics of glaciers and ice sheets: A numerical model study*. Ph.D. thesis, Swiss Fed. Inst. of Technol., Zurich.

Alley, R. B., P. Clark, P. Huybrechts and I. Joughin, 2005. Ice-Sheet and Sea-Level Changes. *Science*, **310**(5747), 456–460.

Ambach, W. and P. Kirchlechner, 1986. Nomographs for the determination of the meltwater from ice and snow surfaces by sensible and latent heat flux. *Wetter und Leben*, **38**, 181–189.

Arakawa, A. and V. R. Lamb, 1977. Computational design of the basic dynamical processes of the UCLA general circulation model. *Methods Comput. Phys.*, **17**, 173–265.

Bamber, J. L., D. G. Vaughan and I. Joughin, 2000. Widespread Complex Flow in the Interior of the Antarctic Ice Sheet. *Science*, **287**(5456), 1248 – 1250.

Baral, D., K. Hutter and R. Greve, 2001. Asymptotic theories of large-scale motion, temperature, and moisture distribution in land-based polythermal ice sheets: a critical review and new developments. *Appl. Mech. Rev.*, **54**, 215–256.

Berger, W. and J. S. Killingley, 1982. The Worthington effect and the origin of the Younger Dryas. *J. Mar. Res.*, **Suppl.**, 27–38.

Blackmon, M., 1976. A climatological spectral study of the 500 mb geopotential height of the Northern Hemisphere. *Journal of the Atmospheric Sciences*, **33**, 1607–1623.

Blatter, H., 1991. Effect of climate in the cryosphere. *Züercher Geogr. Schr.*, **41**, 98 pp.

Braithwaite, R. J. and O. B. Olensen, 1989. Calculation of glacier ablation from air temperature, West Greenland. In *Glacier fluctuations and climatic change* (edited by J. Oerlemans), pp. 219–233. Kluwer.

Broecker, W. S., M. Andree, W. Wolfli, H. Oeschger, G. Bonani, J. Kennet and D. Peteet, 1988. The chronology of the last deglaciation: implications to the cause of the Younger Dryas event. *Paleoceanogr.*, **3**, 1–19.

Budd, W. F. and I. N. Smith, 1979. The growth and retreat of ice sheets in response to orbital radiation changes. In *Sea level,ice, and climatic change, Proceedings of the Canberra Symposium, December 1979,IAHS Publ. 131*.

Bugnion, V. and P. H. Stone, 2002. Snowpack model estimates of the mass balance of the Greenland ice sheet and its changes over the twentyfirst century. *Climate Dynamics*, **20**, 87–106.

Calov, R., 1994. *Das thermomechanische Verhalten des groenlaendischen Eisschildes unter der Wirkung verschiedener Klimaszenarien - Antworten eines theoretisch-numerischen Modells*. Ph.D. thesis, Institut fuer Mechanik, Technische Hochschule Darmstadt, Germany.

Calov, R., A. Ganopolski, M. Claussen, V. Petoukhov and R. Greve, 2005. Transient simulation of the last glacial inception. Part I: Glacial inception as a bifurcation in the climate system. *Climate Dynamics*, **24**, 545–561.

Calov, R., A. Ganopolski, V. Petoukhov, M. Claussen and R. Greve, 2002. Large-scale instabilities of the Laurentide ice sheet simulated in a fully coupled climate-system model. *Geophysical Research Letters*, **29**(24), 2216.

Calov, R. and K. Hutter, 1996. The thermomechanical response of the Greenland ice sheet to various climate scenarios. *Climate Dynamics*, **12**, 243–260.

Calov, R., A. A. Savvin, R. Greve, I. Hansen and K. Hutter, 1998. Simulation of the Antarctic ice sheet with a three-dimensional polythermal ice-sheet model, in support of the EPICA project. *Annals of Glaciology*, **27**, 201–206.

Church, J. A., J. M. Gregory, P. Huybrechts, M. Kuhn, K. Lambeck, M. T. Nhuan, D. Qin and P. L. Woodworth, 2001. Changes in sea level. In *Climate Change 2001: The Scientific Basis, Contribution of Working Group I to the Third Assessment Report of the Intergovernmental Panel on Climate Change (IPCC)*, pp. 639–694. Cambridge University Press, UK.

Cook, K. and I. Held, 1988. Stationary waves of the ice age climate. *J. Clim.*, **1**, 807–819.

Crowley, T. and S. Baum, 1995. Is the Greenland ice sheet bistable. *Paleoceanography*, **10**, 357–363.

Cuffey, K. M. and S. J. Marshall, 2000. Substantial contribution to sea-level rise during the last interglacial from the Greenland ice sheet. *Nature*, **404**, 591–594. Doi:10.1038/35007053.

Curt, H. D., Y. Li, J. R. McConnell, M. M. Frey and E. Hanna, 2005. Snowfall-Driven Growth in East Antarctic Ice Sheet Mitigates Recent Sea-Level Rise. *Science*, **308**(5730), 1898 – 1901. DOI: 10.1126/science.1110662.

Dansgaard, W., S. Johnsen, H. Clausen, D. Dahl-Jensen, N. Gunestrup, C. Hammer, C. Hvidberg, J. Steffensens, A. Sveinbjörnsdottir, J. Jouzel and G. Bond, 1993. Evidence for general instability of past climate from a 250-kyr ice-core record. *Nature*, **364**, 218–220.

DKRZ, 1994. The ECHAM 3 Atmospheric General Circulation Model. Technical Report 6, Deutsches Klimarechenzentrum, Hamburg, Germany.

Eppley, R., 1972. Temperature and phytoplankton growth in the sea. *Fish. Bull.*, **70**, 1063–1085.

ETOPO5, 1988. Data announcement 88-mgg-02, digital relief of the surface of the earth. Technical report, NOAA, National Geophysical Data Center, Boulder, Colorado, USA.

Fichefet, T., C. Poncin, H. Goose, P. Huybrechts, I. Janssens and H. L. Treut, 2003. Implications of changes in freshwater flux from the Greenland ice sheet for the climate of the 21st century. *Geophysical Research Letters*, **30**, 1911.

Fisher, D. A., 1987. Enhanced flow of Wisconsin ice related to solid conductivity through strain history and recrystallization. *International Association of Hydrological Sciences*, **170**, 45–51.

Fouquart, Y. and B. Bonnel, 1980. Computations of solar heating of the earth's atmosphere- A new parameterization. *Beitraege zur Physik der Atmosphaere*, **59**, 35–62.

Giovinetto, M. B. and H. J. Zwally, 1995. Annual changes in sea ice extent and of accumulation on ice sheets: implications for sea level variability. *Zeitschrift für Gletscherkunde und Glazialgeologie*, **31**, 39–49.

Gregory, J., P. Huybrechts and S. Raper, 2004. Climatology: Threatened loss of the Greenland ice-sheet. *Nature*, **428**, 616.

Greve, R., 1995. *Thermomechanisches Verhalten polythermer Eisschilde - Theorie, Analytik, Numerik*. Ph.D. thesis, Institut fuer Mechanik, Technische Hochschule Darmstadt, Germany.

Greve, R., 1997. Application of a polythemal three-dimensional ice sheet model to the Greenland ice sheet: response to steady-state and transient climate scenarios. *jc*, **10**, 901–918.

Greve, R., 2000. On the response of the Greenland ice sheet to greenhouse climate change. *Climatic Change*, **46**, 289–303.

Greve, R. and R. Calov, 2002. Comparation of numerical schemes for the solution of the ice-thickness equation in a dynamic/thermodynamic ice-sheet model. *Journal of Computational Physics*, **179**(2), 649–664.

Greve, R., K. Wyrwoll and A. Eisenhauer, 1999. Deglaciation of the Northern Hemisphere at the onset of the Eemian and the Holocene. *Ann Glaciol*, **28**, 1–8.

Hagemann, S. and L. Dümenil-Gates, 1998. A parameterization of the lateral waterflow for the global scale. *Climate Dynamics*, **14**, 17–31.

Hagemann, S. and L. Dümenil-Gates, 2003. An improved sub grid runoff parameterization scheme for climate models. *Climate Dynamics*, **21**, 349–359.

Hibler III, W. D., 1979. A Dynamic Thermodynamic Sea Ice Model. *Journal of Physical Oceanography*, **9**(4), 815–846. Doi: 10.1175/1520-0485.

Houghton, J., Y. Ding, D. Griggs, M. Noguer, P. Van der Linden, X. Dai, K. Maskell and C. Johnson, 2001. *Climate Change 2001: the scientific basis*. Cambridge University Press, Cambridge, United Kingdom.

Houghton, R. and J. Hackler, 2002. Carbon Flux to the Atmosphere from Land-Use Changes. In *A Compendium of Data on Global Change*. Carbon Dioxide Information Analysis Center, Oak Ridge National Laboratory, U.S. Department of Energy, Oak Ridge, Tenn., USA.

Hutter, K., 1983. *Theoretical Glaciology*. Kluwer Acad., Norwell, Mass., 1983.

Huybrechts, P., 1992. *The Antarctic ice sheet and enviromental change: a three-dimensional modelling study*. Ber. Polarforschung. 241 pp.

Huybrechts, P. and J. de Wolde, 1999. The dynamic response of the Greenland and Antarctic ice sheets to multiple-century climatic warming. *Journal of Climate*, **12**, 2169–2188.

Huybrechts, P., J. M. Gregory, I. Janssens and M. Wild, 2004. Modelling antarctic and greenland volume changes during the 20th and 21st centuries forced by gcm time slice integrations. *Global and Planetary Change*, **42**, 83–105.

Huybrechts, P., I. Janssens, C. Poncin and T. Fichefet, 2002. The response of the Greenland ice sheet to climate changes in the 21st century by interactive coupling of an AOGCM with a thermomechanical ice-sheet model. *Annals of Glaciology*, **35**, 409–415.

Huybrechts, P. and J. Oerlemans, 1990. Response of the Antarctic Ice Sheet to future greenhouse warming. *Climate Dynamics*, **5**, 93–102.

Imbrie, J., J. Martinson, D. McIntyre, A. Mix, J. Morley, N. Pisias, W. Prell and N. Shackleton, 1984. The orbital theory of Pleistocene climate: Support from a revised chronology of the marine delta 0^{18} record. In *Milankovich and climate, part I* (edited by A. Berger), Volume 126. D. Reidel Publishing Company, Dordrecht, Holland.

Jacobs, S. S., H. H. Helmer, C. S. M. Doake, A. Jenkins and R. M. Frolich, 1992. Melting of ice shelves and the mass balance of Antarctica. *Journal of Glaciology*, **38**, 130.

Janssens, I. and P. Huybrechts, 2000. The treatment of meltwater retention in mass-balance parameterisations of the Greenland Ice Sheet. *Annals of Glaciology*, **31**, 133–140.

Joughin, I., W. Abdalati and M. Fahnestock, 2004. Large fluctuations in speed on Greenland's Jakobshavn Isbrae glacier. *Nature*, **432**(7017), 608–610.

Joughin, I., E. Rignot, C. E. Rosanova, B. K. Lucchitta and J. Bohlander, 2003. Timing of Recent Accelerations of Pine Island Glacier, Antarctica. *Geophysical Research Letters*, **30**(13), 1706. Doi:10.1029/2003GL017609.

Jouzel, J., N. I. Barkov, M. B. J. M. Barnola, J. Chappelaz, C. Genthon, V. M. Kotlyakov, V. Lipenkov, C. Lorius, J. R. Petit, D. Raynaud, G. Raisbeck, C. Ritz, T. Sowers, M. Stievenard, F. Yiou and P. Yiou, 1993. Extending the Vostok ice-core record of paleoclimate to the penultimate glacial period. *Nature*, **364**(6436), 407–412.

Jouzel, J., C. Waelbroeck, B. Malaize, M. Bender, J. R. Petit, N. I. Barkov, J. M. Barnola, T. King, V. M. Kotlyakov, V. Lipenkov, C. Lorius, D. Raynaud, C. Ritz and T. Sowers, 1996. Climatic interpretation of the recently extended Vostok ice records. *Climate Dynamics*, **12**, 513–521.

Jungclaus, J., M. Botzet, H. Haak, N. Keenlyside, J.-J. Luo, M. Latif, J. Marotzke, U. Mikolajewicz and E. Roeckner, 2006. Ocean circulation and tropical variability in the AOGCM ECHAM5/MPI-OM. *Journal of Climate*, **19**(16), 3952–3972. Doi: 10.1175/JCLI3827.1.

Junge, M., R. Blender, K. Fraedrich, V. Gayler, U. Luksch and F. Lunkheit, 2005. A world without Greenland: impacts on the Northern Hemisphere winter circulation in low- and high- resolution models. *Climate Dynamics*, **24**, 297–307.

Kageyama, M., S. Charbit, C. Ritz, M. Khodri and G. Ramstein, 2004. Quantifying ice-sheet feedbacks during the last glacial inception. *Geophysical Research Letters*, **31**, L24203,doi:10.1029/2004GL021339.

Krabill, W., E. Hanna, P. Huybrechts, W. Abdalati, J. Cappelen, B. Csatho, E. Frederick, S. Manizade, C. Martin, J. Sonntag, R. Swift, R. Thomas and J. Yungel, 2004. Greenland ice sheet: Increased coastal thinning. *Geophysical Research Letters*, **31**(L24402). Doi:10.1029/2004GL021533.

Kukla, G. and D. Robinson, 1980. Annual cycle of surface albedo. *Mon. Wea. Rev.*, **108**, 56–58.

Kutzbach, J. and H. Wright, 1985. Simulation of the climate of 18,000 yr BP: Results for the North American/North Atlantic/European sector and comparison with the geological record. *Quat. Sci. Rev.*, **4**, 147–187.

Larsen, H., A. Saunders, P. Clift, J. Beget, W. Wei and S. Spezzaferri, 1994. Seven millions years of glaciation in Greenland. *Science*, pp. 952–954.

Le Meur, E. and P. Huybrechts, 1998. Present-day uplift patterns over Greenland from a coupled ice-sheet/visco-elastic bedrock model. *Geophysical Research Letters*, **25**, 3951–3954.

Letreguilly, A., P. Huybrechts and N. Reeh, 1991a. Steady-state characteristics of the Greenland ice sheet under different climates. *Journal of Glaciology*, **37**(125), 149–157.

Letreguilly, A., N. Reeh and P. Huybrechts, 1991b. The Greenland ice sheet through the last glacial-interglacial cycle. *Palaeogeogr. Paleoclimatol. Palaeoecol.*, **90**, 385–394.

Lin, S. and R. Rood, 1996. Multidimensional flux-form semi-lagragian transport schemes. *Mon. Weather Rev.*, **124**, 2046–2070.

Lohman, U. and E. Roeckner, 1996. Design and performance of a new cloud mycrophysics scheme developed for the ECHAM general circulation model. *Climate Dynamics*, **12**, 557–572.

Lunt, D., N. de Noublet-Ducoudré and S. Charbit, 2004. Effects of a melted greenland ice sheet on climate,vegetation, and the cryosphere. *Climate Dynamics*, **23**, 679–694.

Lythe, M., D. Vaughan and the BEDMAP Consortium: Ph. Huybrechts at al., 2001. BEDMAP: a new ice thickness and subglacial topographic model of Antarctica. *Journal of Geophysical Research*, **106**(B6), 11335–11351.

MacAyeal, D. R., 1993. Binge/purge oscillations of the Laurentide ice sheet as a cause of the North Atlantic's Heinrich Events. *Paleoceonography*, **8**(6), 775–884.

Maier-Reimer, E., 1993. Geochemical cycles in an ocean general circulation model. Preindustrial tracer distributions. *Global Biogeochem. Cycles*, **7**, 645–677.

Maier-Reimer, E. and U. Mikolajewicz, 1989. *Experiments with an OGCM on the Cause of the Younger Dryas*, chapter Oceanography 1988, pp. 87–100. UNAM Press, Mexico D F, 208p.

Manabe, S. and A. Broccoli, 1985. The influence of continental ice sheets on the climate of an ice age. *J. Geophys. Res.*, **90**, 2167.

Marland, G., T. Boden and R. Andres, 2005. Global, Regional, and National Fossil Fuel CO_2 emissions. In *Trends: A Compendium of Data on Global Change*. Carbon Dioxide Information Analysis Center, Oak Ridge National Laboratory, U.S. Department of Energy, Oak Ridge, Tenn., U.S.A.

Marsiat, I., 1994. Simulation of the northern hemisphere continental ice sheets over the last glacial-interglacial cycle: Experiments with a latitude-longitude vertically integrated ice sheet model coupled to a zonally averaged climate model. *Paleoclimates*, **I**, 59–98.

Marsland, S., H. Haak, J. Jungclaus, M. Latif and F. Roske, 2003. The Max-Planck-Institute global ocean/sea ice model with orthogonal curvilinear coordinates. *Ocean Modelling*, **5**, 91–127.

Marty, C., R. Philipona, C. Fröhlich and A. Ohmura, 2002. Altitude dependence of surface radiation fluxes and cloud forcing in the alps: results from the alpine surface radiation budget network. *Theoretical and Applied Climatology*, **72**(3-4), 137–155. DOI:10.1007/s007040200019.

Mayer, C., 1996. Numerische Modellierung der Übergangszone zwischen Eisschild und Shelfeis (Numerical modelling of the transition zone between an ice sheet and an ice shelf). *Ber. Polarforsch.*, **214**, 1–150.

Mercer, J. H., 1978. West Antarctic ice sheet and CO_2 greenhouse effect: a threat of disaster. *Nature*, **271**, 321–325.

Mikolajewicz, U., M. Gröger, E. Maier-Reimer, G. Schurgers, M. Vizcaíno and A. Winguth, accepted. Long-term effects of anthropogenic CO_2 emissions simulated with a complex earth system model. *Accepted for publication in Climate Dynamics*.

Mitrovica, J. X., M. E. Tamisiea, J. L. Davis and G. A. Milne, 2001. Recent mass balance of polar ice sheets inferred from patterns of global sea-level change. *Nature*, **409**, 1026–1029.

Morcrette, J., C. S.A., E. Mlawer and M. Iacono, 1998. Impact of a validated radiative transfer scheme, RRTM, on the ECMWF model climate and 10-day forecasts. Technical Memorandum 252, ECMWF, Reading, U.K.

Nakićenović, N., J. Alcamo, G. Davis, B. De Vries, J. Fenhann, S. Gaffin, K. Gregory, A. Grübler, T. Jung, T. Kram, E. Lebre La Rovere, L. Michaelis, S. Mori, T. Morita, W. Pepper, H. Pitcher, L. Price, K. Riahi, A. Roehrl, H. Rogner, A. Sankovski, M. Schlesinger, P. Shukla, S. Smith, R. Swart, S. Van Rooijen, N. Victor and Z. Dadi, 2001. Special report on emissions scenarios. In *A special report of Working Group III of the Intergovernmental Panel on Climate Change*. Cambridge University Press, Cambridge.

Nordeng, T., 1994. Extended versions of the convective parameterizations scheme at ecmwf and their impact on the mean and transient activity of the model in the tropics. Technical Memorandum 206, ECMWF, Reading, U.K.

Ohmura, A., P. Calanca, M. Wild and M. Anklin, 1996. A possible change in mass balance of Greenland and Antarctic ice sheets in the coming century. *Journal of Climate*, **9**, 2124–2135.

Otto-Bliesner, B. L., S. J. Marshall, J. T. Overpeck, G. H. Miller and C. L. I. P. m. A. Hu, 2006. Simulating Arctic Climate Warmth and Icefield Retreat in the Last Interglaciation. *Science*, **311**(5768), 1751 – 1753.

Paterson, W., 1991. Why ice-ige ice is sometimes "soft". *Cold Reg. Sci. Technol.*, **20**, 75–98.

Paterson, W. S. B., 1994. *The physics of glaciers*. Oxford, Pergamon Press, third edition edition. 480 pp.

Pattyn, F., 2003. A new three-dimensional higher-order thermomechanical ice sheet model: Basic sensitivity, ice stream development, and ice flow across subglacial lakes. *Jounal of Geophysical Research*, **108**(B8), 2382. Doi:10.1029/2002JB002329.

Payne, A. J., 1995. Limit cycles in the basal thermal regime of ice sheets. *Journal of Geophysical Research*, **100**(B3), 4249–4263.

Payne, A. J., A. Vieli, A. P. Shepherd, D. J. Wingham and E. Rignot, 2004. Recent dramatic thinning of largest West Antarctic ice stream triggered by oceans. *Geophysical Research Letters*, **31**(L23401).

Petersen, G., J. Kristjánsson and H. Ólafsson, 2004. Numerical simulations of Greenland's impact on the Northern Hemisphere winter circulation. *Tellus*, **56A**, 102–111.

Raper, S. and R. Braithwaite, 2006. Low sea level rise projections from mountain glaciers and icecaps under global warming. *Nature*, **439**, 311–313.

Reeh, N., 1991. Parameterization of melt rate and surface temperature on the Greenland Ice Sheet. *Polarforschung*, **59**(3), 113–228.

Ridley, J. K., P. Huybrechts, J. M. Gregory and J. A. Lowe, 2005. Elimination of the Greenland Ice Sheet in a High CO_2 Climate. *Journal of Climate*, **18**, 3409–3427.

Rignot, E. and P. Kanagaratnam, 2006. Changes in the Velocity Structure of the Greenland Ice Sheet. *Science*, **311**(5763), 986–990.

Rignot, E. and R. H. Thomas, 2002. Mass balance of polar ice sheets. *Science*, **297**(5586), 1502 – 1506. DOI: 10.1126/science.1073888.

Ritz, C., 1987. *The physical basis of ice sheet modelling*, Volume 170, chapter Time dependent boundary conditions for calculation of temperature fields in ice sheets, pp. 207–216. IAHS Publication.

Ritz, C., A. Fabre and A. Letreguilly, 1997. Sensitivity of a Greenland ice sheet model to ice flow and ablation parameters: Consequences for evolution through the last climatic cycle. *Climate Dynamics*, **13**, 11–24.

Robock, A., 1980. The seasonal cycle of snow cover, sea-ice and surface albedo. *Mon. Wea. Rev.*, **108**, 267–285.

Roeckner, E., K. Arpe, L. Bengtsson, S. Brinkop, L. Duemenil, M. Esch, E. Kirk, F. Lunkheit, M. Ponater, B. Rockel, R. Sausen, U. Schlese, S. Schubert and M. Windelband, 1992. Simulation of the present-day climate with the ECHAM model: impact of the model physics and resolution. Technical Report 93, Max-Planck-Institut für Meteorologie, Hamburg.

Roeckner, E., G. Baeuml, L. Bonventura, R. Brokopf, M. Esch, M. Giorgetta, S. Hagemann, I. Kirchner, L. Kornblueh, E. Manzini, A. Rhodin, U. Schlese, U. Schulzweida and A. Tompkins, 2003. The atmospheric general circulation model ECHAM 5. PART I: Model description. Report 349, Max Planck Institute for Meteorology, Hamburg, Germany. Available from http://www.mpimet.mpg.de.

Saito, F., 2002. *Development of a three dimensional ice sheet model for numerical studies of Antarctic and Greenland ice sheet*. Ph.D. thesis, Univ. of Tokyo, Tokyo.

Sausen, R. and R. Voss, 1996. Techniques for asynchronous and periodically synchronous coupling of atmosphere and ocean models, part i: general strategy and application to the cyclo-stationary case. *Climate Dynamics*, **12**, 313–323.

Scambos, T. A., J. A. Bohlander, C. A. Shuman and P. Skvarca, 2004. Glacier acceleration and thinning after ice shelf collapse in the Larsen B embayment, Antarctica. *Geophysical Research Letters*, **31**(L18402). Doi:10.1029/2004GL020670.

Schiller, A., U. Mikolajewicz and R. Voss, 1997. The stability of the North Atlantic thermohaline circulation in a coupled ocean-atmosphere general circulation model. *Climate Dynamics*, **13**, 325–347.

Schwerdtfeger, 1963. Theoretical derivation of the thermal conductivity and diffusivity of snow. *IASH*, **61**, 75–81.

Schytt, V., 1958. *The inner structure of the ice shelf at Maudheim as shown by core drilling*, Volume 4 of *Glaciology 2, Scientific Results*, chapter Scientific Results, pp. 115–151. Norsk Polarinstitutt, Oslo.

Sclatter, J. G., C. Jaupart and D. Galson, 1980. The heat flow through oceanic and continental crust and the heat loss of the earth. *Reviews of Geophysics and Space Physics*, **18**(1), 269–311.

Shepherd, A., D. Wingham, T. Payne and P. Skvarca, 2003. Larsen Ice Shelf Has Progressively Thinned. *Science*, **302**(5646), 856 – 859. DOI: 10.1126/science.1089768.

Shepherd, A., D. J. Wingham and J. A. D. Mansley, 2002. Inland thinning of the Amundsen Sea sector, West Antarctica. *Geophysical Research Letters*, **29**(10), 1364. Doi:10.1029/2001GL014183.

Sitch, S., B. Smith, I. Prentice, A. Arneth, A. Bondeau, W. Cramer, J. Kaplan, S. Levis, W. Lucht, M. Sykes, K. Thonicke and S. Venevsky, 2003. Evaluation of ecosystem dynamics, plant geography and terrestrial carbon cycling in the LPJ dynamic global vegetation model. *Global Change Biology*, **9**(2), 161–185.

Smith, E., 1936. Photosynthesis in Relation to Light and Carbon Dioxide. In *Proc. Natl. Acad. Sci.*, Volume 22, pp. 504–511.

Smith, I., 1999. Estimating mass balance components of the Greenland Ice Sheet from a long-term GCM simulation. *Global and Planetary Change*, **20**, 19–32.

Smith, I. N., W. F. Budd and P. Reid, 1998. Model estimates of Antarctic accumulation rates and their relationship to temperature changes. *Annals of Glaciology*, **27**, 246–250.

Stirling, C., T. Esat, K. Lambeck and M. McCulloch, 1998. Timing and duration of the Last Interglacial: evidence for a restricted interval of widespread coral reef growth. *Earth and Planetary Science Letters*, **160**(3-4), 745–762.

Stouffer, R. J., K. W. Dixon, M. J. Spelman and W. Hurlin, 2006. Investigating the Causes of the Response of the Thermohaline Circulation to Past and Future Climate Changes. *Journal of Climate*, **19**(8), 1365–1387.

Svendsen, B. and K. Hutter, 1996. A continuum approach for modelling induced anisotropy in glaciers and ice sheets. *Ann. Glaciol*, **23**, 262–269.

Thomas, R., E. Rignot, G. Casassa, P. Kanagaratnam, C. Acuña, T. Akins, H. Brecher, E. Frederick, P. Gogineni, W. Krabill, S. Manizade, H. Ramamoorthy, A. Rivera, R. Russell, J. Sonntag, R. Swift, J. Yungel, and J. Zwally, 2004. Accelerated Sea-Level Rise from West Antarctica. *Science*, **306**(5694), 255 – 258. DOI: 10.1126/science.1099650.

Tiedke, M., 1989. A comprenhensive mass flux scheme for cumulus parameterization in large-scale models. *Mon. Weather Rev.*, **117**, 1779–1800.

Toniazzo, T., J. Gregory and P. Huybrechts, 2004. Climatic Impact of a Greenland deglaciation and Its Possible Irreversibility. *Journal of Climate*, **17**, 21–33.

Uppala, S. M., P. W. Kallberg, A. J. Simmons, U. Andrae, V. da Costa Bechtold, M. Fiorino, J. Gibson, J. Haseler, A. Hernandez, G. Kelly, X. Li, K. Onogi, S. Saarinen, N. Sokka, R. Allan, E. Andersson, K. Arpe, M. Balmaseda, A. Beljaars, L. van de Berg, J. Bidlot, N. Bormann, S. Caires, F. Chevallier, A. Dethof, M. Dragosavac, M. Fisher, M. Fuentes, S. Hagemann, E. Holm, B. Hoskins, L. Isaksen, P. Janssen, R. Jenne, A. McNally, J.-F. Mahfouf, J.-J. Morcrette, N. Rayner, R. Saunders, P. Simon, A. Sterl, K. Trenberth, A. Untch, D. Vasiljevic, P. Viterbo and J. Woollen, 2005. The ERA-40 re-analysis. *Quart. J. Roy. Meteor. Soc.*, **131**, 2961–3012.

Valcke, S., A. Caubel, D. Declat and L. Terray, 2003. OASIS Ocean Atmosphere Sea Ice Soil user's guide. Technical Report TR/CMGC/03/69, CERFACS, Toulouse, France. 85pp.

Van de Wal, R. S. W. and S. Elkholm, 1996. On elevation models as input for mass balance calculations of the Greenland ice sheet. *Annals of Glaciology*, **23**, 181–186.

Van de Wal, R. S. W. and J. Oerlemans, 1997. Modelling the short term response of the Greenland ice sheet to global warming. *Climate Dynamics*, **13**, 733–744.

Velicogna, I. and J. Wahr, 2006. Measurements of Time-Variable Gravity Show Mass Loss in Antarctica. *Science*, **311**(5768), 1754 – 1756. 10.1126/science.1123785.

Vezina, J., B. Jones and D. Ford, 1999. Sea-level highstands over the last 500,000 years: evidence from the ironshore formation on grand cayman, british west indies. *J. Sedim. Res.*, **69**, 317–327.

Volk, T. and M. I. Hoffert, 1985. Ocean carbon pumps: analysis of relative strengths and efficiencies in ocean-driven atmospheric CO_2 changes. In *The Carbon Cycle and Atmospheric CO_2 : Natural Variations Archean to Present* (edited by E. T. Sundquist and W. S. Broecker), Volume 32 of *Geophysical Monograph*, pp. 99–110. American Geophysical Union, Wash., D.C.

Voss, R. and U. Mikolajewicz, 2001. Long-term climate changes due to increased CO_2 concentration in the coupled atmosphere-ocean general circulation model ECHAM3/LSG. *Climate Dynamics*, **17**, 45–60.

Voss, R. and R. Sausen, 1996. Techniques for asynchronous and periodically synchronous coupling of atmosphere and ocean models, part ii: impact of variability. *Climate Dynamics*, **12**, 605–614.

Voss, R., R. Sausen and U. Cubasch, 1998. Periodically synchronously coupled integrations with the atmosphere-ocean general circulation model ECHAM3/LSG. *Climate Dynamics*, **14**, 249–266.

Wang, Z. and L. Mysak, 2002. Simulation of the last glacial inception and rapid ice sheet growth in the McGill Paleoclimate model. *Geophysical Research Letters*, **29**(23), doi:10.1029/2002GL015120.

Warner, R. and W. Budd, 1998. Modelling the long term response of the Antarctic ice sheet to global warming. *Ann. Glaciol.*, **27**, 161.

Wild, M., P. Calanca, S. Scherrer and A. Ohmura, 2003. Effects of polar ice sheets on global sea level in high resolution greenhouse scenarios. *J. Geophys. Res.*, **108**, 4165.

Wild, M. and A. Ohmura, 2000. Changes in the mass balance of the polar ice sheets and sea level from high resolution GCM simulations of global warming. *Annals of Glaciology*, **30**, 197–203.

Wingham, D. J., A. J. Ridout, R. Scharroo, R. J. Arthern and C. K. Shum, 1998. Antarctic Elevation Change from 1992 to 1996. *Science*, **282**(5388), 456 – 458. DOI: 10.1126/science.282.5388.456.

Winguth, A., E. Maier-Reimer, U. Mikolajewicz and J. Segschneider, 1994. El Nino-Southern Oscillation related fluctuations of the marine carbon cycle. *Global Biogeochemical Cycles*, **8**, 39–63.

Wolff, J., E. Maier-Reimer and S. Legutke, 1997. The Hamburg Ocean primitive equation model - HOPE. Technical Report 13, German Climate Computer Centre (DKRZ), Hamburg, Germany.

Yen, Y. C., 1981. Review of thermal properties of snow, ice and sea ice. *CRREL Report*, **81-10**.

Zachos, J., M. Pagani, L. Sloan, E. Thomas and K. Billups, 2001. Trends, Rhythms, and Aberrations in Global Climate 65 ma to Present. *Science*, **27**, 686 – 693.

Zwally, H., W. Abdalati, T. Herring, K. Larson, J. Saba and K. Steffen, 2002. Surface melt-induced acceleration of Greenland ice-sheet flow. *Science*, **297**, 218–222.

Acknowledgements

I would like to thank here the persons who made possible that this thesis was completed.

Thanks to my supervisor Uwe Mikolajewicz, for his support, his advice, and for the wonderful scientific project he involved me in.

To my colleagues Guy Schurgers, Matthias Gröger, Arne Winguth, Ernst Maier-Reimer, and Johann Jungclaus, for the work done together.

To Prof. Hartmut Graßl, for the corrections to the manuscript, for his enthusiasm, for his support.

To the members of my Panel, for their support and advice.

To Prof. Guy Brasseur, for his encorauging words, his support, and for his idea of the International Max Planck Research School.

To the International Max Planck Research School: students, executive committee, organizators, teachers, funders. Because it was extremely interesting to learn about the different components of the Earth System, because it was fabulous to meet people from so diverse countries and cultures, and because it was helfpul to work together.

To the people from the ocean department, for the shared knowledge, for the shared chat, for the together fun. To Johann and Helmuth for their support during my first months in Hamburg.

To the fantastic community of glaciologists in the world. Very special thanks to to Prof. Johannes Oerlemanns (University of Utrecht) for his scientific advice, which was very helpful to me during my first steps into the field of Glaciology. To teachers and students of the Summer School of Karthaus on Ice Sheets and Glaciers 2003, for the fun together, for the science learnt.

To Prof. Ralf Greve (University of Hokkaido), for his support with the ice sheet model and his scientific advice.

And many special thanks to my favourite scientist, Luis, for his wise advice, his enthusiasm, and his support. And to Juan and Luisma, and to my parents.

Publikationsreihe des MPI-M
„Berichte zur Erdsystemforschung“ , „*Reports on Earth System Science*“, ISSN 1614-1199
Sie enthält wissenschaftliche und technische Beiträge, inklusive Dissertationen.

Publikationsreihe des MPI-M
„Berichte zur Erdsystemforschung“ , „*Reports on Earth System Science*“, ISSN 1614-1199
Sie enthält wissenschaftliche und technische Beiträge, inklusive Dissertationen.


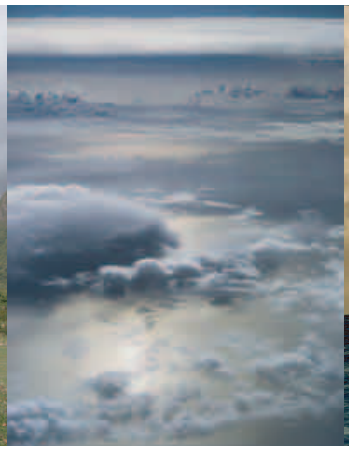


ISSN 1614-1199